

Impact of Turbulence on Detonation Dynamics

Bernard Joseph Marjaba

A thesis
in
The Department
of
Mechanical, Industrial, and Aerospace Engineering

Presented in Partial Fulfillment of the Requirements
for the Degree of
Masters of Applied Science (Mechanical Engineering)
Concordia University
Montréal, Québec, Canada

April 2021
© Bernard Joseph Marjaba, 2021

CONCORDIA UNIVERSITY

School of Graduate Studies

This is to certify that the thesis prepared

By: **Bernard Joseph Marjaba**

Entitled: **“Impact of Turbulence on Detonation Dynamics”**

and submitted in partial fulfillment of the requirements for the degree of

 Master of Applied Science (Mechanical Engineering)

complies with the regulations of the University and meets the accepted standards with respect to originality and quality.

Signed by the final examining committee:

_____ Chair & Examiner
Dr. Hoi Dick Ng

_____ Examiner
Dr. Rolf Wuthrich

_____ Thesis Supervisor
Dr. Charles Basenga Kiyanda

Approved by _____
Dr. Sivakumar Naranswamy, MASc Program Director
Department of Mechanical, Industrial, and Aerospace Engineering

Dr. Mourad Debbabi, Interim Dean
Gina Cody School of Engineering and Computer Science

Abstract

Impact of Turbulence on Detonation Dynamics

Bernard Joseph Marjaba

This study provides a macroscopic, experimental analysis of the impact of turbulence on the dynamics of a detonation wave. The interaction of detonation waves with turbulence is widely encountered in detonation-based propulsion devices such as the rotating detonation engine (RDE), and a good understanding of this interaction is needed for suitable orifice design and wave stability and sustainability. In this study, experiments were conducted in a detonation tube with multiple inlets. One inlet is used to slowly fill the tube with a reactive mixture, while the other is used for the rapid injection of a jet into an initially quiescent medium, thereby generating turbulence. Detonation waves are initiated from one end of the tube using a high power ignition system. A schlieren visualization system is used to capture images as blasts and detonation waves pass through an optical viewing section at the other end of the tube. Five levels of turbulence were generated for each fill pressure of 10 kPa, 20 kPa, and 30 kPa. Detonation speeds were measured from the captured images and compared to those of detonations propagating in a quiescent medium at the same pressures. It was found that turbulence enhances the propagation of detonations with larger cell size (at 10 kPa) bringing its speed closer to the ideal, Chapman-Jouguet, detonation speed, and hinders the propagation of detonations with smaller cells (at 20 kPa and 30 kPa) increasing the deficit below the wave's CJ speed at the given pressure. This result implies that there exists a critical cell size, characteristic of the reactive mixture, at which a switch in behaviour occurs under the influence of turbulence. Consequently, a minimum cell size must be attained, in order to recover lost energy of a detonation wave and use turbulence favourably.

Acknowledgements

First and foremost, I would like to thank my supervisor Professor Charles Kiyanda for giving me this opportunity of exploring the fascinating world of detonations, and for the continuous support I received from him throughout this project. Second, I would like to thank my parents, Joseph Marjaba & Nawal Marjaba, and my brother and sister Nizar Marjaba & Nadine Marjaba, for their unconditional love and relentless support since day one, specifically since deciding to travel half way across the world to pursue my Master's degree. Lastly, I would like to thank my family of uncle and cousins in Ottawa for their support and for relieving the stress of being far from home, as well as my friends who have been nothing but supportive throughout this journey.

Table of Contents

List of Symbols	vii
List of Figures.....	ix
List of Tables	xi
1 Introduction.....	1
1.1 Detonative Cycles.....	1
1.2 Pulse Detonation and Rotating Detonation Engines.....	2
1.3 Detonation-Turbulence Interaction	5
2 Detonation Theory	7
2.1 Chapman-Jouguet Theory	7
2.2 ZND Model and Detonation Structure	9
2.3 Detonation Cell Size.....	10
2.4 Propagation Limits and Cell Size.....	13
3 Experimental Setup	14
3.1 Injection and Filling	16
3.2 Schlieren Diagnostics.....	17
3.3 Vacuum System	18
3.4 Ignition System	18
3.5 Arduino Control System	19
4 Shock-Turbulence Interaction.....	21
4.1 Injection Characteristics.....	21
4.1.1 Jet Dynamics.....	21
4.1.2 Characterizing Turbulence.....	22
4.2 Initial Conditions	23
4.3 Results.....	25
4.3.1 Shock Waves Propagating Through a Quiescent Medium.....	25
4.3.2 Shocks with Jet Injection Through Inlet 1	28
4.3.3 Shocks with Jet Injection Through Inlet 2	31
4.3.4 Shocks with Jet Injection Through Inlet 3	34
4.4 Errors and Uncertainties	37
5 Detonation-Turbulence Interaction	38
5.1 Initial Conditions	38
5.2 Results.....	38
5.2.1 Detonation Propagation Through an Undisturbed Medium	38
5.2.2 Detonation-Turbulence Interaction with Argon Injection.....	40
5.2.3 Detonation-Turbulence Interaction with Ethylene-Oxygen Injection.....	43
5.3 Errors and Uncertainties	59

6 Conclusion	60
6.1 Future Works.....	60
Bibliography	62
Appendix.....	64
A1 List of Components.....	64
A2 Schlieren Setup Procedure.....	65
A3 Shock Test Procedure.....	66
A3.1 Shocks with no Turbulence.....	66
A3.2 Shocks with Turbulence.....	67
A4 Detonation Test Procedure	68
A4.1 Detonations with no Turbulence	68
A4.2 Detonations with Turbulence	69
A5 Arduino Scripts.....	70
A5.1 Detonations with no turbulence	70
A5.2 Detonations with turbulence	71
A6 Schlieren Images of Detonations with Turbulence	75

List of Symbols

c_0	Speed of sound in an undisturbed fluid in the piston-cylinder example
c_p	Specific heat capacity at constant pressure
E_0	Pre-shock energy of a fluid in the piston-cylinder example
h_j	Specific enthalpy of the gas in the turbulent jet
h_s	Specific enthalpy of the gas in the supply line
P_0	Pre-shock pressure of a fluid in the piston-cylinder example
P_f	Final pressure in the shock tube after jet injection
P_i	Initial pressure
$P_{s,f}$	Final supply pressure in injection cylinder C2 after injection
$P_{s,i}$	Initial supply pressure in injection cylinder C2 before injection
P_s	Supply pressure
PR_f	Final pressure ratio
PR_i	Initial pressure ratio
t_{delay}	Delay time between jet injection and ignition
t_{inj}	Injection time
T_j	Temperature of the gas in the turbulent jet
T_s	Temperature of the gas in the supply line
U_{av}	Average speed of the detonation wave in a turbulent medium
$U_{average}$	Average speed of the shock front
U_{bottom}	Speed of the shock front at the bottom of the test section
U_{CJ}	CJ speed of the detonation wave at a given pressure
U_j	Speed of the turbulent jet
$U_{N,P}$	Normalized speed of a detonation wave in a quiescent medium
U_N	Normalized speed of a detonation wave in a turbulent medium
U_P	Speed of the detonation wave at a given fill pressure in a quiescent medium
U_{top}	Speed of the shock front at the top of the test section

x_i	Distance between inlet and start of schlieren beam
y_0	Reaction progress variable at initial state
Z_{Argon}	Mole fraction of argon in the medium
$Z_{reactant}$	Mole fraction of the reactive gas in the medium
Z_T	Ratio of pressure contribution of turbulence to final pressure in the reactive medium
v_0	Pre-shock specific volume of a fluid in the piston-cylinder example
ρ_0	Pre-shock density of a fluid in the piston-cylinder example
ρ_j	Density of the turbulent jet
ρ_j	Density of gas in the turbulent jet
ρ_s	Density of gas in the supply line
c	Speed of sound in a shocked fluid in the piston-cylinder example
C	Capacitance
D	CJ speed of a detonation wave in the piston-cylinder example
D	Diameter of the turbulent jet
E	Post-shock energy of a fluid in the piston-cylinder example
M	Mach number of the turbulent jet
P	Post-shock pressure of a fluid in the piston-cylinder example
Re	Reynold's number
V	Voltage
y	Reaction progress variable
γ	Specific heat ratio of the gas
Γ	Location of inlet relative to turbulent region
E	Stored energy in bank of capacitors
λ	Detonation cell size
μ	Kinematic viscosity of the injected gas
v	Post-shock specific volume of a fluid in the piston-cylinder example
ρ	Post-shock density of a fluid in the piston-cylinder example
τ	Difference between initial pressure ratio and final pressure ratio

List of Figures

1	Comparison of P - V diagrams for Humphrey, Brayton, and Fickett-Jacobs cycles	2
2	PDE Schematic	3
3	A schematic representing the different processes that occur in a PDE, including injection, ignition, detonation propagation, and thrust	3
4	Schematic of a typical RDE showing its essential components.	4
5	A schematic showing the different regions of the RDE's flow field, in the engine (top) and in an unwrapped version of the engine (bottom)	5
6	Piston-cylinder example used to explain detonation wave propagation	8
7	P - V diagram showing the Rayleigh line, reacted, and unreacted Hugoniot curves	9
8	Schematic of ZND structure of gaseous detonation and pressure profile of the structure	10
9	Ideal structure of a detonation cell: I, region of transverse wave collision; 1 and 2, shock fronts; 3, flame fronts; 4, induction zone; 5, transverse waves; 6, tail of transverse wave; R and r , radius of shock waves produced by neighboring I regions	11
10	Schlieren photos of the detonation structure of (a) $C_3H_8 + 5O_2$ at an initial pressure of 5.6 kPa in the solid section of a channel and (b) $2H_2 + O_2 + 40\%Ar$ at an initial pressure of 13 kPa in the smooth section of a channel	11
11	A soot imprint of the cellular structure of a detonation wave	12
12	Cell size vs initial pressure for an ethylene-oxygen mixture diluted in argon	12
13	Shock tube setup diagram	15
14	Z-type schlieren setup diagram	18
15	Igniter circuit diagram	19
16	Control system circuit diagram	20
17	Velocity vs time graph describing a turbulent flow-field	23
18	Example of a free turbulent jet	23
19	Average wave speed versus fill pressure	26
20	A frame of the normal shock wave propagating through an undisturbed medium of air for each of the 6 fill pressures	27
21	Average wave speed versus injection time (Inlet 1)	29
22	A frame of each shock wave for experiments 1, 4, 5, 8, 9, 12, 13, 16, referring to table 4	30
23	Average wave speed versus injection time (Inlet 2)	32
24	A frame of the shock wave for experiments 1, 4, 5, 8, 9, 12, 13, 16, referring to table 5 . .	33

25	Average wave speed versus injection time (Inlet 3)	35
26	A frame of the shock wave for experiments 1, 4, 5, 8, 9, 12, 13, 16, referring to table 6	36
27	Schlieren images of a propagating detonation wave in an undisturbed medium for (a) 5 kPa (b) 10 kPa (c) 20 kPa (d) 30 kPa	39
28	A frame from the detonation at 20 kPa fill pressure showing the visible portions of the cellular pattern	40
29	One frame from each of the 12 shots of detonation with argon. The numbers next to each image correspond to the rows from table 8	41
30	Five frames from a detonation with turbulence though inlet 1 at $P_s = 75$ kPa, $P_f = 10$ kPa, $P_i = 8$ kPa, $t_{inj} = 0.238$ s	44
31	Pressure versus time graph during jet injection	46
32	Pressure versus time graph read by the 15 psi sensor during jet injection and manifold evacuation, for experiment 22 from table 7	47
33	Normalized wave speed, U_N , vs Γ for $P_f = 10$ kPa	50
34	Normalized wave speed, U_N , vs Γ for $P_f = 20$ kPa	50
35	Normalized wave speed, U_N , vs Γ for $P_f = 30$ kPa	51
36	Normalized wave speed U_N versus Z_T for $P_f = 10$ kPa	52
37	Normalized wave speed U_N versus Z_T for $P_f = 20$ kPa	53
38	Normalized wave speed U_N versus Z_T for $P_f = 30$ kPa	54
39	Normalized wave speed U_N versus τ	56
40	One frame from each of the 16 detonations that have exhibited change in shape or orientation upon interaction with turbulence	58
41	Schlieren images of detonations with ethylene-oxygen turbulence at $P_s = 100$ kPa and $Z_T = 0.99$ & $Z_T = 0.2$	75

List of Tables

1	Comparison of thermodynamic efficiencies for Humphrey, Brayton, and Fickett Jacobs cycles for 3 different fuels	2
2	Schlieren setup components	17
3	Initial conditions for shock experiments	24
4	Calculated shock speeds for 6 fill pressures	25
5	Calculated shock speeds for 16 shocks interacting with turbulence through inlet 1	28
6	Calculated shock speeds for 16 shocks interacting with turbulence through inlet 2	31
7	Calculated shock speeds for 16 shocks interacting with turbulence through inlet 3	34
8	Calculated wave speeds from the schlieren images and from the ZND model, as well as the deviation of the experimentally obtained speeds from the CJ speed obtained from Cantera	39
9	Initial conditions and measured velocities for all 12 experiments	40
10	Initial conditions, calculated parameters, and measured velocities for all 99 experiments	48
11	Values of Γ for all 9 values of Z_T and 3 inlets	49
12	List of components used in the experiments	64

Chapter 1

Introduction

The intriguing structure of detonation waves, which can be described as the coupling of shock waves with exothermic chemical reactions, has been studied for over a century now with one of the primary goals being exploitation of its rapid energy release for propulsion or as a power source. Besides the first concepts that emerged over the years, it was not until the 1940s/1950s that serious consideration was placed into developing compact, lightweight, detonation-based propulsion devices [1]. Much of the focus early on was towards the fundamental concepts and experimental observations of detonation phenomena. This much later gave rise to a heightened interest of the pulsed detonation engine (PDE), the rotating detonation engine (RDE), and the oblique detonation wave engine (ODWE). Detonative propulsion concepts were popularized due to their potentially superior thermodynamic cycles in comparison to traditional constant pressure deflagrative cycles which are the basis for modern day rocket and gas turbine engines that use the well-known Brayton cycle. Practical implementations of propulsion systems inevitably involve the generation of significant levels of turbulence within the combustion chamber. Detonation-based concepts are no exception. The propagation of detonation waves is, however, usually studied for an initially quiescent, reactive mixture. There is thus a need to study the impact of turbulence on detonation propagation.

1.1 Detonative Cycles

The main difference between deflagration and detonation is that a deflagration wave propagates with a subsonic velocity and results in a decrease in density, while a detonation consists of a strong shock wave followed by the reaction front which is coupled to the leading front [2]. Figure 1 compares the P - V diagrams¹ of the ideal combustion cycles Humphrey (isochoric), Brayton-Joule (isobaric), and Fickett-Jacobs (detonation). The largest pressure increase in the compression process is noted in the Fickett-Jacobs cycle. The detonation process in this cycle is $2 \rightarrow 3$ ". A comparison of the calculated efficiency for the three cycles for three different fuels is shown in Table 1. The Fickett-Jacobs cycle yields the highest efficiency as well. This significant increase in thermodynamic efficiency in detonative cycles along with their pressure gain properties give detonation-based engines promise and more reasons to be investigated further.

¹ The scale of the vertical axis used in this graph is logarithmic, area at higher pressures corresponds to a greater amount of work.

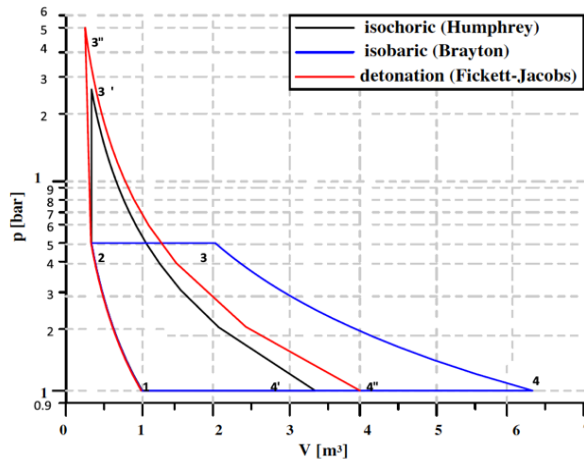


Figure 1: Comparison of P-V diagrams for Humphrey, Brayton, and Fickett-Jacobs cycles [2]. The detonation process occurs between states 2 and 3''.

Fuel	Brayton (%)	Humphrey (%)	Fickett-Jacobs (%)
Hydrogen-H ₂	36.9	54.3	59.3
Methane-CH ₄	31.4	50.5	53.2
Acetylene-C ₂ H ₂	36.9	54.1	61.4

Table 1: Comparison of thermodynamic efficiencies for Humphrey, Brayton, and Fickett-Jacobs cycles for 3 different fuels [2]

1.2 Pulse Detonation and Rotating Detonation Engines

The PDE and the RDE are the two detonation-based propulsion devices for which working, proof-of-concept lab-scale models have been realized.

A PDE is composed of a long tube (combustor) in which a detonation wave propagates axially, as shown in figure 2. One end of the tube is closed, and the other is open for exhaust. Once the tube is filled with a reactive gas mixture and the supply valves are closed, the ignition system is activated. The initiated flame rapidly transitions to detonation through a very short distance. The high pressures produced by the detonation wave are then converted to thrust. Once all the reactants have been consumed by the detonation and expanded to produce thrust, a fresh mixture is injected back into the tube to repeat the cycle. Purging with an inert gas is typically used to separate the exhaust from the fresh reactants. Therefore, one PDE cycle consists of purging, filling, detonation initiation and propagation, and blowdown [1], as shown in figure 3. The relatively long filling times limit the frequency of the engine to typically less than 100 Hz. The term “pulse” in the name is given to describe the process involved in one cycle.

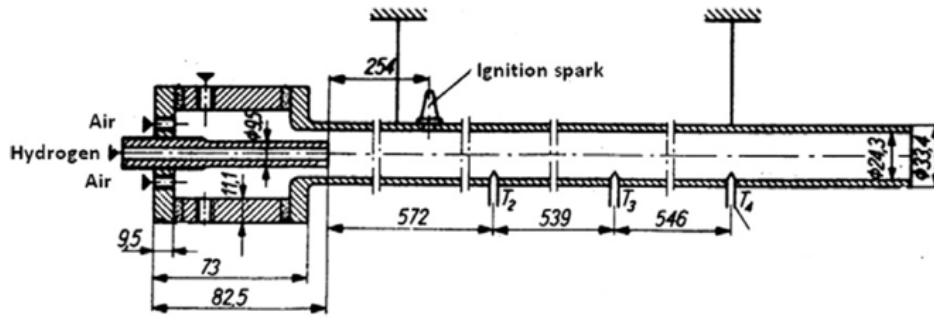


Figure 2: PDE Schematic [2]

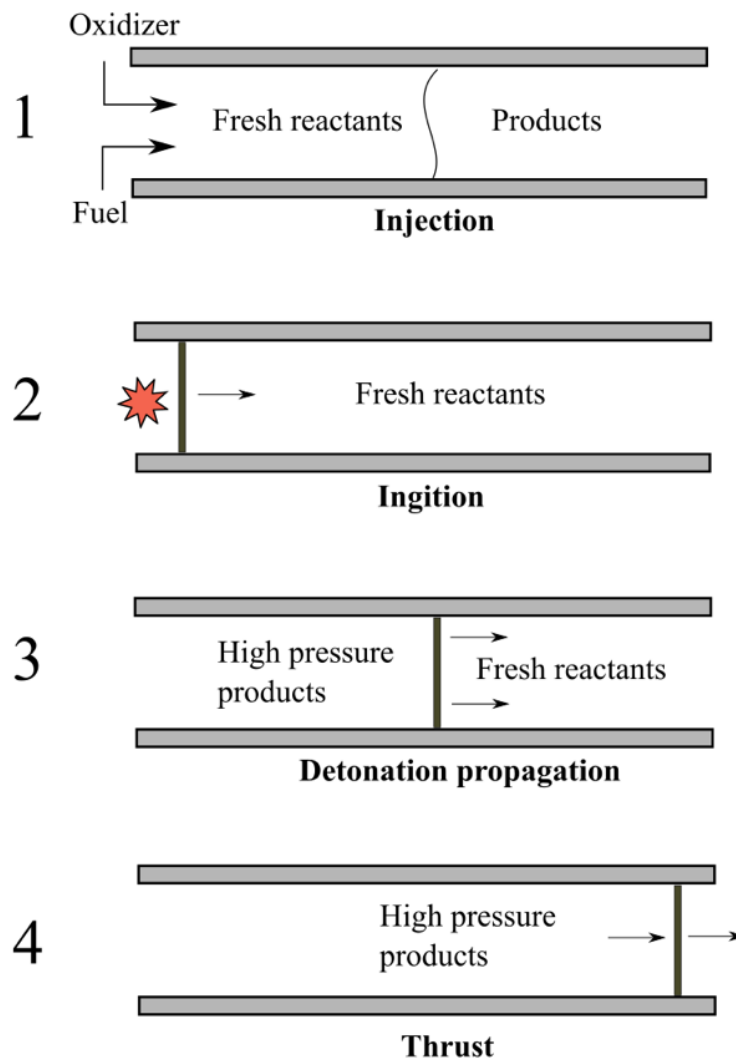


Figure 3: A schematic representing the different processes that occur in a PDE, including injection, ignition, detonation propagation, and thrust

An RDE is composed of an annular combustion chamber around which sustained detonation waves travel circumferentially, as shown in figure 4. The fuel and oxidizer are typically injected axially into the annulus, either separately (non-premixed) or premixed. As the wave (or waves) rotates around the combustor, it consumes the continuously fed reactants after which it has penetrated only a certain axial distance. In the case of non-premixed engines, the fuel and oxidizer need to be sufficiently mixed before they are consumed in order to sustain the RDE cycle. As the combustion products expand, the pressure behind the front is lowered with an expansion wave. This expansion allows the flow to naturally turn and be accelerated further through a nozzle [1]. After passage of the wave, the high pressure then decays to below that of the inlet manifold, which allows the reactants to again feed into the annulus, thereby allowing detonation waves to propagate continuously [1]. The basic flow-field of an RDE is shown in fig. 5, both in a physical cylindrical geometry and in an “unrolled” geometry where the annular combustion chamber is “cut” and the left and right boundaries of the rectangular domain are periodic boundary conditions. The blue region (a) is the fresh reactant region into which the detonation wave is propagating. Typical frequencies of RDEs are in the range of 1-10 kHz due to the very high rotational speed of the wave.

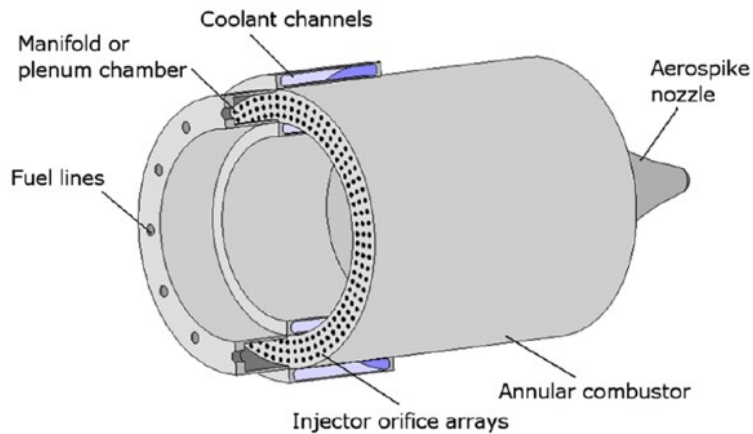


Figure 4: Schematic of a typical RDE showing its essential components [1]

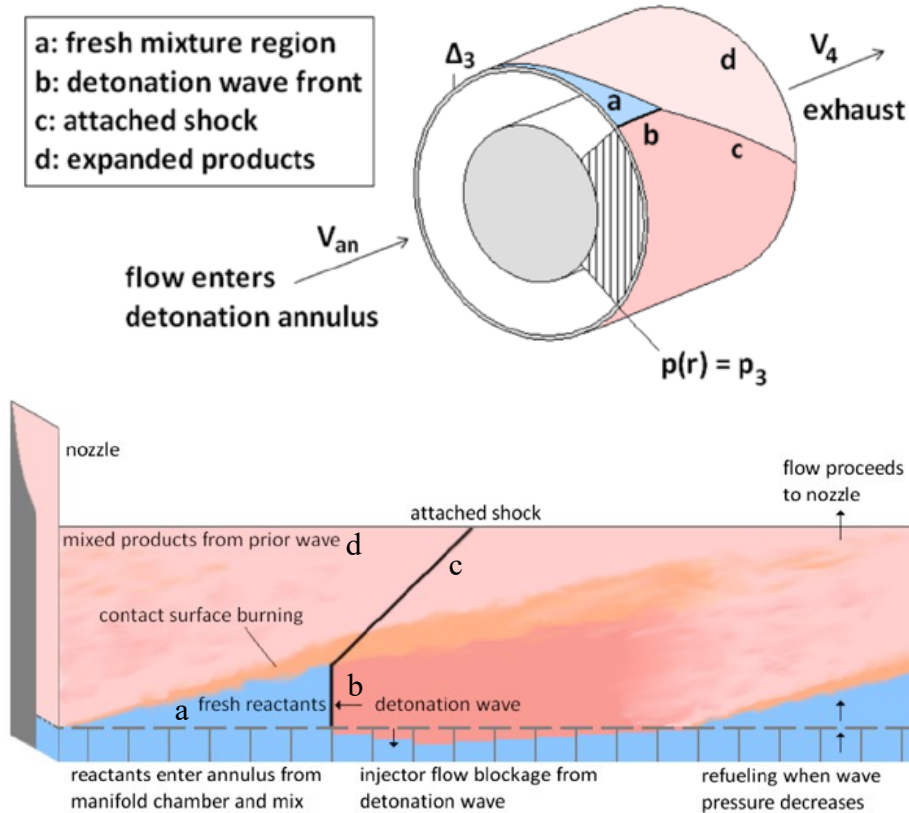


Figure 5: A schematic showing the different regions of the RDE's flow field, in the engine (top) and in an unwrapped version of the engine (bottom) [1]

Due to the unsteady cyclic nature of a PDE, ignition of reactants is done at the start of every pulse, which puts a heavy demand on the ignition system. Additionally, and possibly more importantly, the entirely unsteady nature of the PDE means there is no frame of reference in which the exhaust flow is steady. As a result, there is no known nozzle design that can optimize the thrust of the device. The lack of a realizable nozzle implies a severe loss of propulsion efficiency from the losses in the expansion. In an RDE, on the other hand, ignition is needed only once, as the wave sustains itself so long as reactants are continuously being fed into the chamber. The flow is also potentially quasi-steady as the unsteadiness stems from constant, rotational wave motion. As a result, the expansion is much more likely to be optimizable. The higher operable frequencies of RDEs allow for the use of higher reactant mass flow rates. PDEs induce more noise and vibration than RDEs due to their unsteady nature. All the mentioned advantages of RDEs offer a more compact, light-weight, and simple design of the ignition system and combustor. RDEs therefore have more potential than PDEs to replace traditional deflagration-based engines.

1.3 Detonation-Turbulence Interaction

The primary concern with the RDE is to ensure that the established detonation waves that circle the annular detonation chamber are stable, sustainable and controllable, and to prevent them from

degenerating into deflagration waves [1]. The relatively large pressure ratio (usually between 2-4) between the injector manifold and the annulus means that the axially injected reactants are highly turbulent jets, consequently leading to the inevitable interaction of the detonation wave in cross-flow with turbulence. While turbulence is inherently present within the structure of a detonation (see for example [3]), the addition of a turbulent flow ahead of the wave is still not well understood. The study of the interaction between detonation waves and turbulence is relatively recent, starting in earnest in the early 1990s with the analytical works of Jackson, Kapila, Hussaini, Lasseigne and Ribner [4–6]. The distinction is being made here between the study of a detonation interacting with a “disturbed turbulent flow field” as would be the case for isotropic turbulence, and the study of the interaction of a detonation wave with a single disturbance such as an obstacle, or an interaction with a flow perturbation of a single wavelength, such as sinusoidal density perturbations in a reactive medium. Other researchers who have studied the interaction of detonations with turbulence have done so using numerical simulations [7–12]. Semi-analytical and linearized approaches have also been employed [13–16]. No experimental examination of the interaction of a detonation wave with a distributed, turbulent field could be identified. A good understanding of detonation-turbulence interaction is needed to ensure suitable design of injector orifice, wave stability, and sustainability. This study aims to provide a macroscopic analysis of the impact a turbulent flow-field has on the speed of a detonation wave.

The following questions were raised and discussed: What characteristics should the turbulence have in order to impact the incoming detonation? At what level of turbulence do we begin to see an impact on detonation dynamics?

Before examining detonation-turbulence interactions, though, it is good to first have an understanding of how turbulence affects non-reactive shock waves. Detonation-turbulence differs from shock-turbulence interaction due to exothermicity, the presence of its structure’s length scale, and the intrinsic fluctuations in the unstable detonation front [9]. Previous experimental and numerical investigations have observed that a shock wave can exhibit substantial unsteadiness and deformation as a result of its interaction with turbulence [17].

Chapter 2 covers an overview of the basic theory of detonation. Chapter 3 covers the experimental setup and diagnostics used. Chapter 4 summarizes the results obtained in the experiments of shock waves in air. Chapter 5 summarizes the results obtained in the experiments of detonation waves in stoichiometric ethylene-oxygen. Finally, Chapter 6 outlines the main conclusions and future improvements required.

Chapter 2

Detonation Theory

Detonation waves are composed of shock waves that are sustained by the chemical energy release in the highly compressed explosive medium behind them. A detonation is composed of a strong shock wave followed by a reaction front which propagates with supersonic velocity, on the order of km/s. The products of a detonation wave have a higher density and pressure than the reactants. The extremely high temperatures and pressures produced by the passage of the wave provide huge thermodynamic potential for propulsion and power generation applications. The detonation process involves complex interactions between reactive chemical dynamics and fluid dynamics [18].

The well-known works of Chapman [19] and Jouguet [20], the Chapman-Jouguet (CJ) theory, first calculated the easily observable, global parameters such as the natural detonation propagation velocity, post wave pressure, temperature, etc. These thermodynamic parameters are known to be mostly independent of the actual structure of the detonation wave and each subsequent model of the detonation structure must reconcile itself with those thermodynamic parameters. The first model of the detonation structure, the one-dimensional Zel'dovich, von Neumann, Döring (ZND) model [21] is both consistent with the CJ theory and remains today the only easily computable theory of detonation structure. Length scales encountered in this model, for example the half-reaction zone length, are still widely used to scale detonation parameters such as the detonation cell size, the hydrodynamic thickness, the critical tube diameter, etc. This reliance on the ZND model persists despite it being well known since the late 1950s that the internal detonation structure is not one dimensional [22–24]. Multi-dimensional detonations are in fact composed of a complex of lead shocks, normal to the wave's propagation direction, and transverse shock waves travelling perpendicularly to the wave's path and all participate in the establishment of the detonation structure. The detonation cell size, the spacing between consecutive transverse waves, and the hydrodynamic thickness - the physical extent of the zone of influence of chemical reaction on the lead shock structure - have been recognized as the fundamental length scales in the multidimensional detonation structure.

2.1 Chapman-Jouguet Theory

Detonations can be thought of as a thermodynamic path that transforms the unreacted explosive into stable products at the CJ state, which is a steady chemical equilibrium state that conserves mass, momentum, and energy [25]. The CJ speed is defined as the minimum speed that a wave can attain while remaining consistent with the governing conservation laws.

A detonation wave is thus a self-propagating shock wave whose energy is supplied by the chemical reaction of the reactive material [25]. The fundamental equations that describe the steady

propagation of a detonation wave can best be derived using the classical example of a fluid in a semi-infinite cylinder compressed by a piston, shown in figure 6, moving with constant velocity, with the piston analogous to the compression caused by the detonation products produced behind the shock front [25]. Proper analysis and combination of the mass, momentum, and energy conservation equations gives us:

$$P - P_0 = \rho_0^2 D^2 (v_0 - v) \quad (1)$$

$$E - E_0 = \frac{1}{2} (P + P_0) (v_0 - v) \quad (2)$$

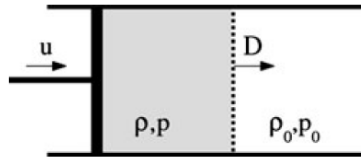


Figure 6: Piston-cylinder example used to explain detonation wave propagation [25]

Equation 1 is called the Rayleigh line, which expresses the linear relationship between the pressure P and specific volume v of the wave for a given velocity D . Equation 2 is called the Hugoniot relation, which expresses the energy E of the product as a function of its pressure and specific volume. This relation, along with the thermodynamic function $E = E(v, P, y)$ yield the Hugoniot curve which incorporates all thermodynamic states that can be reached by detonating a material from its initial state (P_0, v_0, y_0) , where y_0 and y are the reaction progress variables at the initial and final states, respectively. For any shock velocity, D , the product pressure and specific volume can be found at the intersection of the Rayleigh line with the Hugoniot curve, since mass, momentum, and energy must always be conserved.

Not all intersections between the Rayleigh line and Hugoniot curve correspond to stable detonation waves. The two main criteria that determine the stability of a wave are $D > c_0$ and $|D - u| < c$, where c_0 and c are the speeds of sound for the undisturbed and shocked fluids respectively [25]. The first inequality implies that the speed of the propagating wave must be faster than the speed of sound in the undisturbed medium, which is what defines a shock wave. The second inequality implies that sound waves from the piston should be able to reach the wave in order to provide it with the energy required to sustain its propagation [25].

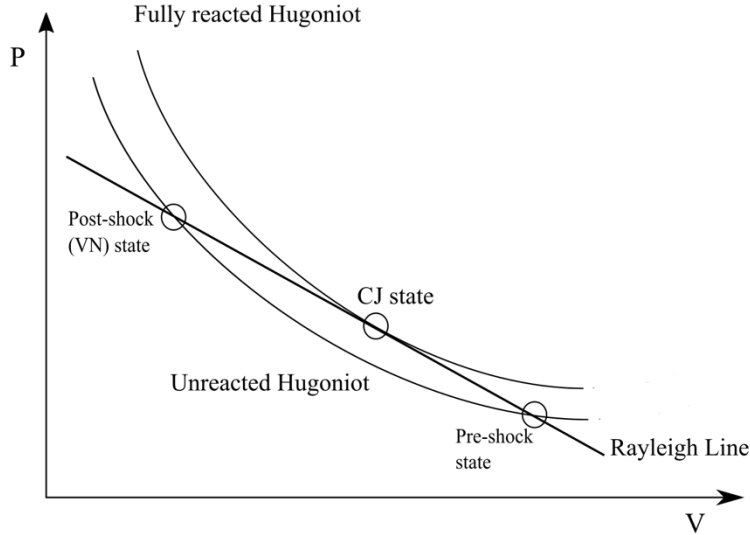


Figure 7: P - V diagram showing the Rayleigh line, reacted, and unreacted Hugoniot curves

In the CJ model, the transformation of reactants to products at the CJ state can be thought of as occurring through an infinitesimally thin surface and hence the reaction reaches completion instantly. The detonation products reach thermodynamic equilibrium and their properties can be calculated using standard thermodynamics. The unreacted Hugoniot curve is the set of possible post-shock states for shock waves of different velocities. The fully reacted Hugoniot is the set of possible end states with combustion, i.e. the high pressure state that consists of burnt products. Consequently, this curve does not pass through the initial state (P_0, v_0) . The CJ theory assumes that a self-sustained detonation occurs when the Rayleigh line is tangent to the shock Hugoniot [25]. The tangent point is a sonic point as the flow velocity in the wave frame of reference equals the local equilibrium sound speed. Since any other intersections of the Rayleigh line with the Hugoniot curve are above the tangent line, the CJ detonation wave is the slowest supersonic wave that can transform an explosive into equilibrated products [25]. This minimum velocity wave is the kind normally encountered experimentally. Figure 7 is a P - V diagram showing the Rayleigh line, reacted, and unreacted Hugoniot curves.

2.2 ZND Model and Detonation Structure

Analysis of the detonation structure of a wave is necessary for understanding its dynamics and limits of propagation. The issue of defining detonability limits naturally leads to an investigation of the reaction zone length [26]. The solutions obtained from applying the CJ criterion will relatively accurately predict the detonation velocity and the product thermodynamic state so long as the wave propagates within its detonability limits with minimal losses, but will not provide any information about whether or not the wave will initiate or fail under different conditions.

The main assumption of the Zeldovich-von Neumann Döring (ZND) model, a one-dimensional model of the structure of a detonation wave, is that the shock initially raises the pressure and temperature of the incoming reactants without changing the chemical composition; the state is said

to be “frozen” across the leading shock front, and is often called the von Neumann state [26]. This assumption stems from the fact that shock waves are almost infinitesimally thin and that the chemical reaction occurs extremely fast. The post-shock flow then reacts to reach the final equilibrium state obtained by the CJ solution. Figure 8 summarizes the ZND structure of a detonation wave travelling through a gaseous mixture at atmospheric conditions.

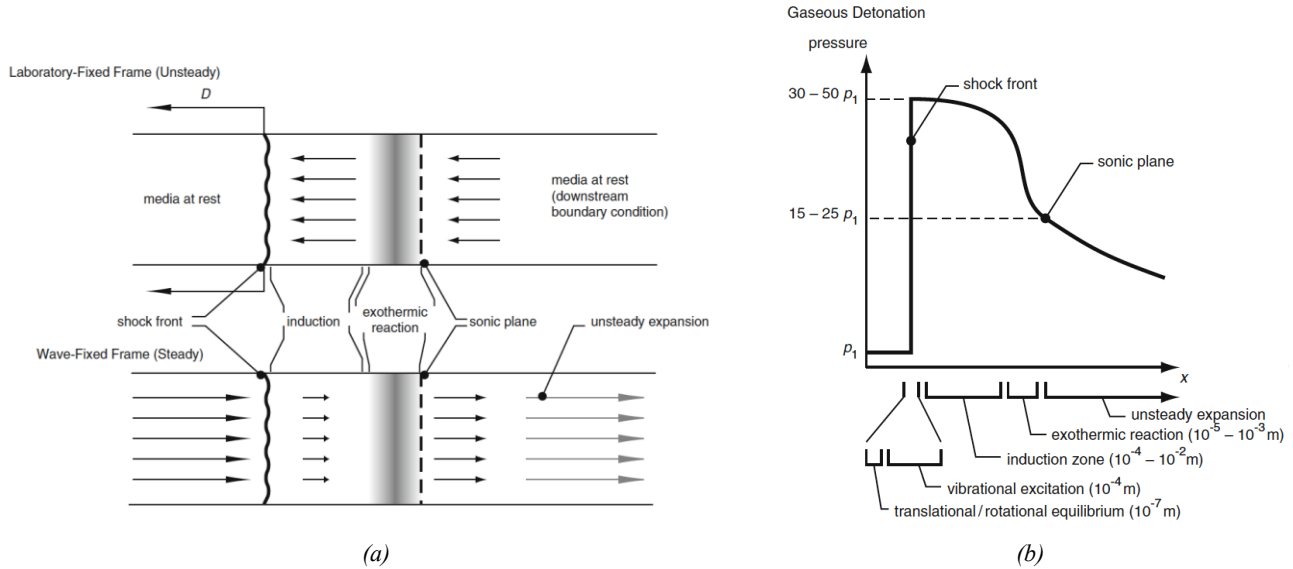


Figure 8: (a) Schematic of ZND structure of gaseous detonation and (b) pressure profile of the structure [26]

2.3 Detonation Cell Size

Detonation dynamic parameters of detonations are ones that characterize its dynamic behavior, and they include detonation cell size, critical initiation energy, and critical diameter [27]. This section discusses the parameter that is most relevant to this study: the detonation cell size.

The one-dimensional ZND model does not accurately capture the true, multidimensional nature of detonation waves. The detonation front is not smooth. Instead, the lead shock is made of several, intersecting shocks. Further shock waves travel perpendicular to the direction of propagation of the detonation. Where the transverse waves intersect the lead shock, we find the triple points: the location of intense reaction and vorticity. Figure 9 outlines the ideal structure of a detonation cell.

When observed at high speed using specialized techniques such as schlieren photography, the multidimensional structure is revealed, such as in figure 10, which shows the reaction zone structures of a diluted hydrogen-oxygen mixture in a channel with smooth walls (a) and of a propane-oxygen mixture in a channel with solid walls (b). The clearly visible periodic transverse waves characterize a regular cellular structure in the channel with smooth walls. The fine wrinkles in the solid wall channel characterize the structure as irregular and are associated with unburned pockets at the front [28].

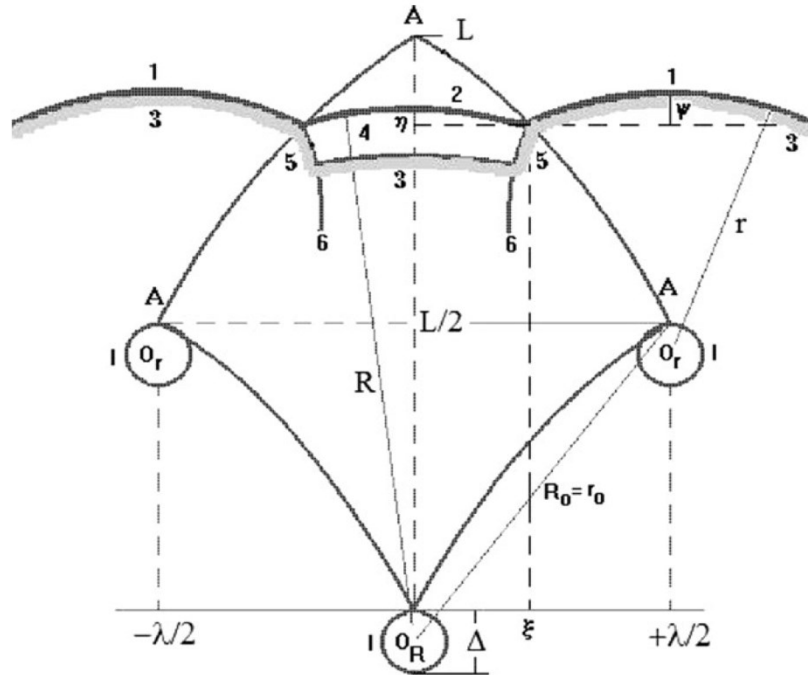
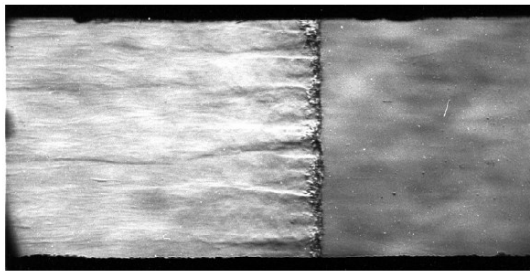
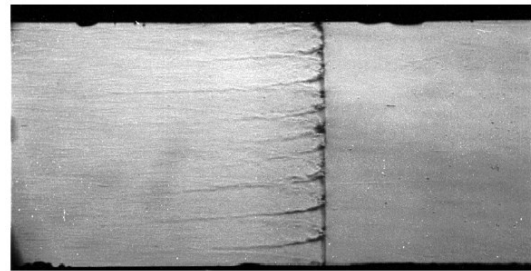


Figure 9: Ideal structure of a detonation cell: I, region of transverse wave collision; 1 and 2, shock fronts; 3, flame fronts; 4, induction zone; 5, transverse waves; 6, tail of transverse wave; R and r, radius of shock waves produced by neighboring I regions [27]



(a)



(b)

Figure 10: Schlieren photos of the detonation structure of (a) $C_3H_8 + 5O_2$ at an initial pressure of 5.6 kPa in the solid section of a channel and (b) $2H_2 + O_2 + 40\%Ar$ at an initial pressure of 13 kPa in the smooth section of a channel [28]

The spacing between two consecutive transverse waves is referred to as the cell width or cell size with “cell” referring to the fish-scale like pattern etched by detonations in soot foils, as shown in figure 11 below. Soot foils are the commonly used method to experimentally determine the cell size, and the resulting pattern is imprinted on the foil allowing for the cells to be measured using a ruler. In order to reduce the uncertainties induced by the inherent irregularity of some of the mixtures, a 2D Fourier analysis is sometimes conducted on a digital image of the film in order to capture the dominant frequencies in the pattern.

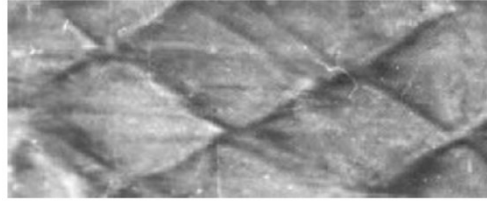


Figure 11: A soot imprint of the cellular structure of a detonation wave [27]

The basic cellular pattern is as follows. The origin apex of the cell O_R , corresponds to the location of two transverse waves colliding. In the first half of the cell, a strong shock is expanding. Reactions are triggered promptly by the shock compression and energy is released. In the second half of the cell, the “shrinking” part, the shock is weaker and can decouple. In this case, the reaction front lags and the shocked yet unburned material may be prompted to react by transverse wave compression, turbulent mixing with hot material, etc. This basic dynamic process occurs in all detonations. When lowering the initial pressure, the cell size enlarges, but the process remains. The cell size is therefore an intrinsic property of a detonation wave that depends on the species of fuel and oxidizer involved in the mixture, fuel-oxidizer ratio, percentage dilution, pressure, temperature, etc.

Figure 12 shows the variation of the cell size versus initial pressure for an ethylene-oxygen mixture diluted in argon. The solid line is data calculated using an analytical model, and the remaining points are previously gathered experimental data.

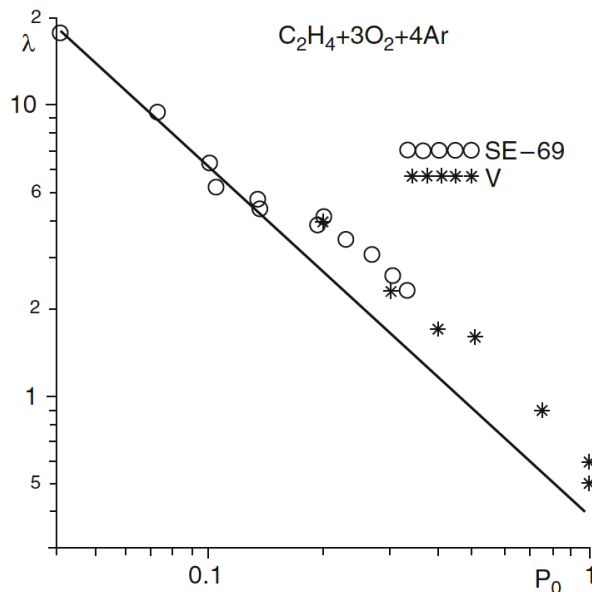


Figure 12: Cell size vs initial pressure for an ethylene-oxygen mixture diluted in argon [27]

2.4 Propagation Limits and Cell Size

Through the years, several experiments have been performed to understand the cellular nature of detonation waves and its impact on the dynamics of those waves. In the critical tube experiment, a detonation travelling in a tube of diameter D emerges into a much larger space. Successful transmission into the unconfined space occurs only for large enough values of the ratio D/λ . That is to say, a minimum number of cells must be present across the donor tube for successful transmission [29]. Several detonation-obstacle interactions have also been studied: detonations interacting with perforated plates [30], with arrays of solid, cylindrical tubes [31], with beads and arrays of beads [32], with porous walls [28] among others. In all cases, the profound influence of the cell size on the ensuing behavior was remarked.

Chapter 3

Experimental Setup

In this work, we employ a 2 meter long, horizontally mounted, detonation tube with a square cross section of 3.81 cm by 6.35 cm and optical access at one end. Solenoid valves are controlled through an arduino-based control system to inject a jet of air or reactive mixture. The gases are injected through one of two inlets. One inlet is located near the initiation location and serves for traditional, slow injection of gases. The second inlet is located near or in the optical section and can be moved between experiments. The use of two injection ports allows the study of waves in atmospheres that have been disturbed by turbulence. A detonation (or shock) is initiated promptly via a high power ignition system in a medium of uniform, detonable mixture (or air in the case of shock analysis, since shock waves propagate in non-reactive mediums). A schlieren visualization system allows the imaging of the detonation front as it passes through the optically clear section.

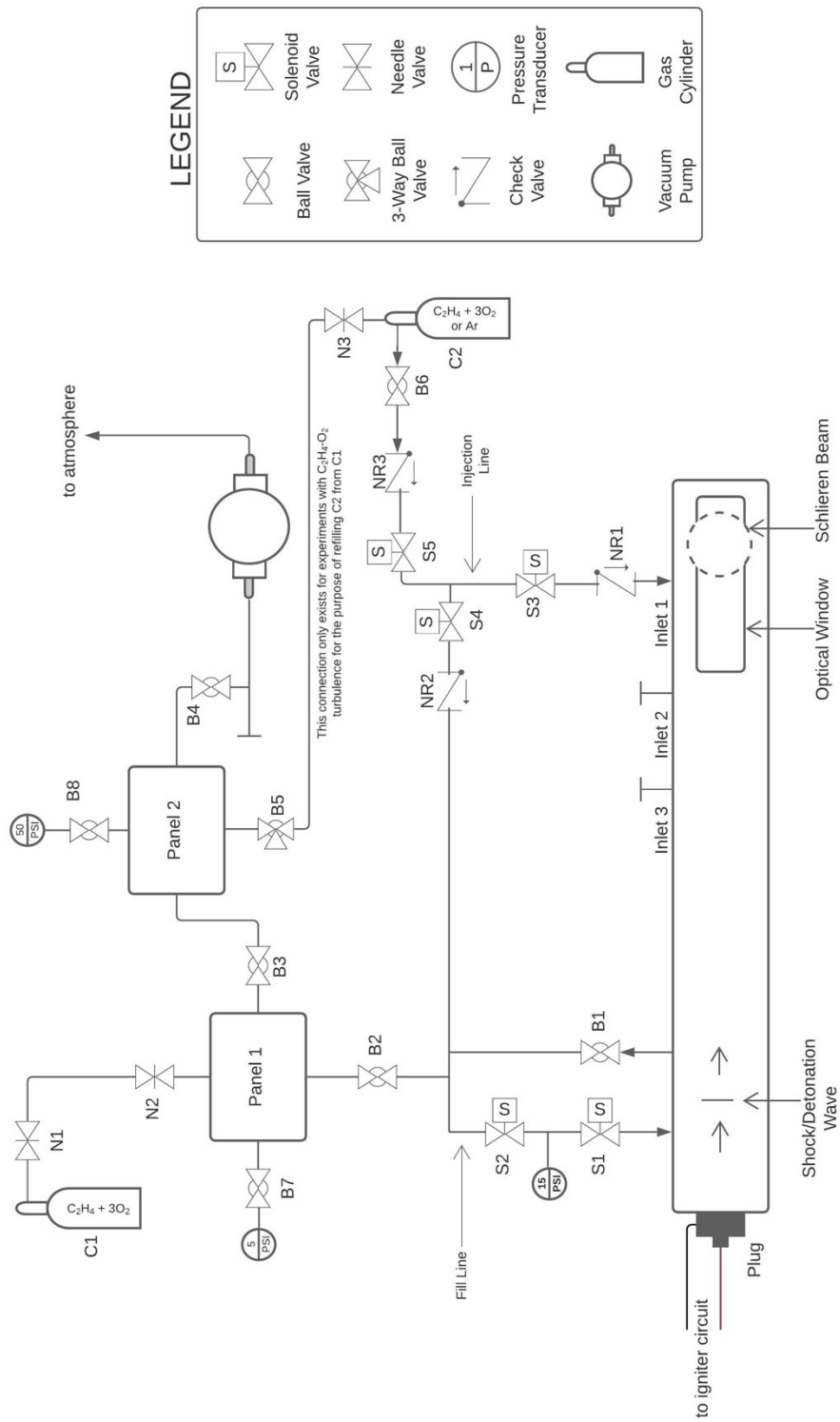


Figure 13: Shock tube setup diagram

The following experiments were conducted in this study:

- 1- Shock waves propagating in quiescent air: In quiescent air, shocks (more specifically blast waves), are generated by the discharge of the igniter. Their propagation are observed.
- 2- Shock-turbulence interaction: The tube is prefilled with quiescent air. A rapid injection is performed through the downstream port, leading to the generation of a turbulent atmosphere inside the tube. Shocks are generated by electrical discharge and their propagation is observed.
- 3- Detonation waves in a quiescent reactive medium: In a quiescent, reactive medium of stoichiometric ethylene-oxygen, a rapidly initiated detonation wave is imaged and observed.
- 4- Detonation-turbulence interaction (non-reactive): The tube is prefilled with a quiescent, reactive medium of stoichiometric ethylene-oxygen. A rapid injection of a non-reactive gas, argon, is performed and a detonation wave is subsequently observed as it propagates in the tube.
- 5- Detonation-turbulence interaction (reactive): The tube is prefilled with a quiescent, reactive medium of stoichiometric ethylene-oxygen. A rapid injection of the reactive gas is performed, leading to the establishment of a turbulent flow field inside a chemically homogeneous and reactive gas. A detonation is promptly initiated and its propagation through the turbulent atmosphere is observed.

Figure 13 shows the setup diagram used for those experiments. The test procedures for each of the 5 sets of experiments are outlined in appendices A3 and A4, as well as the list of components with their corresponding part numbers and manufacturers.

3.1 Injection and Filling

The turbulent jet is injected through a 3/8" inlet located at the top of the tube. Three inlets are used to inject turbulence, and one to slowly fill. The reason for the three inlets is to study the effect of interaction time between the incoming wave and the generated turbulence. Inlet 1 is located right at the beginning of the schlieren field of view. Inlet 2 is located 38.1 cm upstream of the start of the schlieren beam. Inlet 3 is 63.5 cm upstream of the beam.

The basic injection procedure is to:

- 1- Evacuate the tube to vacuum.
- 2- Manually inject the desired medium inside the tube to an intermediate pressure.
- 3- Initiate the Arduino-controlled procedure that:
 - a. Injects the second gas (which may or may not be different from the first gas) to create a turbulent atmosphere with the desired chemical composition.
 - b. Close all valves to isolate the tube from the manifold.
 - c. Evacuate the manifold to a low pressure and prevent shocks and detonation waves from propagating in the manifold and the fill tanks.
 - d. Trigger the high speed camera.
 - e. Trigger the igniter circuit.

The specific timings and procedures can be found in appendices A3 and A4.

The purpose of each of the valves installed on the manifold, as well as the sensors used in the setup, is described below. Referring to figure 14:

- 1- The purpose of check valves NR1, NR2, and NR3 is to prevent any undesired flow up the inlet or across the manifold in case the pressure downstream of the valves is higher than that upstream.
- 2- The purpose of S1 and S2 is to isolate the tube from the 15 psi sensor and from the panels when required. This is needed to prevent damage to the sensors and equipment.
- 3- The purpose of S3 is to control the injection of the jet.
- 4- The purpose of S4 is to evacuate the injection and fill lines before triggering a detonation.
- 5- The purpose of S5 is to isolate C2 from the tube and manifold when required, and serves as an extra protection from potential detonation waves propagating back into the cylinder.
- 6- The purpose of B1 is to manually fill the tube with air during the shock experiments, and to manually evacuate the tube from the products after detonation experiments.
- 7- A 15 psi (or 30 psi during shock experiments) sensor was installed between valves S1 and S2 to monitor the pressure in the tube during injection in detonation experiments.
- 8- A 5 psi sensor was installed on Panel 1 during all experiments to monitor the pressure during the filling process.
- 9- A 50 psi sensor was installed on Panel 2 to monitor and set the supply pressure in cylinder C2 during its filling.

3.2 Schlieren Diagnostics

The diagnostic used to visualize processes in the shock tube viewing section is schlieren optical diagnostics. Schlieren, named after the German word “schliere”, which means “streaks”, refers to gradient disturbances of inhomogeneous transparent media which bend light rays in directions other than the normal. A schlieren setup is built by integrating high quality lenses in a system to detect small differences in the refractive index of the medium, caused by variations in temperature, pressure, and density. A Z-type schlieren system was used. The components of the system are listed in table 2 and the schlieren setup diagram is shown in figure 14. The procedure used to set the system is outlined in appendix A2.

Description	Manufacturer
Two spherical concave mirrors of aperture 6”, and focal length 48” – giving them an f-number of f/8.	Aerolab
LS 150 Light Source with an embedded 1” diameter condenser and 1” diameter converging lens, of f-numbers f/1 and f/5 respectively	Abet Technologies
A slit and a knife edge	Aerolab
Two square 30 cm x 30 cm flat first surface mirrors for the purpose of folding the system and minimizing space	Edmund Optics
A high speed camera, FASTCAM SA1.1 RV, connected to a PC to record the schlieren image.	Fastcam

Table 2: Schlieren setup components

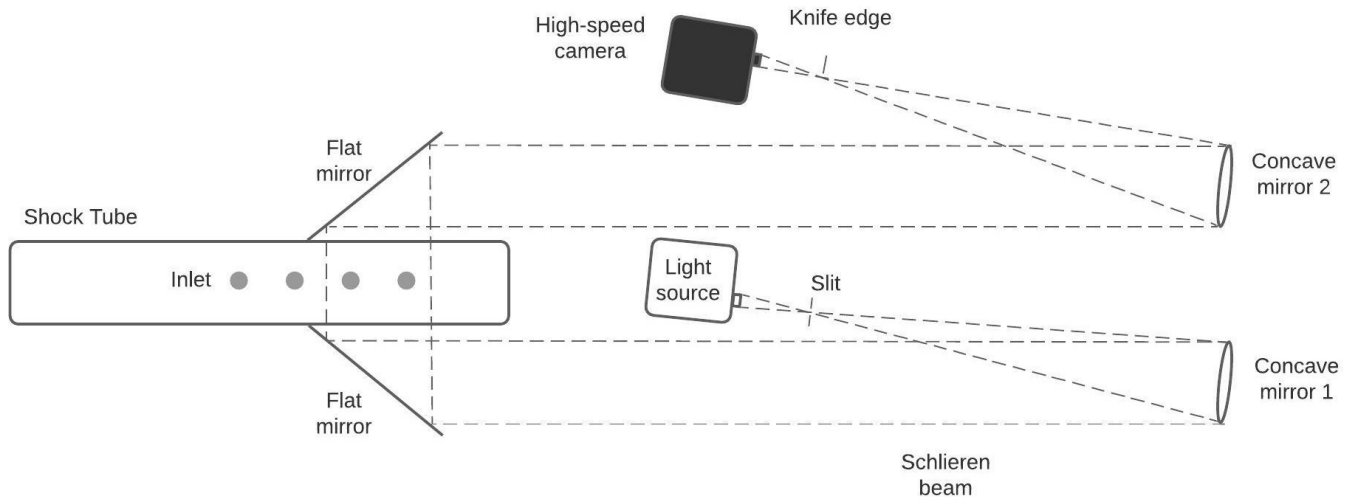


Figure 14: Z-Type schlieren setup diagram

3.3 Vacuum System

Since our test pressures are below atmospheric, the shock tube is to be evacuated to reach those pressures. This is done through the tapping point on the far left of the tube, shown in figure 14. A two-stage EDWARDS RV-5 rotary vane vacuum pump is used and an evacuation hose that connects the outlet of the pump to the outside atmosphere is connected to an evacuation motor to provide suction. Before conducting the experiment, a leak test is to be performed to ensure that all joints are tightened and the tube is ready to be filled. The achieved leak rate is an average of 0.15 kPa/min when the tube is at a pressure of 1 kPa.

3.4 Ignition System

The ignition system is a capacitive discharge igniter. The total capacitance of the system is 0.4 μF , and the typical voltage used is 16-16.5 kV. This gives a stored energy of roughly $E = \frac{1}{2}CV^2 = 54.45 \text{ J}$ at a charge of 16.5 kV. The igniter is triggered by a TM-11A 30kV EG&G trigger module connected to an air-gap switch and the capacitor bank is built of 4 individual EC104-30M (0.1 μF , 30kV max) capacitors in parallel. The system is self-discharging through a high value resistance ladder so it cannot be left charged unattended. It is also equipped with a manual shunt that, when closed, prevents charging from electrostatic or other stray sources, allowing the system to be left unattended for long periods of time. This high energy igniter makes it possible to directly initiate detonation waves in a combustible mixture. It also has enough energy to be used to create a blast wave in a non-reactive mixture. All blast waves and detonation waves were fired at a voltage of 16.5 kV. The igniter circuit diagram is shown in figure 15.

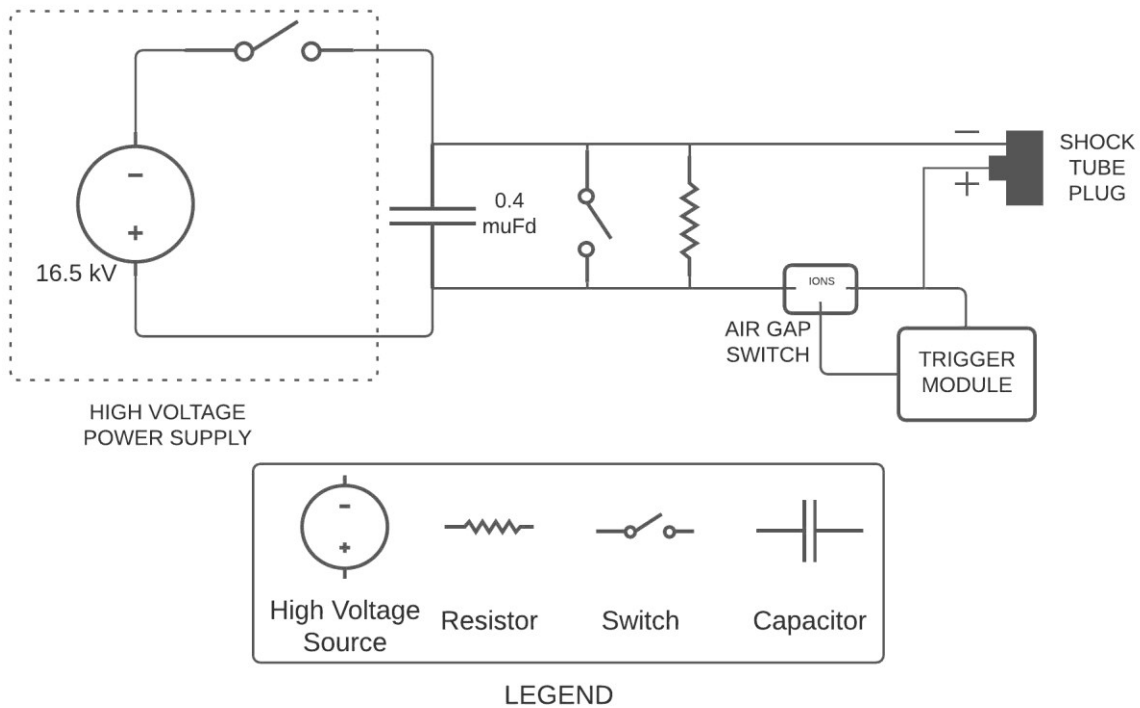


Figure 15: Igniter circuit diagram

3.5 Arduino Control System

The characteristics of the turbulence inside the tube are controlled by varying (i) the pressure of the gas injected rapidly and (ii) the duration of injection. Since turbulent motion dissipates through diffusion, it is necessary to accurately and reproducibly time the gas injection and minimize the amount of time elapsed between the end of the injection process and the shock/detonation process. It was also found that it is critical to evacuate the manifold properly, especially for reactive experiments, to prevent the propagation of compressive waves in conduits leading to sensing equipment and storage tanks. To this end, an Arduino Mega is used to control the sequence of operations followed in the experiments, including valve actuation, pressure readings, ignition, and camera triggering. The circuit diagram for the control system is shown in figure 16. Signals are sent to the Arduino using a green button and a red button, shown in figure 16 as switches. The Arduino codes used for the shock and detonation experiments are included in appendix A6 where the sequence of operations is outlined.

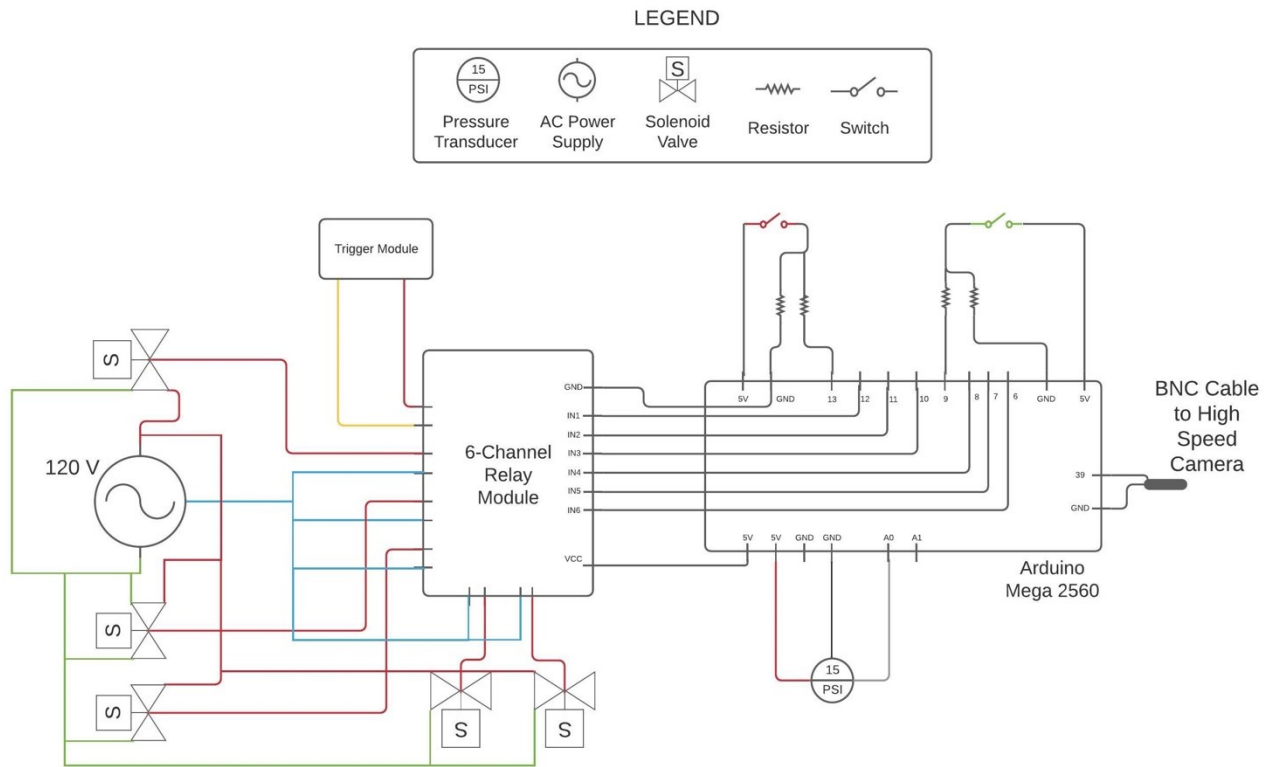


Figure 16: Control system circuit diagram

Chapter 4

Shock-Turbulence Interaction

Initial experiments involve non-reactive phenomena. The production of a turbulent atmosphere is tested and its impact on the propagation of a non-reactive wave is used to qualitatively assess the magnitude or impact of the turbulence generated under different conditions.

4.1 Injection Characteristics

4.1.1 Jet Dynamics

The parameters governing the degree of turbulence generated are the initial supply pressure of the injected gas P_s , the initial pressure in the tube P_i , and the duration of the injection t_{inj} . Various supply pressures were coupled with different injection times to determine which initial conditions actually had an impact on the incoming shocks and detonations. The different impacts expected include change in average wave speed across the camera's field of view, fluctuations in instantaneous velocities, and orientation of the wave.

Before choosing any initial conditions, it is important to check what pressure ratio, or values of P_s and P_i , will generate a turbulent jet. P_i is the initial pressure in the shock tube before jet injection. A jet is considered turbulent if the associated Reynold's number is above 2000 [33].

$$Re = \frac{\rho_j U_j D}{\mu} > 2000 \quad (3)$$

Since the flow is compressible, we can use the isentropic flow relations to determine the fluid conditions under steady-state, quasi-1D assumptions.

$$PR_i = \frac{P_s}{P_i} = \left(\frac{T_s}{T_j}\right)^{\frac{\gamma}{\gamma-1}} = \left(\frac{\rho_s}{\rho_j}\right)^{\gamma} = \left(1 + \frac{\gamma-1}{2} M^2\right)^{\frac{1-\gamma}{\gamma}} \quad (4)$$

The subscript “s” stands for supply and denotes the stagnation conditions. The subscript “j” stands for jet.

From the steady, first law of thermodynamics, the jet velocity and specific enthalpy are related through

$$h_s = h_j + \frac{U_j^2}{2} \quad (5)$$

or, assuming a perfect gas

$$U_j = \sqrt{2C_p(T_s - T_j)} = \sqrt{2C_p T_s \left(1 - \frac{T_j}{T_s}\right)} \quad (6)$$

This leads to

$$\frac{DP_s}{\mu RT_s} \frac{\sqrt{2C_p T_s (PR_i^{\frac{\gamma-1}{\gamma}} - 1)}}{PR_i^{\frac{\gamma+1}{2\gamma}}} > 2000 \quad (7)$$

Examining equations 3-7 tells us that for a supply pressure of 3 kPa and a pressure ratio of 1.11, $Re = 2065$. In actual experiments, higher supply pressure and pressure ratios are used, leading to the establishment of clearly turbulent jets.

4.1.2 Characterizing Turbulence

The eddy currents and vortices generated in turbulent flows cause irregular fluctuations in the flow's instantaneous pressure and velocity components, as depicted in figure 17. Any instantaneous parameter can be written as the sum of a mean term (denoted by a bar on top of the letter) and a fluctuating term. For instance, the instantaneous velocity component $u(t)$ becomes

$$u(t) = \bar{u} + u'(t) \quad (8)$$

where $u'(t)$ is the term that accounts for the fluctuations. Expression (8) is commonly known as the Reynold's decomposition, and when applied to the equations of motion, the Reynold's equations are derived. The degree of turbulence is usually characterized by the kinetic energy (per unit mass) of the velocity fluctuations, e , and turbulence intensity, i , which is defined as the ratio of the root mean square of the velocity fluctuation term $u'(t)$ to the mean velocity \bar{u} :

$$e = \frac{1}{2} u_{rms}^2 \quad (9)$$

$$i = \frac{u_{rms}}{\bar{u}} \quad (10)$$

where $u_{rms} = \sqrt{\overline{u'(t)^2}}$.

The results of turbulence simulations are typically in the form of equations 9 and 10.

Figure 18 shows an example of a free turbulent jet exiting a confined space and expanding into an unconfined one.

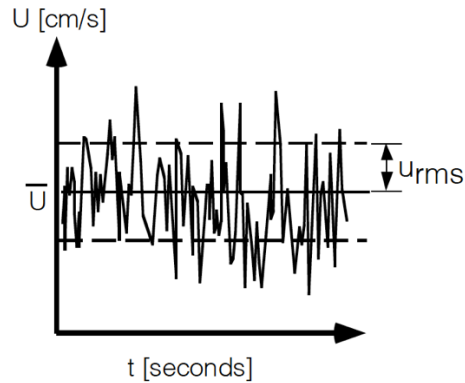


Figure 17: Velocity vs time graph describing a turbulent flow-field

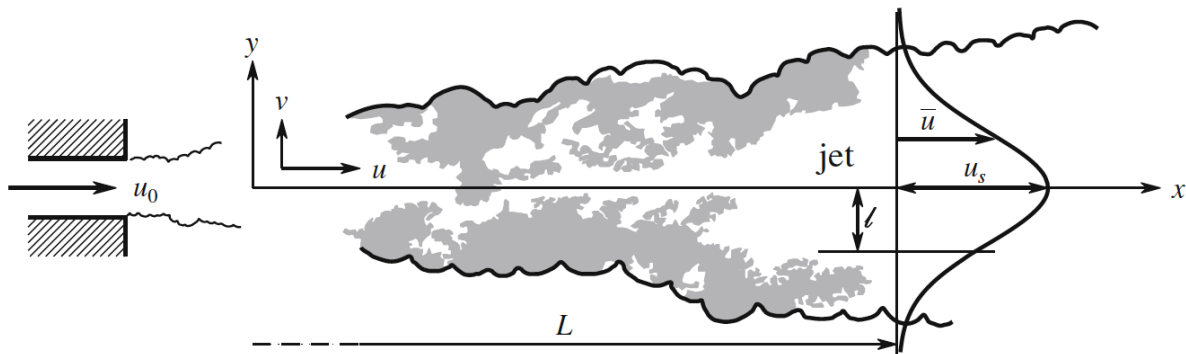


Figure 18: Example of a free turbulent jet [16]

4.2 Initial Conditions

A total of 54 experiments were fired for the case of shocks in air – 6 without turbulence, and 48 with turbulence present.

Shocks were first sent through an undisturbed medium of air at 6 different fill pressures: 50 kPa, 75 kPa, 100 kPa, 135 kPa, 169 kPa, 200 kPa. Those shocks are indeed weak blast waves generated by a spark discharge. The range of Mach numbers of the shock waves encountered in this experiment is $1.06 \rightarrow 1.16$.

For interaction of shocks in air with turbulence, two supply pressures were chosen, 150 kPa and 200 kPa absolute. The supply pressures are constant here as the shop air line is regulated. For each supply pressure, a shock was initiated at two different fill pressures, each with four corresponding

injection times and initial pressures, P_i , before injection. P_i was approximated (using a measured average of rate of increase in pressure due to the jet) from arbitrarily chosen injection times that had previously either shown no impact or had shown impact on the wave. The approximated initial pressures were then used as a starting point, and were slowly reached by manually operating the vacuum valve. The final fill pressure, P_f , was controlled by the Arduino, and a corresponding injection time was measured for each experiment.

Below is a table of the initial conditions with which the shock-turbulence experiments were conducted. In all cases, the jet was injected through inlet 1.

P_s (kPa)	No.	$PR_i = P_s/P_i$	$PR_f = P_s/P_f$	P_i (kPa)	t_{inj} (s)	P_f (kPa)
150	1	4.2	3	35.35	0.505	50
	2	6.6	3	22.83	0.984	50
	3	14.5	3	10.32	1.561	50
	4	71.1	3	2.11	1.891	50
	5	1.8	1.5	84.12	0.67	100
	6	2.1	1.5	73	1.121	100
	7	2.5	1.5	60.24	1.63	100
	8	3.3	1.5	45.58	2.242	100
200	9	4.9	4	40.78	0.223	50
	10	6.6	4	30.16	0.508	50
	11	14.6	4	13.74	0.986	50
	12	80.3	4	2.49	1.341	50
	13	2.5	2	81.09	0.488	100
	14	3.2	2	63.02	0.965	100
	15	7.3	2	27.51	2.02	100
	16	21.5	2	9.31	2.565	100

Table 3: Initial conditions for shock experiments

For each experiment fired, the instantaneous shock wave speed at each location in the field of view of the schlieren beam (~13 cm in length) was measured. A frame rate setting of 30,000 fps meant that the camera would capture 10-11 frames of the shock wave, which gave 10-11 instantaneous positions and, consequently, 9-10 instantaneous velocities. The average speed over this distance of 13 cm was calculated using the average of those instantaneous speeds, and is equivalent to calculating the speed from the first and last positions in the field of view, as the time increments are constant between consecutive positions/frames ($dt = \frac{1}{30,000} s = 0.03\overline{3} ms$). An on-screen pixel ruler was used to calculate dx , and was converted to real-time distance using a conversion factor obtained from measuring an object placed in the schlieren's field of view. The conversion factor obtained is 1 pixel = 4.96 mm for the zoom setting used for those experiments.

The purpose of calculating the instantaneous velocities was to attempt to capture the unsteady nature of the shock front as it propagates through a turbulent medium, and to see if velocity

fluctuations are amplified when the front interacts with increasing levels of turbulence. This, however, is subject to quite a significant error, because ± 2 pixel/dt (1 pixel per location measurement, and 2 measurements per speed calculation) corresponds to approximately ± 12.1 m/s ($\pm 3.2\%$). This error is too large to be able to rely on the calculated velocity fluctuation terms to quantitatively measure levels of unsteadiness due to turbulence.

4.3 Results

In most cases where turbulence was present, the front exhibited a change in orientation and a deformation of structure. To further capture this and the resulting unsteadiness, the positions and speeds of the front at the top and bottom of the test section were separately measured and calculated.

Before presenting any results, it is important to note the error included in the velocity calculations. The velocities presented in this section are average velocities over 10 or 11 frames which correspond to 0.3 or 0.333 milliseconds. One measurement using the pixel ruler is subject to a ± 1 pixel error, and two location measurements are made per speed calculation. This corresponds to ± 1.21 m/s for a 0.3 ms timeframe and ± 1.34 m/s for a 0.333 ms time frame, using the conversion factor of 4.96 mm/pixel. An error bar of 1.3 m/s was added to each of the velocity plots made.

4.3.1 Shock Waves Propagating Through a Quiescent Medium

The calculated shock speeds for all 6 fill pressures are shown in table 4, and are plotted in figure 19, which shows a trend of decreasing wave speed with increasing fill pressures. The shock Mach number, M , is also calculated to indicate the generation of weak shock waves. The speed of sound in the medium is calculated to be 340 m/s at a temperature of 288 K.

No	P_f (kPa)	U_{top} (m/s) \pm % Deviation		U_{bottom} (m/s) \pm % Deviation		$U_{average}$ (m/s)	M
1	50	366.4	0.16	367.6	-0.16	367.0	1.08
2	75	364.1	0.37	366.8	-0.37	365.5	1.075
3	100	362.8	0.08	363.4	-0.08	363.1	1.068
4	130	361.6	0.17	362.8	-0.17	362.2	1.065
5	167	361.5	0.28	363.5	-0.28	362.5	1.066
6	200	361.6	-0.08	361.0	0.08	361.3	1.063

Table 4: Calculated shock speeds for 6 fill pressures

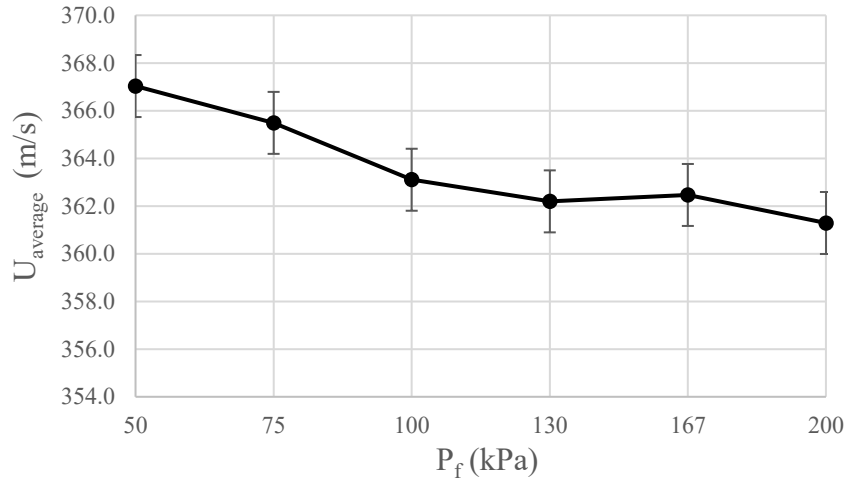


Figure 19: Average wave speed versus fill pressure

It can be seen that at lower fill pressures, the shock travels faster than at higher pressures because the speed of a shock wave is a function of the ratio of the energy supplied to the gas from the spark to the pressure in the tube. So the lower the fill pressure, the larger this ratio is, and the faster the front will propagate. This observation is verified with the tests done with turbulence, where all the calculated shock speeds at 100 kPa fill pressure are lower than those at 50 kPa. At some point above atmospheric, the shock speed starts to plateau.

Figure 20 lays out one frame from each of the six experiments where the shock wave is in approximately the same position in the schlieren beam's field of view. The number next to each image represents the experiment number from table 3. The shock fronts appear to be perfectly normal to the tube walls, as expected. Another observation is that the shock fronts are sharper for higher fill pressures. This is due to the sensitivity of the schlieren optical system. The schlieren intensity is proportional to the changes (or derivative) of density, $\Delta\rho = \rho_2 - \rho_1$. For the same Mach number, a shock generates the same density ratio ρ_2/ρ_1 . At a higher initial pressure, and consequently density, the value of ρ_2 is higher and $\Delta\rho$ is consequently higher.

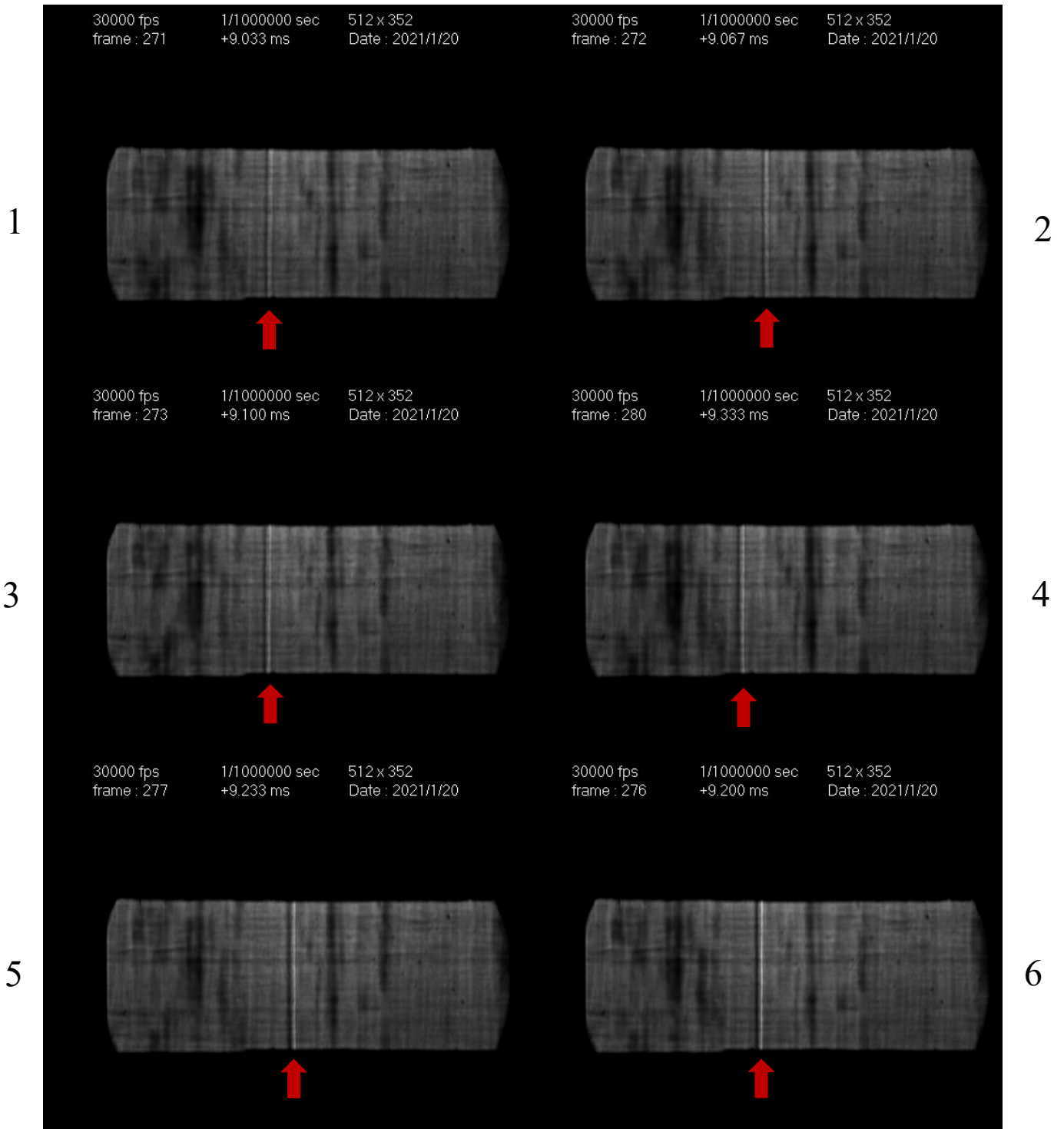


Figure 20: A frame of the normal shock wave propagating through an undisturbed medium of air for each of the 6 fill pressures. The red arrow indicates the location of the shock wave.

4.3.2 Shocks with Jet Injection Through Inlet 1

Inlet 1 is situated on top of the viewing section and exactly at the very start of the schlieren beam. As in the case with no turbulence, the average speed of the wave, as well as the speed of the front top and bottom were calculated for each scenario. The following observations were made based on the calculated shock speeds shown in table 5, and plotted in figure 21:

- 1- For all 16 cases, the wave speed is higher, for the same fill pressure P_f , than in the case with no turbulence. So the injected jet seems to speed up the wave as it passes underneath the inlet.
- 2- The bottom of the shock front travels faster than the top of the front, and that gap is quite significant compared to the cases with no turbulence. This can be attributed to an increase in unsteadiness upon contact with the turbulent jet.
- 3- The wave speed for fill pressures of 100 kPa are lower than that of 50 kPa. This solidifies the claim made in the previous section that shocks travel faster in lower pressures.
- 4- An increase in injection time for the same fill pressure and supply pressure does not seem to have much of an impact on the propagation of the shock.

Inlet 1										
P_s (kPa)	No.	PR_f	P_i (kPa)	t_{inj} (seconds)	P_f (kPa)	U_{top} (m/s) \pm % Deviation		U_{bottom} (m/s) \pm % Deviation		$U_{average}$ (m/s)
150	1	3	35.35	0.51	50	367.6	0.65	372.5	-0.65	370.1
	2	3	22.83	0.98	50	368.2	0.72	373.6	-0.72	370.9
	3	3	10.32	1.56	50	367.5	0.64	372.2	-0.64	369.9
	4	3	2.11	1.89	50	367.0	0.74	372.5	-0.74	369.8
	5	1.5	84.12	0.67	100	364.0	0.58	368.2	-0.58	366.1
	6	1.5	73.00	1.12	100	366.8	0.18	368.2	-0.18	367.5
	7	1.5	60.24	1.63	100	365.8	0.25	367.6	-0.25	366.7
	8	1.5	45.58	2.24	100	366.2	0.09	366.8	-0.09	366.5
200	9	4	40.78	0.22	50	365.2	1.31	374.9	-1.31	370.1
	10	4	30.16	0.51	50	370.2	0.54	374.2	-0.54	372.2
	11	4	13.74	0.99	50	367.0	1.06	374.9	-1.06	371.0
	12	4	2.49	1.34	50	368.2	0.65	373.1	-0.65	370.7
	13	2	81.09	0.49	100	365.8	0.41	368.8	-0.41	367.3
	14	2	63.02	0.97	100	366.4	0.66	371.3	-0.66	368.8
	15	2	27.51	2.02	100	365.8	0.66	370.7	-0.66	368.2
	16	2	9.31	2.57	100	365.8	0.58	370.1	-0.58	367.9

Table 5: Calculated shock speeds for 16 shocks interacting with turbulence through inlet 1

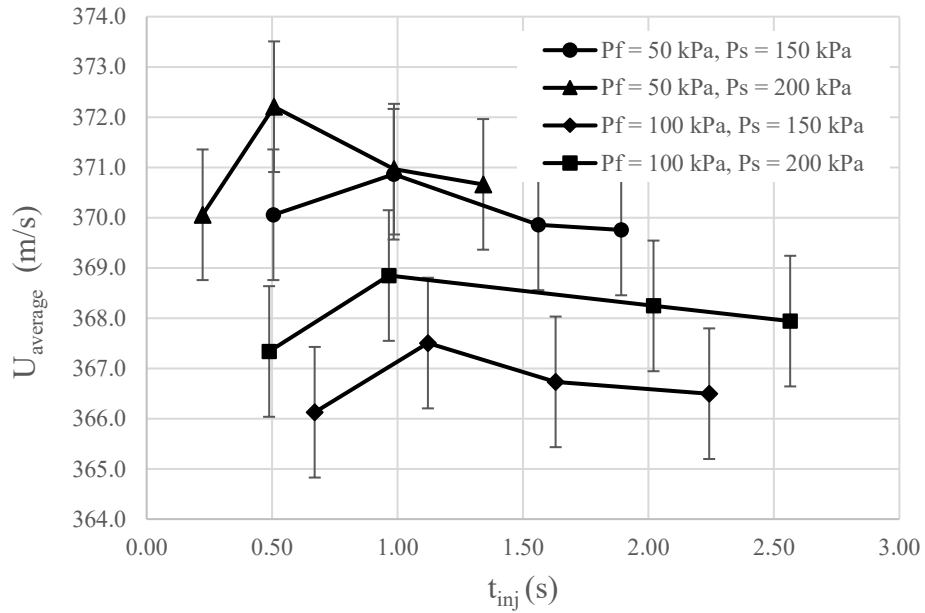


Figure 21: Average wave speed versus injection time (inlet 1)

Figure 22 shows one frame from each of eight shots, where the shock is approximately in the same position after it has interacted with the turbulent jet injected through inlet 1. The shock front's structure and orientation barely changes for the different pressure ratios and injection times. However, there is a slight deformation in the front in comparison to the shocks sent through an undisturbed medium, shown in figure 20.

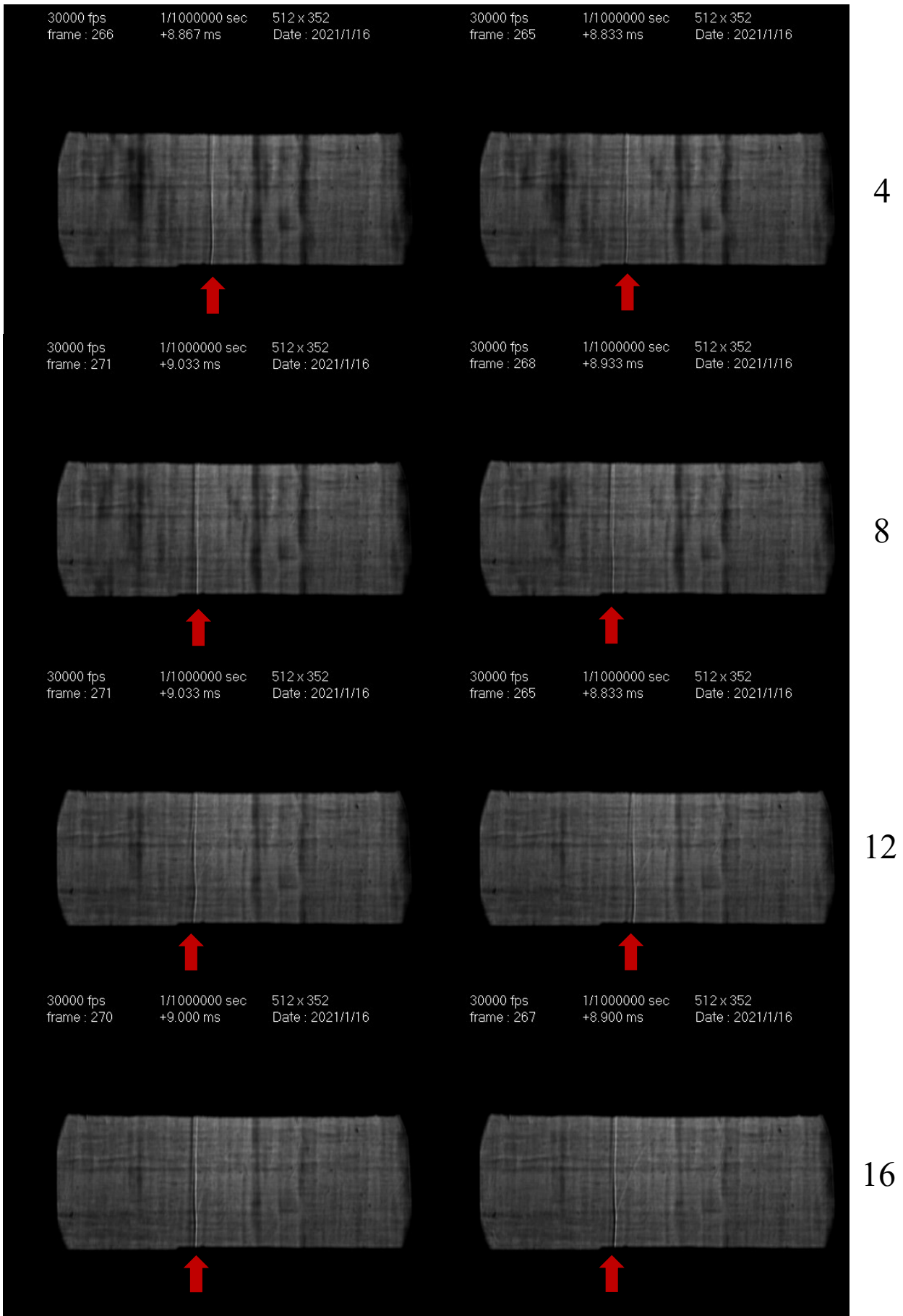


Figure 22: A frame of each shock wave for experiments 1, 4, 5, 8, 9, 12, 13, 16, referring to table 5. The red arrow indicates the location of the shock wave.

4.3.3 Shocks with Jet Injection Through Inlet 2

Inlet 2 is situated 38.1 cm upstream of inlet 1 and the start of the schlieren beam, giving the wave more time to interact with the injected jet before entering the test section and field of view. Table 6 shows the resulting shock speeds, figure 23 plots them, and the following observations were made:

- 1- All 16 shock waves here travel faster than those that interacted with turbulence through inlet 1. This solidifies the claim that turbulence does indeed speed up a shock wave, as in this set of experiments, the shock was given more time to interact with the injected jet and hence was analyzed at a point in time when turbulence had a larger impact on it.
- 2- The injection times play a bigger role here in altering the shock speeds (top, bottom, and average). The shocks generally travel faster with higher injection times, and this increase in speed seems to be steadier with a supply pressure of 200 kPa. The gap between the speeds of the front top and bottom seem to increase with the injection time as well.
- 3- The impact of supply pressure can be seen by comparing shots 1-4 to shots 9-12, and 5-8 to 13-16. The shocks travel faster for the higher supply pressure of 200 kPa and the gap between U_{top} and U_{bottom} increases as well, implying a larger degree of unsteadiness.
- 4- As opposed to inlet 1, the top of the front travels faster than the bottom in all cases.

Inlet 2										
P_s (kPa)	No.	PR_f	P_i (kPa)	t_{inj} (seconds)	P_f (kPa)	U_{top} (m/s) \pm % Deviation		U_{bottom} (m/s) \pm % Deviation		$U_{average}$ (m/s)
150	1	3	35.35	0.50	50	382.3	-0.18	380.9	0.18	381.6
	2	3	22.71	0.97	50	389.0	-0.43	385.6	0.43	387.3
	3	3	10.45	1.47	50	386.3	-0.35	383.6	0.35	385.0
	4	3	2.11	1.81	50	388.3	-0.26	386.3	0.26	387.3
	5	1.5	84.38	0.61	100	373.6	0.00	373.6	0.00	373.6
	6	1.5	73.26	1.03	100	378.9	-0.18	377.6	0.18	378.3
	7	1.5	60	1.55	100	389.0	-0.43	385.6	0.43	387.3
	8	1.5	45.58	2.21	100	384.3	-0.53	380.3	0.53	382.3
200	9	4	40.78	0.22	50	376.9	-0.09	376.2	0.09	376.6
	10	4	30.16	0.51	50	387.0	0.00	387.0	0.00	387.0
	11	4	13.86	0.97	50	393.8	-0.68	388.5	0.68	391.1
	12	4	2.49	1.32	50	395.3	-0.97	387.7	0.97	391.5
	13	2	81.22	0.47	100	374.3	0.00	374.3	0.00	374.3
	14	2	63.15	0.95	100	385.6	-0.53	381.6	0.53	383.6
	15	2	27.64	1.99	100	388.3	-1.14	379.6	1.14	384.0
	16	2	9.44	2.53	100	391.7	-1.13	383.0	1.13	387.3

Table 6: Calculated shock speeds for 16 shocks interacting with turbulence through inlet 2

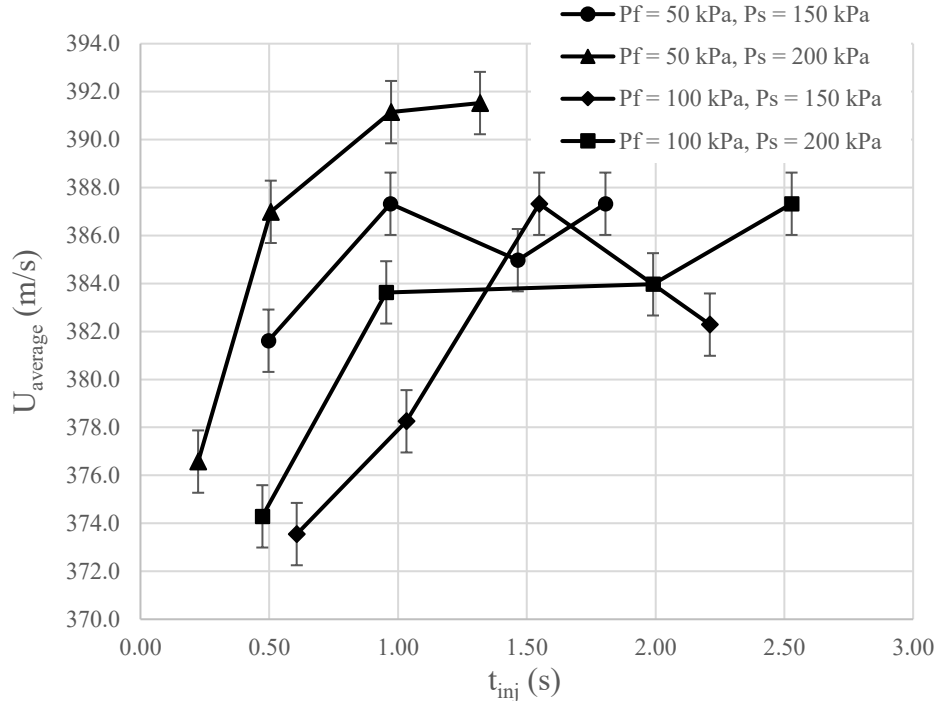


Figure 23: Average wave speed versus injection time (inlet 2)

Figure 24 shows one frame from each of eight shots, where the shock is approximately in the same position after it has interacted with the turbulent jet injected through inlet 2. It captures the deformation of the shock's structure with an increasing injection time for each pressure ratio. The left column is the smallest injection time used for each pressure ratio, and the right column is the largest injection time used for each final pressure ratio.

- 1- The supply pressure doesn't seem to have much of an impact on the shock structure or orientation.
- 2- Upon interaction with turbulence, the shock front loses its sharpness. Increasing the injection time increases the degree of turbulence, and the generated vortices flatten the density gradient and the resulting front looks fainter. This is observed for all 8 experiments when comparing the left column to the right column, and also when comparing figure 24 to figure 20.
- 3- Higher injection times also change the orientation of the front, as it is seen to tilt forward. This agrees with the observations made from table 5 about the top of the front travelling faster than the bottom.

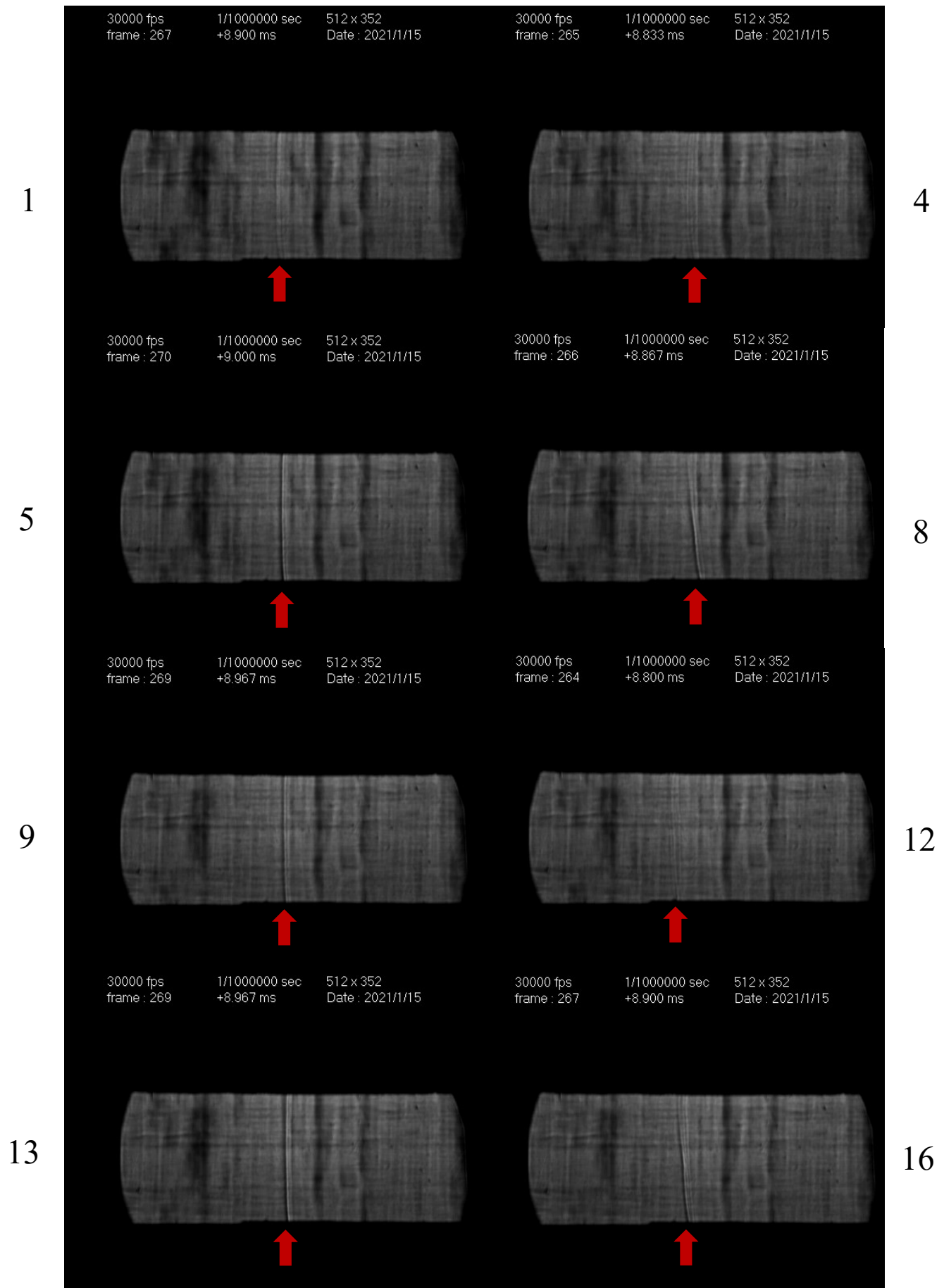


Figure 24: A frame of the shock wave for experiments 1, 4, 5, 8, 9, 12, 13, 16, referring to table 6. The red arrow indicates the location of the shock wave.

4.3.4 Shocks with Jet Injection Through Inlet 3

Inlet 3 is situated 63.5 cm upstream of inlet 1 and the start of the schlieren beam, giving the wave more time to interact with the injected jet before entering the test section and field of view. Table 7 shows the resulting shock speeds, also plotted in figure 25, and the following observations were made:

- 1- Shock speeds here are also higher than in inlet 1, and overall higher than in inlet 2 as well.
- 2- Injection times have an even more formidable impact through inlet 3, raising the shock speeds to more than 391 m/s for both fill pressures and supply pressures.
- 3- Again, the gap between U_{top} and U_{bottom} increases for higher supply pressures, implying a higher degree of unsteadiness. The overall shock speeds increase as well.
- 4- The observed trends from inlet 2 are more noticeable, consistent, and steady in inlet 3. This can be explained by the fact that injecting through inlet 3, the furthest inlet upstream of the schlieren beam, allows the shock ample time to interact with turbulence.

Inlet 3										
P_s (kPa)	No.	PR_f	P_i (kPa)	t_{inj} (seconds)	P_f (kPa)	U_{top} (m/s) \pm % Deviation		U_{bottom} (m/s) \pm % Deviation		$U_{average}$ (m/s)
150	1	3	35.35	0.52	50	379.6	-0.18	378.3	0.18	378.9
	2	3	22.83	1.03	50	390.3	-0.52	386.3	0.52	388.3
	3	3	10.20	1.57	50	393.0	-0.69	387.7	0.69	390.3
	4	3	2.11	1.91	50	392.4	-0.34	389.7	0.34	391.0
	5	1.5	84.12	0.68	100	371.5	0.00	371.5	0.00	371.5
	6	1.5	73.00	1.15	100	375.6	0.00	375.6	0.00	375.6
	7	1.5	60.24	1.67	100	383.0	-0.53	378.9	0.53	380.9
	8	1.5	45.71	2.29	100	387.0	-0.61	382.3	0.61	384.6
200	9	4	40.65	0.23	50	374.9	0.00	374.9	0.00	374.9
	10	4	30.16	0.51	50	385.6	0.00	385.6	0.00	385.6
	11	4	13.86	0.99	50	394.4	-0.09	393.7	0.09	394.0
	12	4	2.49	1.33	50	395.7	-0.26	393.7	0.26	394.7
	13	2	80.71	0.49	100	371.3	0.16	372.5	-0.16	371.9
	14	2	63.02	0.97	100	383.0	-0.26	380.9	0.26	381.9
	15	2	27.64	2.00	100	393.7	-0.86	387.0	0.86	390.3
	16	2	9.44	2.53	100	399.8	-1.45	388.3	1.45	394.0

Table 7: Calculated shock speeds for 16 shocks interacting with turbulence through inlet 3

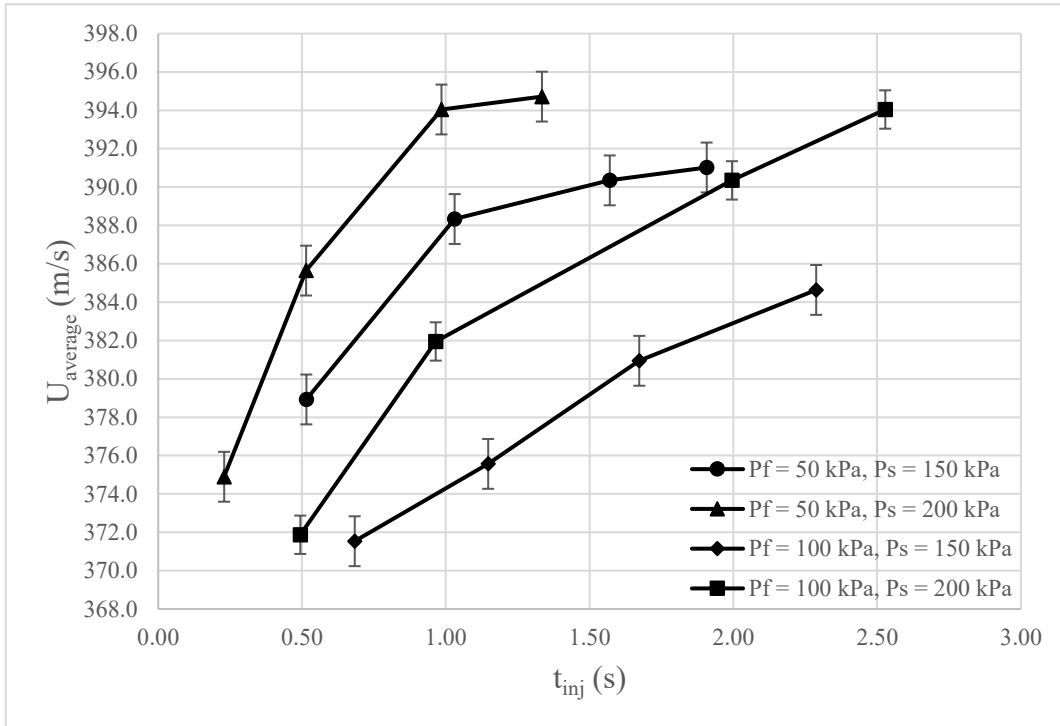


Figure 25: Average wave speed versus injection time (inlet 3)

Figure 26 shows one frame from each of eight shots, where the shock is approximately in the same position after interaction with the turbulent jet injected through inlet 3. It captures the deformation of the shock's structure with an increasing injection time for each pressure ratio. The left column is the smallest injection time used for each pressure ratio, and the right column is the largest injection time used for each pressure ratio.

- 1- Again, the supply pressure doesn't seem to have much of an impact on the shock structure or orientation.
- 2- Upon interaction with turbulence, the shock front loses its sharpness, even more than in the cases with inlet 2. The shock front can barely be seen in the cases with the highest injection times for each pressure ratio.
- 3- The same observations are made with regards to the orientation of the front; it tilts forward upon interaction with higher degrees of turbulence.

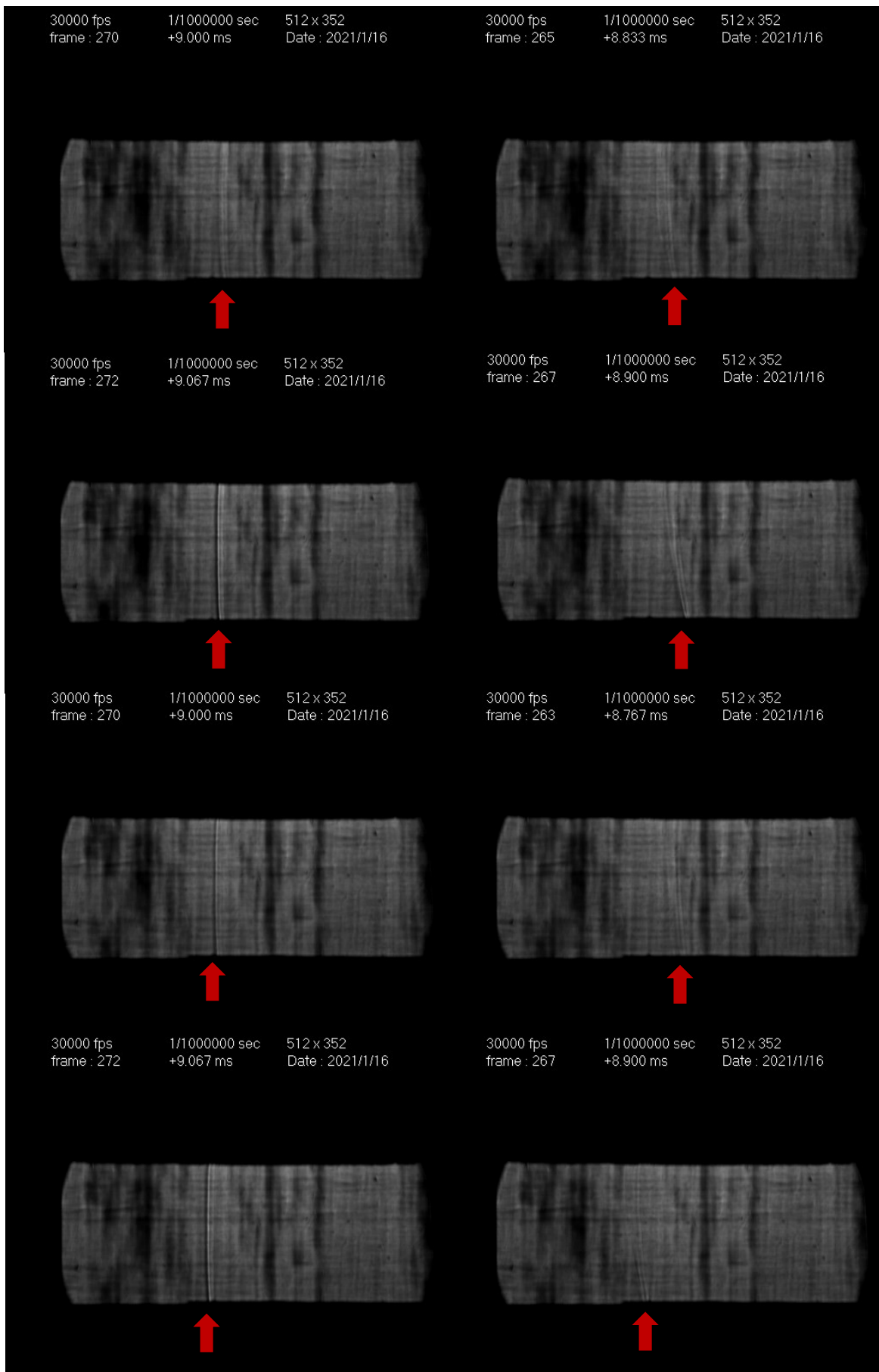


Figure 26: A frame of the shock wave for experiments 1, 4, 5, 8, 9, 12, 13, 16, referring to table 7. The red arrow indicates the location of the shock wave.

To recap, while some changes were seen in the propagation of the shock in inlet 1 and 2 experiments, the greatest impact and most noticeable/consistent trends were seen when turbulence was injected through inlet 3. The shock speeds steadily increased with an increasing injection time and supply pressure, while the front top and bottom speeds deviated more from the average speed, indicating higher levels of unsteadiness. Also, turbulence deforms the structure of a shock wave, and flattens the density gradient around the front, as it is barely visible at higher injection times, specifically when injecting through inlet 3. Finally, shock speeds propagating in a turbulent medium are higher than shock speeds travelling in a quiescent medium, at the given pressure, for all cases.

4.4 Errors and Uncertainties

The errors incurred in the shock experiments with air are:

- 1- As mentioned earlier in this chapter, measuring the velocity of the shock front using the on-screen pixel ruler incorporates an error of 2 pixels/second which corresponds to ± 1.21 - 1.34 m/s. All considered variations were greater than at least one error bar.
- 2- The accuracy of the 30 psi sensor is $\pm 0.25\%$, which amounts to ± 0.52 kPa on all pressure readings.

Chapter 5

Detonation-Turbulence Interaction

The interaction of detonations with a turbulent flow field is investigated for a stoichiometric mixture of ethylene and oxygen, $C_2H_4 + 3O_2$. The propagation of detonation waves in a quiescent medium is first examined to establish a baseline. Following this, non-reactive argon, and reactive, $C_2H_4 + 3O_2$, gases are injected to create a turbulent atmosphere.

5.1 Initial Conditions

The fill pressures used for the detonations range between 5 and 30 kPa, to (1) ensure that the von-Neumann pressure does not exceed the shock tube's maximum yield of 200 psi, and (2) to observe a range of cell sizes. For the experiments with turbulence, initial, pre-jet injection pressures were chosen and injection times were calibrated at the different supply pressure to obtain specific fill pressures after the turbulent jet injection. During live experiments, the pressure sensors were disconnected to prevent equipment damage and the experiments were performed, pressure-wise, "blind".

5.2 Results

5.2.1 Detonation Propagation Through an Undisturbed Medium

Detonations were fired at four fill pressures of 5 kPa, 10 kPa, 20 kPa, and 30 kPa. The pressure in the tube was measured using the 5 psi sensor hooked to Panel 1, shown in figure 14. The respective wave speeds were measured and compared to the ideal CJ detonation speed, which was calculated using the Shock & Detonation Toolbox, an open-source software library that enables the solution of standard problems for gas-phase explosions using realistic thermochemistry and detailed chemical kinetics [34]. The SD toolbox uses the Cantera software package and is implemented using MATLAB or Python. Detonations are computed and analyzed using the 1D ZND model.

The test procedure followed is outlined in the appendix A4. The images were captured at a frame rate of 90,000 fps, capturing 5-6 frames of the wave front. The average speed across the field of view was calculated by the distance covered divided by the time elapsed between the first and last frames. An error of ± 1 pixel per location measurement is considered, which leads to ± 9.9 m/s for a 0.0556 ms time frame and ± 12.4 m/s for a 0.0444 ms time frame. A conversion factor of 3.63 pixels/mm was found by placing an object of known dimensions in the schlieren field of view, and measuring it's width in a captured image.

Figure 27 shows one frame from each of the four pre-detonation pressures. Table 8 shows the calculated detonation speeds from the experiments (U_P), and from the ZND model (U_{CJ}).

Detonations were observed to travel faster at higher fill pressures. The theoretical CJ velocity is weakly dependent upon the pre-detonation pressure. Additionally, boundary layers along the tube walls have a weaker effect at higher pressures. The resulting experimentally measured detonation velocity is thus also closer to the corresponding theoretical CJ velocity. The cell size of a detonation wave decreases with an increasing fill pressure. This can be observed in figure 27, where the corrugation is finer and less visible for higher pressures. The inevitable presence of more cells across the wave front means there are more triple points, which are the strong points of the detonation. This leads to the boundary layer having an impact on a smaller percentage of the total number of cells and triple points, and therefore allowing the wave to overcome the frictional forces in the vicinity of the boundary layer and bringing its speed closer to CJ. Also, the brighter color in the post-detonation region of the 20 kPa and 30 kPa images indicates more light emitted at higher pressures.

Figure 28 shows the features of a detonation structure that are visible from the detonation fired at 20 kPa. The features include the leading shock front, the reaction zone - which is the thick dark-colored region behind the shock front, the transverse waves - which can be seen as very fine wrinkles behind the reaction zone, and the post-detonation region.

P_f (kPa)	5	10	20	30
U_P (m/s)	1826	2057	2191	2238
U_{CJ} (m/s)	2234	2266	2299	2318
U_P/U_{CJ} (%)	82	91	95	97

Table 8: Calculated wave speeds from the schlieren images and from the ZND model, as well as the deviation of the experimentally obtained speeds from the CJ speed obtained from Cantera

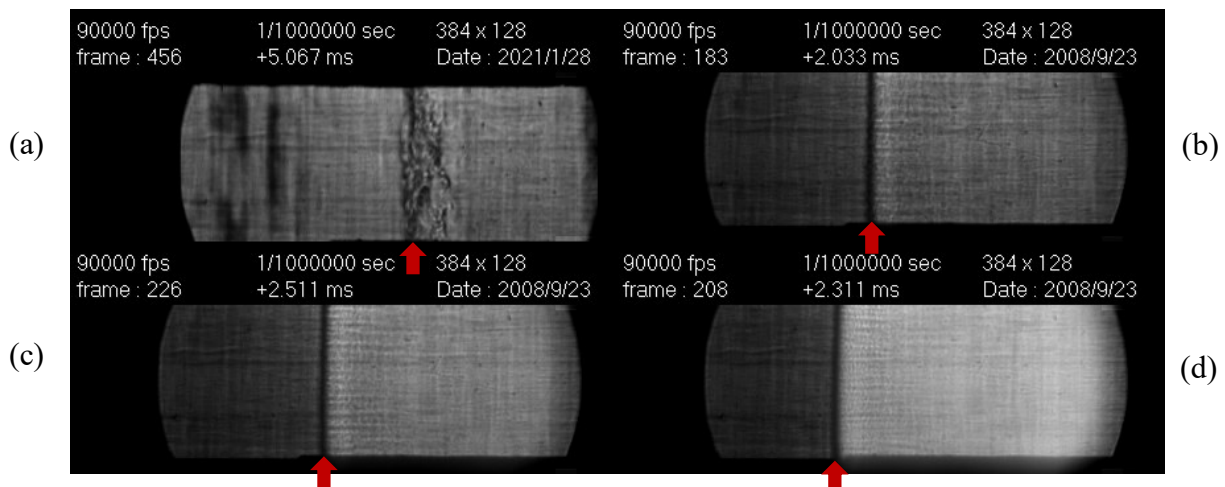


Figure 27: Schlieren images of a propagating detonation wave in an undisturbed medium for (a) 5 kPa (b) 10 kPa (c) 20 kPa (d) 30 kPa. The red arrow indicates the location of the detonation wave.

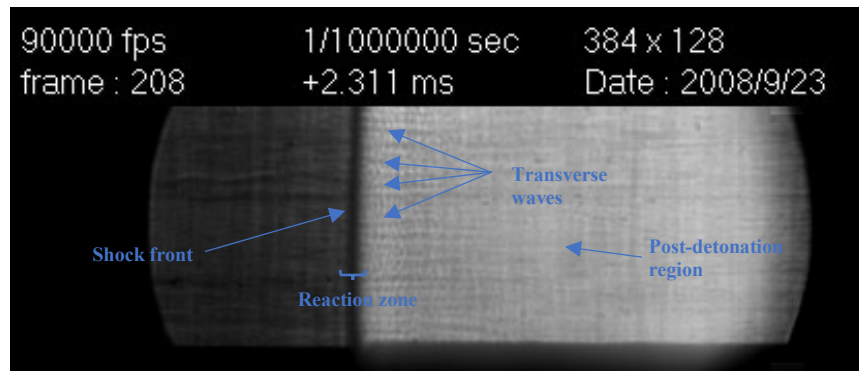


Figure 28: A frame from the detonation at 20 kPa fill pressure showing the visible portions of the cellular pattern

5.2.2 Detonation-Turbulence Interaction with Argon Injection

An argon jet was used to generate turbulence and interact with the detonation wave. Injection was done through inlet 2 only, and at one supply pressure of 95 kPa, as the main objective here is only to study the impact of turbulence and non-reactivity on detonation propagation. A total of 12 shots were fired, 4 at each fill pressure. The initial conditions and calculated wave speeds (U_{av}) are shown in table 8. Z represents the mole fraction of the reactive mixture and of argon in the medium after injection and is the ratio of the partial pressure of each gas to the final pressure P_f . Z also represents the extent of the gas's length scale in the medium, according to Boyle's law. The initial pressures were set to correspond to values of Z_{Ar} equal to those listed in table 9.

No.	P_s (kPa)	P_i (kPa)	P_f (kPa)	t_{inj} (s)	$Z_{Reactant}$	Z_{Ar}	U_{av} (m/s)
1	95	2	10	0.79	0.2	0.8	541.3
2	95	5	10	0.45	0.5	0.5	874.2
3	95	8	10	0.175	0.8	0.2	2001.2
4	95	9	10	0.08	0.9	0.1	2029.1
5	95	5	20	1.44	0.25	0.75	720.5
6	95	10	20	0.95	0.5	0.5	936.8
7	95	16	20	0.33	0.8	0.2	2162.3
8	95	18	20	0.13	0.9	0.1	2153.0
9	95	10	30	1.94	0.33	0.67	804.5
10	95	15	30	1.42	0.5	0.5	905.7
11	95	24	30	0.5	0.8	0.2	2193.3
12	95	27	30	0.205	0.9	0.1	2196.4

Table 9: Initial conditions and measured velocities for all 12 experiments

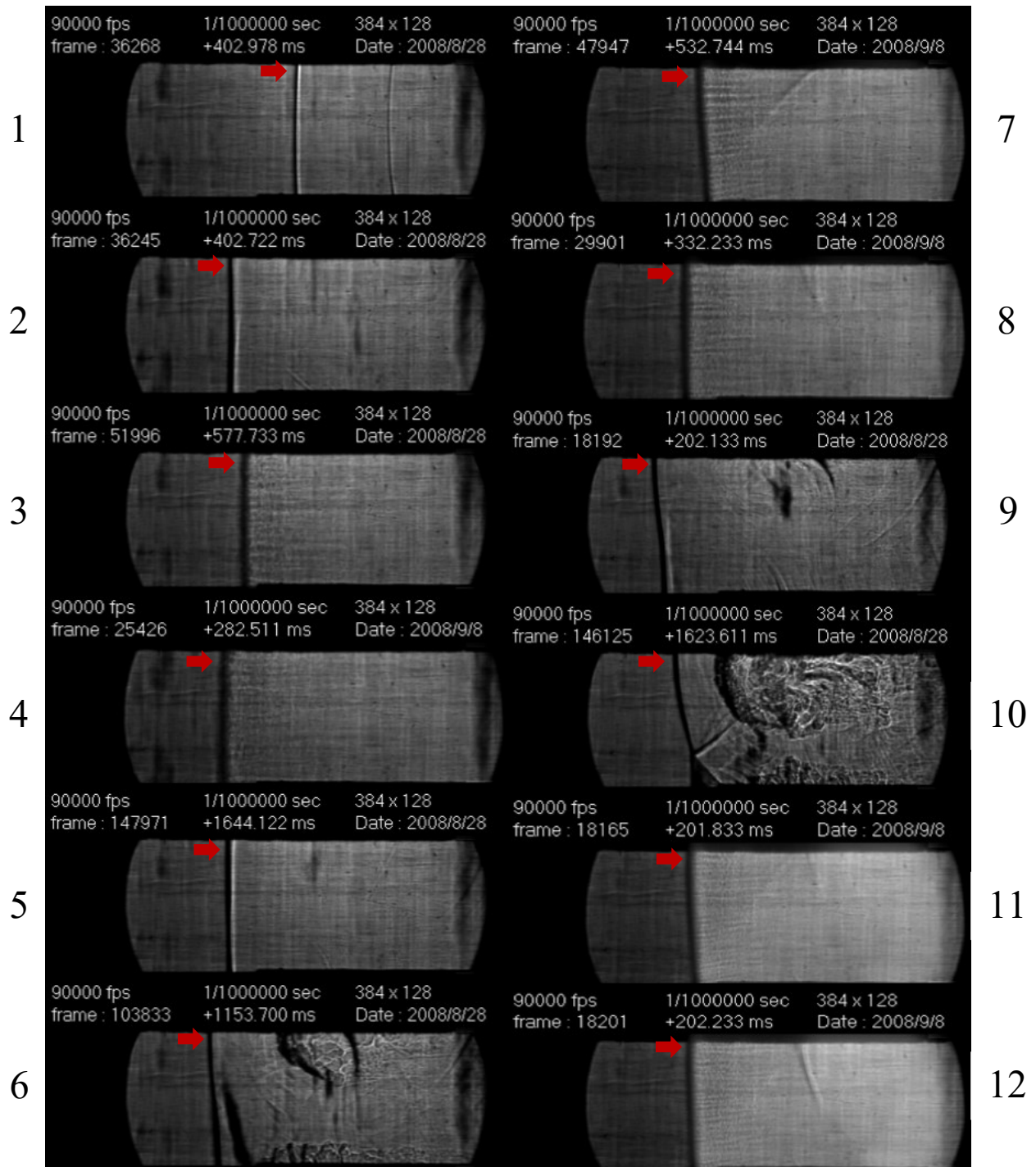


Figure 29: One frame from each of the 12 shots of detonation with argon. The numbers next to each image correspond to the rows from table 9. The red arrow indicates the location of the detonation wave.

From the structure observable for each experiment represented in figure 29, we can see that the calculated wave speed for the experiment 1 is far lower than a typical detonation speed. It looks very much like a non-reactive shock wave with no apparent reaction zone behind the front. This apparent non-reactivity is expected as the partial pressure of ethylene-oxygen is very low (2 kPa) and the medium is mostly non-reactive (80%).

The wave in the experiment 2 travels faster at 874 m/s, as the partial pressure of ethylene-oxygen is increased to 5 kPa. Consequently, the front slightly thickens and begins to develop a reaction zone behind it. Turbulence doesn't seem to have an impact on the orientation of the front.

In experiment 3, the medium is mostly reactive, and the front is a typical detonation wave with an apparent reaction zone behind it. It's speed is on the order of 2 km/s.

In experiment 4, the front is a typical detonation wave with a 90% reactive medium, its speed is slightly faster than in experiment 3 at 2029 m/s.

In experiment 5, the front is slightly thicker than that of a non-reactive shock wave, and a reaction zone has not yet developed as the medium is 75% diluted with argon. The wave speed is much lower than typical detonation speeds due to argon dilution.

In experiment 6, initial pressure is increased to 10 kPa, and the reaction zone becomes more apparent and pockets of burnt products and non-reactive gas develop behind the front. The front is faster than in experiment 4 as partial pressure of ethylene-oxygen is higher. The front also tilts forward as we begin to see an effect of interaction with turbulence.

In experiment 7, the medium is 80% reactive, and the wave looks like a typical detonation wave and is propagating near CJ speed. The front is also slightly tilted forward due to turbulence.

In experiment 8, the front is a typical detonation and is almost completely normal with no observable effect by turbulence, as the medium is 90% reactive.

In experiment 9, the medium is mostly non-reactive but small pockets of burnt products develop behind the front. Interaction with turbulence tilts the front forward. The wave propagates far lower than typical detonation speeds.

In experiment 10, an initial pressure of 15 kPa increases combustion activity in the reaction zone but pockets of inert gas remain. The turbulent flow-field is also very visible here as the density gradient is high between the burnt products and the unreacted argon. The front is tilted forward due to interaction with turbulence.

In experiment 11, the wave is a typical detonation wave traveling at a speed near CJ in an 80% reactive medium. The front is tilted forward due to interaction with turbulence.

In experiment 12, the wave is a typical detonation wave traveling at a speed near CJ in an 90% reactive medium. The front is tilted forward due to interaction with turbulence.

5.2.3 Detonation-Turbulence Interaction with Ethylene-Oxygen Injection

Turbulence was injected through three inlets in order to examine the impact of interaction time/distance of the detonation front with the turbulent flow-field. Inlet 1 is situated right at the start of the schlieren beam, Inlet 2 is 38.1 cm upstream of the schlieren beam, and Inlet 3 is 63.5 cm upstream of the schlieren beam. Two supply pressures of 75 kPa and 100 kPa were used to inject the turbulent jet through the inlets, for pre-detonation fill pressures of 10 kPa, 20 kPa, and 30 kPa. Five levels of turbulence were generated for every pre-detonation pressure, varying the initial pressure in each case, resulting in five injection times for each fill pressure.

Velocity Measurement

Figure 30 shows 5 frames from the detonation wave with turbulence through inlet 1 at a supply pressure of 75 kPa, 10 kPa final pressure, 8 kPa initial pressure and 0.238 seconds of injection. The velocity is calculated by dividing the distance between the first and last frames by the time elapsed between them. The location of the wave in each frame is measured at the front-most location of the wave front. The average velocity across the width of the field of view, found using this method, is equal to the average of the velocity between subsequent frames since the time between every two frames is constant at 0.011 ms. Initially the goal was also to attempt to capture the unsteadiness of the wave after coming in contact with turbulence by measuring the velocity between every two frames and calculating the resulting fluctuations from the mean, if any, but the error incurred there is around 50 m/s, which is too large to capture this unsteadiness.

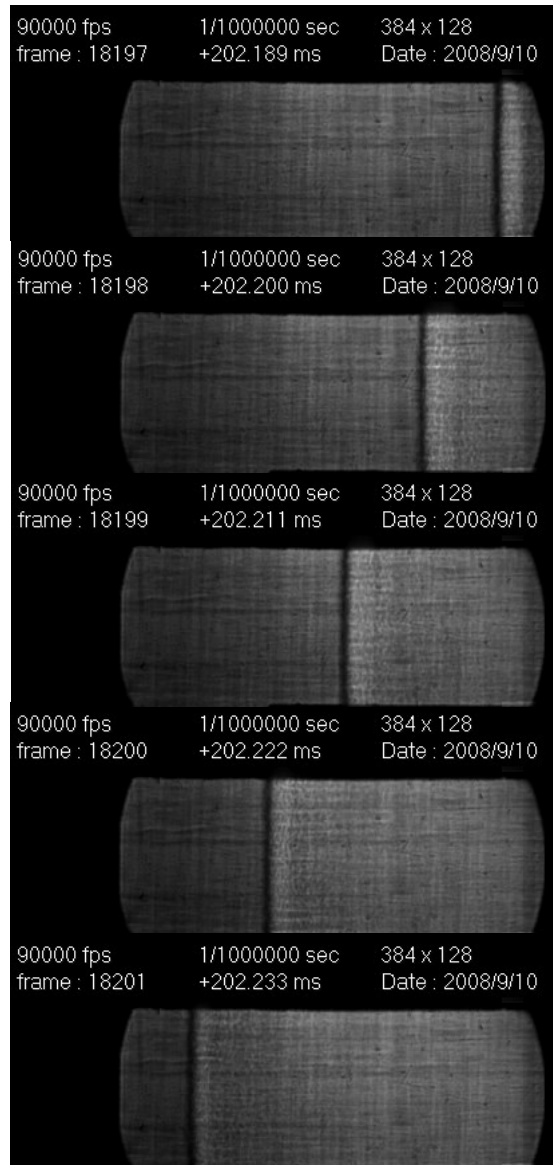


Figure 30: Five frames from a detonation with turbulence through inlet 1 at $P_s = 75$ kPa, $P_f = 10$ kPa, $P_i = 8$ kPa, $t_{inj} = 0.238$ s

Defined Parameters

To analyze the experimental results and compare across different conditions, the following parameters are defined:

Z_T is a non-dimensional parameter defined to quantify the physical extent of the turbulent flow-field in the shock tube and it is the ratio $\frac{P_f - P_i}{P_f}$. In the limit of non-mixing interfaces, Z_T is thus the fraction of the tube occupied by the turbulent fluid and $(1 - Z_T)$ is the fraction occupied by the initially injected material. The five injection times resulted in five Z_T values: 0.2, 0.5, 0.8, 0.9 for 10 kPa; 0.25, 0.5, 0.8, 0.9 for 20 kPa and 0.33, 0.5, 0.8, 0.9 for 30 kPa.

PR_i is the initial pressure ratio between the C2 injection tank and the shock tube, and is defined as $\frac{P_{s,i}}{P_i}$, where $P_{s,i}$ is the initial pressure in C2 before jet injection.

PR_f is the final pressure ratio between the C2 injection tank and the shock tube, and is defined as $\frac{P_{s,f}}{P_f}$, where $P_{s,f}$ is the final pressure reached in C2 after jet injection.

τ is defined as the difference between the initial and final pressure ratios, and is meant to provide an idea of the extent of the generated turbulence. $\tau = PR_i - PR_f$

Γ is a non-dimensional parameter defined to quantify the distance of the inlet from the schlieren beam relative to one side (half) of the physical extent of the generated turbulence, assuming non-mixing interfaces. A value of $\Gamma < 1$ implies the camera's field of view is well in the vicinity of the turbulent flow-field while as Γ increases above 1 the field of view moves further away from the generated turbulence.

$$\Gamma = \frac{x_{inlet} - x_{beam}}{0.5L_{tube}Z_T} \quad (11)$$

Pressure Variation in the Injection Cylinder and Shock Tube

The gas cylinder used to quickly inject the ethylene-oxygen is unregulated for safety purposes, hence the supply pressures are not constant, as opposed to the experiments with argon and shocks in air. For every experiment, the final pressure in the cylinder was measured to obtain initial and final pressure ratios. Figure 31 sketches the pressure variation with time in cylinder C2 and in the shock tube during jet injection. For the same $P_{s,i}$ and P_i , increasing the injection time increases the final pressure P_f and the final supply pressure $P_{s,f}$, which in turn decreases the final pressure ratio PR_f to approach 1, and increases τ . While a larger value of τ may not necessarily mean more turbulence, it does provide us with the ability to combine data from all supply pressures and final pressures into one plot to globally examine the effect of turbulence on detonation propagation.

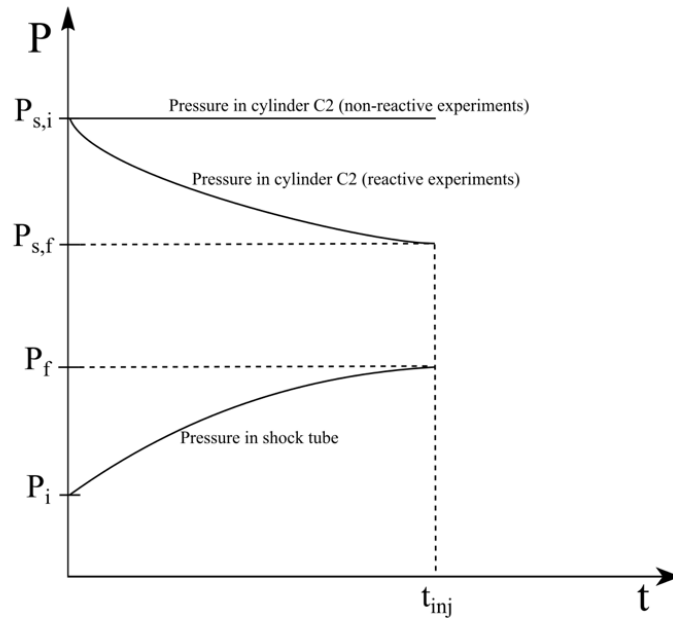


Figure 31: Pressure versus time graph during jet injection

Figure 32 shows an example of the variation of pressure with time in the shock tube and manifold during jet injection and manifold evacuation before ignition. The measurements were made using the 15 psi pressure sensor, and the same procedure was followed for determining the required injection times as in the experiments with argon. The pressure measurements and corresponding times were printed on the Arduino's serial monitor. In order to prevent a detonation from propagating back into the gas cylinders, the manifold was evacuated to a pressure of no more than 5.5 kPa. This induces a delay between the moment the injection valve (S3) closes and ignition. The delay ranged from 200 ms to 400 ms, depending on the supply and fill pressures. For the scenario in figure 31, the initial pressure is 5 kPa, the final pressure is 20 kPa, the injection time is 1.2 seconds, and the delay before ignition is around 0.36 seconds.

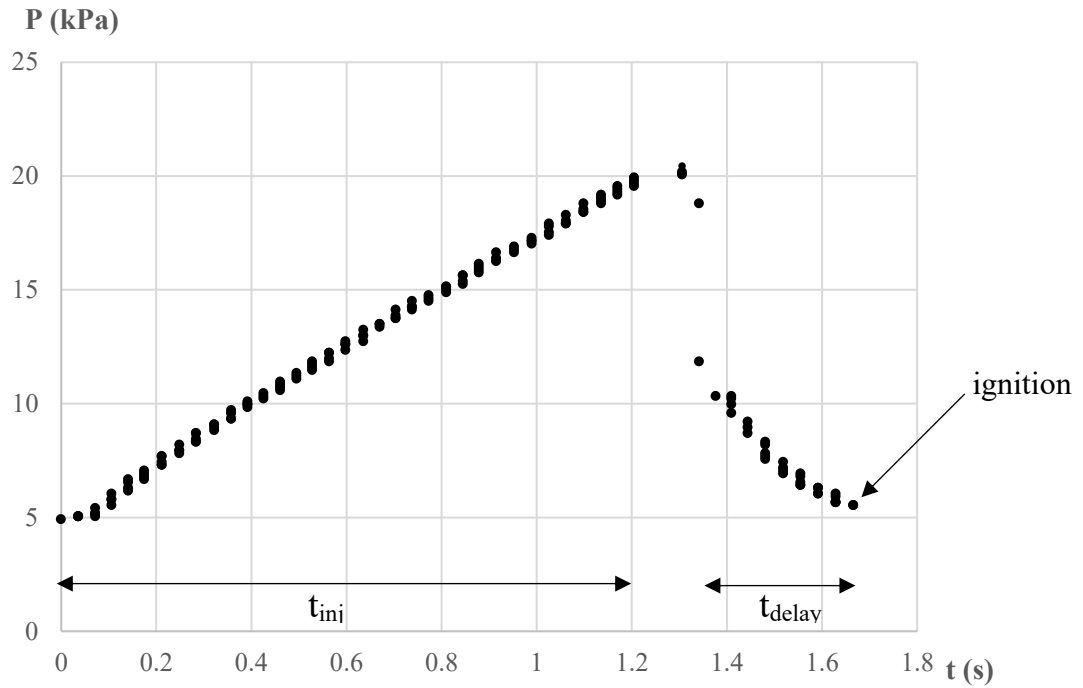


Figure 32: Pressure versus time as read by the 15 psi sensor during jet injection and manifold evacuation, for experiment 22 from table 7.

Initial Conditions and Results

Table 10 shows the initial conditions, calculated parameters and measured wave speeds for each experiment. The highlighted fields are those experimental conditions that resulted in detonations exceeding the undisturbed speeds by more than 5-6 error bars (60 m/s). Table 11 contains the calculated values of Γ for all 9 values of Z_T used, and x_1 , x_2 , and x_3 are the respective distances of the inlets from the schlieren beam.

No	P _{s,i} (kPa)	P _{s,f} (kPa)	P _i (kPa)	P _r (kPa)	t _{inj} (s)	τ	Z _T	Inlet 1	Inlet 2	Inlet 3	U _P (m/s)	U _{CJ} (m/s)
								U _{av} (m/s)	U _{av} (m/s)	U _{av} (m/s)		
1	75	66.29	0.3	10	1.07	243.37	0.97	2143.7	2149.9	2143.7	2057	2266
2	75	67.13	2	10	0.92	30.79	0.80	2131.3	2112.7	2057.0		
3	75	69.23	5	10	0.56	8.08	0.50	2131.3	2075.5	2050.8		
4	75	70.91	8	10	0.238	2.28	0.20	2125.1	2071.8	2057.0		
5	75	72.17	9	10	0.1	1.12	0.10	2118.9	2063.2	2057.0		
6	75	59.98	0.3	20	2.4	247.00	0.99	2195.7	2199.5	2187.1	2191	2299
7	75	64.61	5	20	1.778	11.77	0.75	2193.3	2112.7	2143.7		
8	75	67.97	10	20	1.12	4.10	0.50	2180.9	2081.7	2137.5		
9	75	71.33	16	20	0.38	1.12	0.20	2180.9	2094.1	2143.7		
10	75	72.17	18	20	0.175	0.56	0.10	2156.1	2111.5	2149.9		
11	75	53.26	0.3	30	5.28	248.22	0.99	2225.5	2211.8	2195.7	2238	2318
12	75	66.71	10	30	2.65	5.28	0.67	2193.3	2180.9	2193.3		
13	75	68.81	15	30	1.82	2.71	0.50	2195.7	2162.3	2180.9		
14	75	71.33	24	30	0.6	0.75	0.20	2199.5	2180.9	2195.7		
15	75	72.59	27	30	0.275	0.36	0.10	2205.7	2187.1	2195.7		
16	100	90.67	0.3	10	0.72	324.27	0.97	2211.8	2146.2	2131.3	2057	2266
17	100	92.77	2	10	0.66	40.72	0.80	2162.3	2125.1	2091.7		
18	100	94.03	5	10	0.39	10.60	0.50	2151.1	2063.2	2047.0		
19	100	95.29	8	10	0.17	2.97	0.20	2137.5	2071.8	2061.9		
20	100	96.97	9	10	0.1	1.41	0.10	2118.9	2057.0	2066.9		
21	100	84.78	0.3	20	1.56	329.09	0.99	2180.9	2193.3	2168.5	2191	2299
22	100	87.3	5	20	1.2	15.64	0.75	2193.3	2134.4	2168.5		
23	100	91.51	10	20	0.75	5.42	0.50	2205.7	2134.4	2143.7		
24	100	95.29	16	20	0.3	1.49	0.20	2175.9	2156.1	2136.3		
25	100	95.71	18	20	0.158	0.77	0.10	2180.9	2171.6	2168.5		
26	100	78.48	0.3	30	2.55	330.72	0.99	2193.3	2218.0	2218.0	2238	2318
27	100	85.62	10	30	1.61	7.15	0.67	2218.0	2189.1	2185.8		
28	100	88.98	15	30	1.14	3.70	0.50	2205.7	2156.1	2180.9		
29	100	92.35	24	30	0.42	1.09	0.20	2224.2	2187.1	2185.8		
30	100	95.71	27	30	0.185	0.51	0.10	2195.7	2193.3	2193.3		
31	120	110.42	0.3	10	0.59	388.96	0.97	2146.2	2143.7	2131.3	2057	2266
32	120	105.38	0.3	20	1.24	394.73	0.99	2180.9	2185.8	2175.9	2191	2299
33	120	96.55	0.3	30	2	396.78	0.99	2211.8	2225.5	2199.5	2238	2318

Table 10: Initial conditions, calculated parameters, and measured velocities for all 99 experiments

Γ			
Z_T	$x_1 = 0 \text{ cm}$	$x_2=38.1 \text{ cm}$	$x_3=63.5 \text{ cm}$
0.99	0	0.38	0.64
0.985	0	0.39	0.64
0.97	0	0.39	0.65
0.8	0	0.48	0.79
0.75	0	0.51	0.85
0.67	0	0.57	0.95
0.5	0	0.76	1.27
0.2	0	1.91	3.18
0.1	0	3.81	6.35

Table 11: Values of Γ for all 9 values of Z_T and 3 inlets

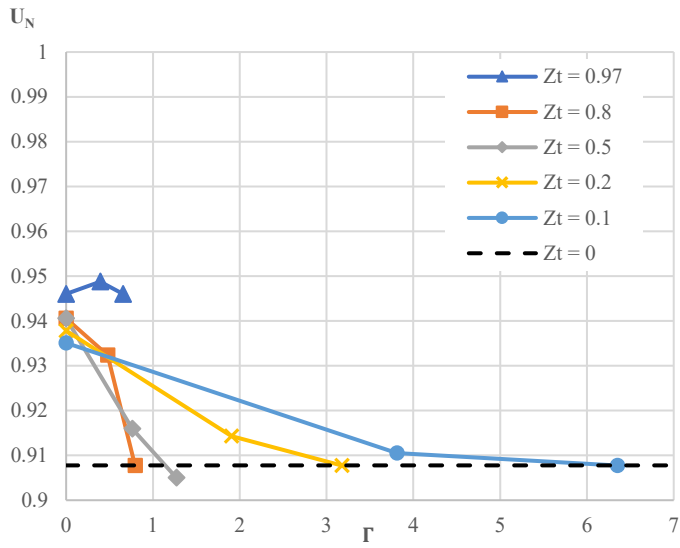
Different levels of turbulence seem to both inhibit and enhance the propagation of a detonation wave. The effects of injection time, supply pressure, and inlet through which turbulence is injected are examined below.

Effect of Inlet:

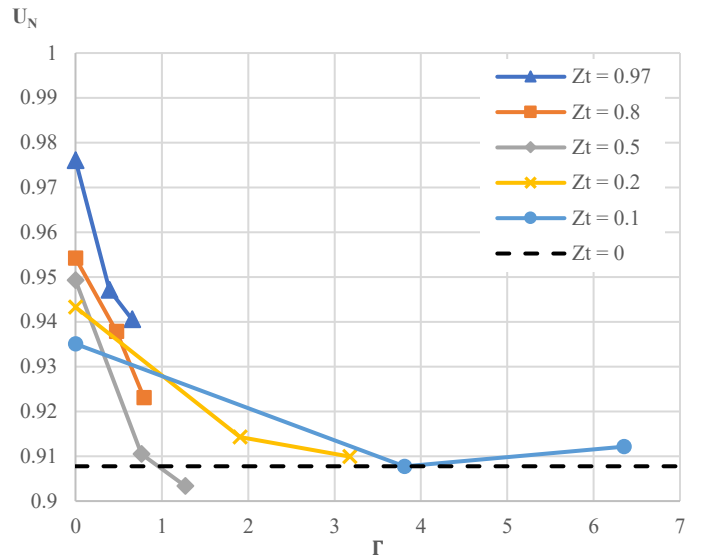
Figures 33, 34, and 35 show the variation of the wave speed, U_{av} , normalized by the CJ velocity at the given pressure versus Γ for all three pre-detonation pressures P_f

$$U_N = \frac{U_{av}}{U_{CJ}} \quad (12)$$

This variation is examined against Γ , the non-dimensional position. The five extents of turbulence, Z_T , are shown for each fill and supply pressure.

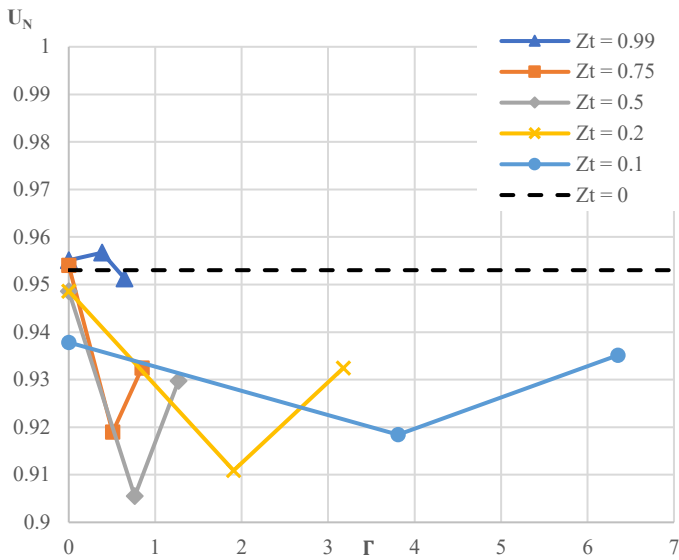


(a) $P_s = 75 \text{ kPa}$

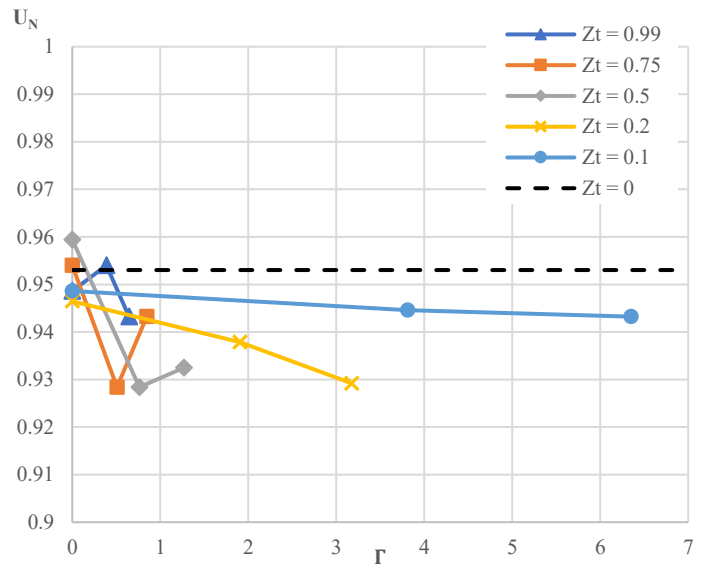


(b) $P_s = 100 \text{ kPa}$

Figure 33: Normalized wave speed, U_N , vs Γ for $P_f = 10 \text{ kPa}$



(a) $P_s = 75 \text{ kPa}$



(b) $P_s = 100 \text{ kPa}$

Figure 34: Normalized wave speed, U_N , vs Γ for $P_f = 20 \text{ kPa}$

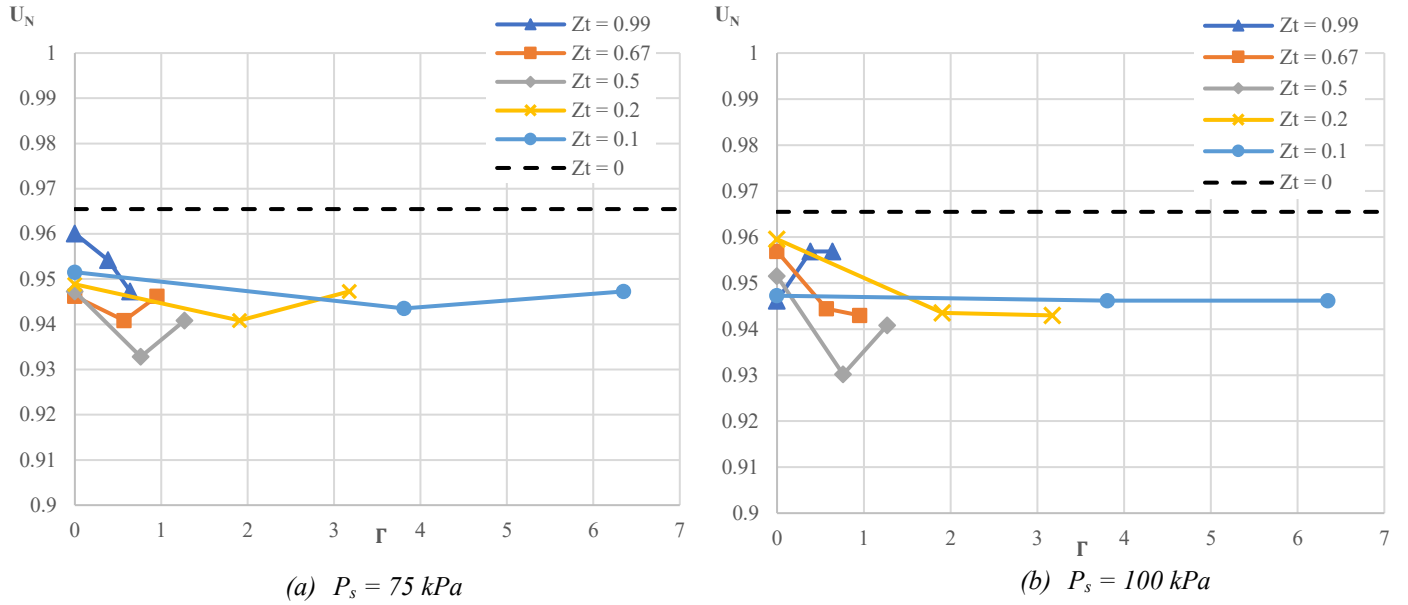


Figure 35: Normalized wave speed, U_N , vs Γ for $P_f=30$ kPa

The effect of turbulence is different at a pressure of 10 kPa than it is at higher pressures of 20 kPa and 30 kPa. When injecting through inlet 1, the captured images, and consequently the measured velocities, are inside the turbulent flow-field for all modes of turbulence. This is seen to have a significant positive impact on the wave speed for 10 kPa, but not for 20 kPa and 30 kPa. When injecting through inlets 2 and 3, the influence of turbulence on the wave propagating in 10 kPa fill pressure decreases as the wave speed is measured further away from the turbulent flow-field. At 20 kPa and 30 kPa, however, a significant drop in detonation speed is observed, which can mean that the wave had sufficient time to interact with the turbulent zone, as opposed to the cases where injection is done through inlet 1. The cell size must play a role in the difference in behavior between the fill pressures, as detonations in lower pressures have a larger cell size than those in higher pressures.

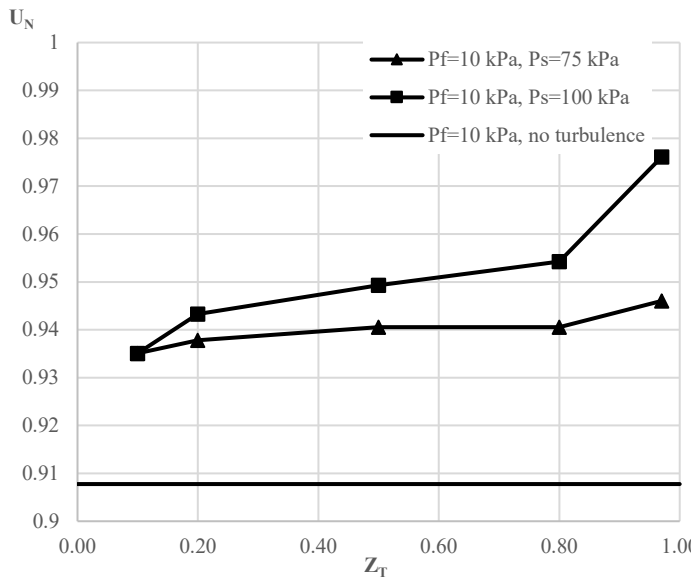
For a fill pressure of 10 kPa (figure 33 a,b), all turbulence extents Z_T , and intensities using P_s as a proxy, result in an increase of 4-7% of U_N . This effect is observable while the detonation is inside the turbulent region ($\Gamma < 1$). The wave velocity relaxes to the undisturbed velocity near $\Gamma=1$ and is equal to the undisturbed detonation velocity for $\Gamma > 1$.

For a fill pressure of 20 kPa (figure 34 a,b), turbulence results in velocity drops of 4% at $P_s=75$ kPa and 2% drop at $P_s=100$ kPa. For this fill pressure, the hindering effect of turbulence persists for $\Gamma > 1$. At the larger turbulence extent, $Z_T=0.99$, the hindering effect of turbulence appears to be absent.

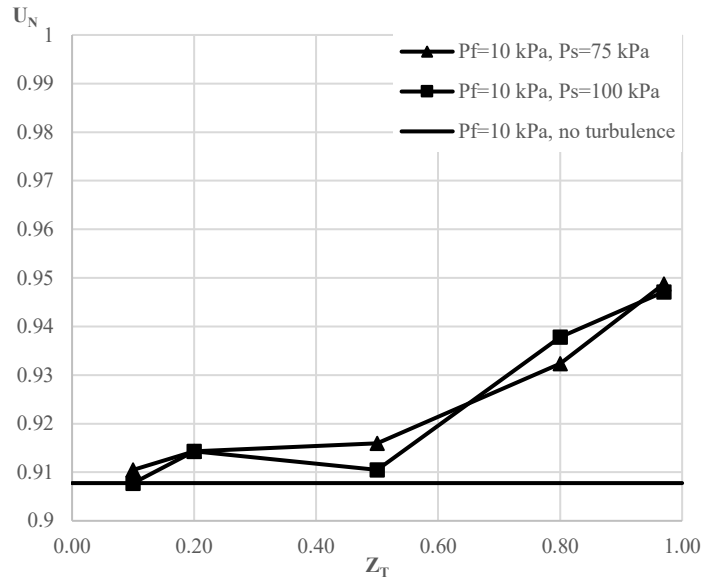
For a fill pressure of 30 kPa (figure 35 a,b), a 2% velocity reduction is observed for both supply pressures. This effect also persists for $\Gamma > 1$.

Effect of Injection Time (or Z_T):

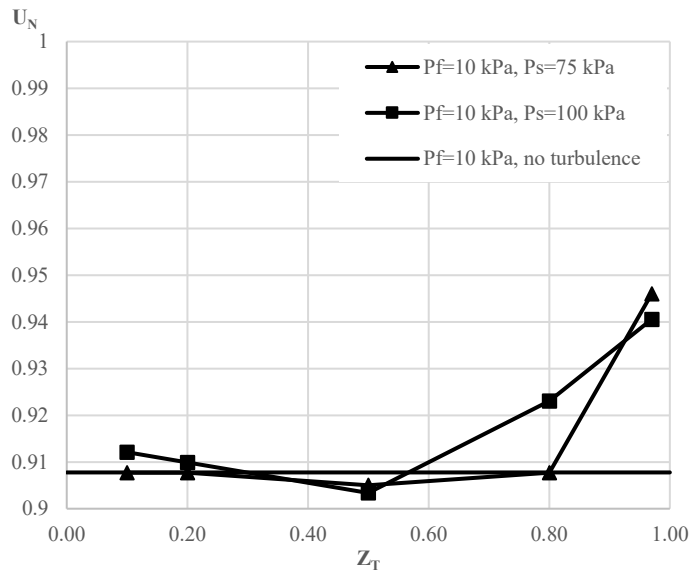
As injection time increases, the contribution of the jet to the change in pressure to reach P_f increases, and so does the physical extent of the turbulent zone, Z_T . In figures 36, 37, and 38 the normalized velocity U_N is plotted versus Z_T for each fill pressure and inlet, and the effect of the injection time is examined.



(a) Inlet 1

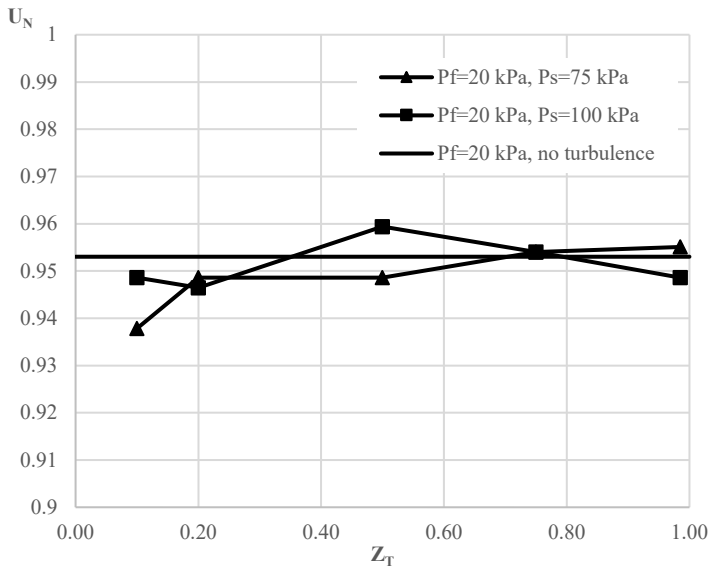


(b) Inlet 2

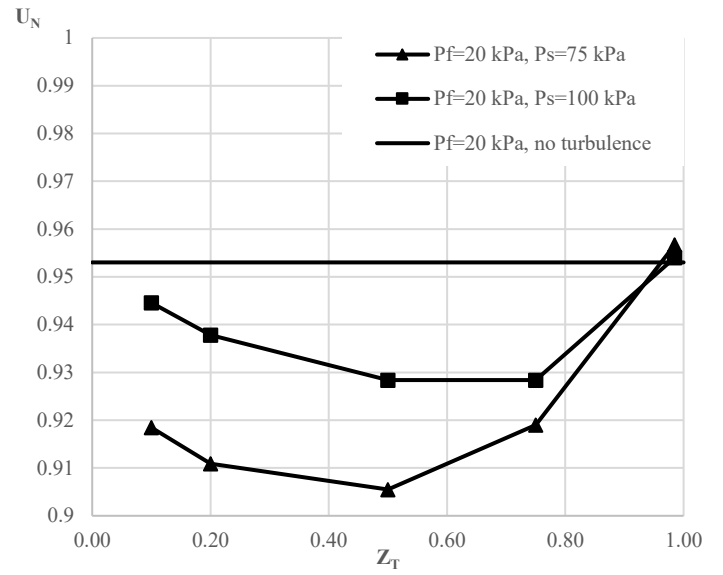


(c) Inlet 3

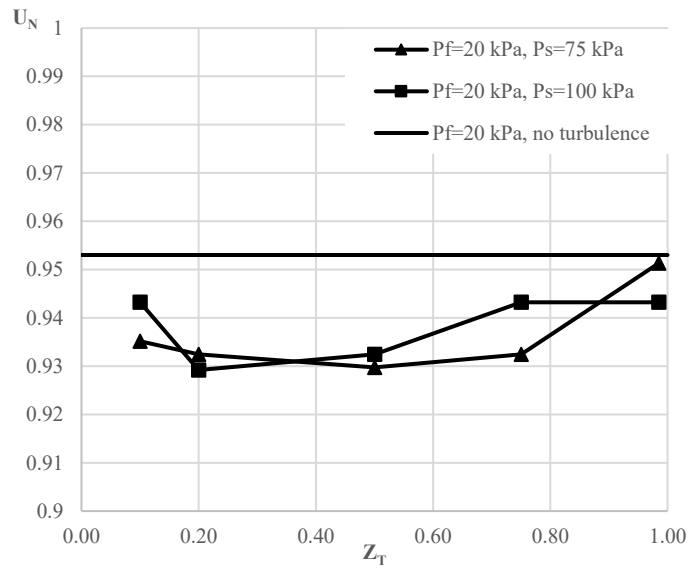
Figure 36: Normalized velocity U_N versus Z_T for $P_f = 10$ kPa



(a) Inlet 1

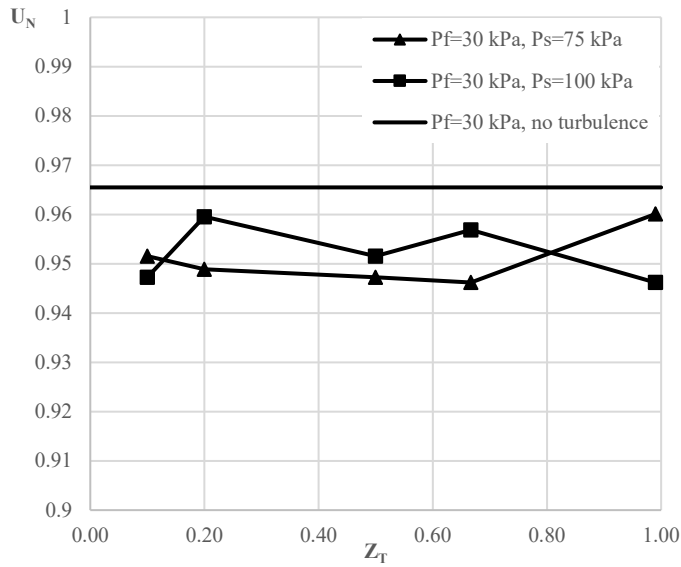


(b) Inlet 2

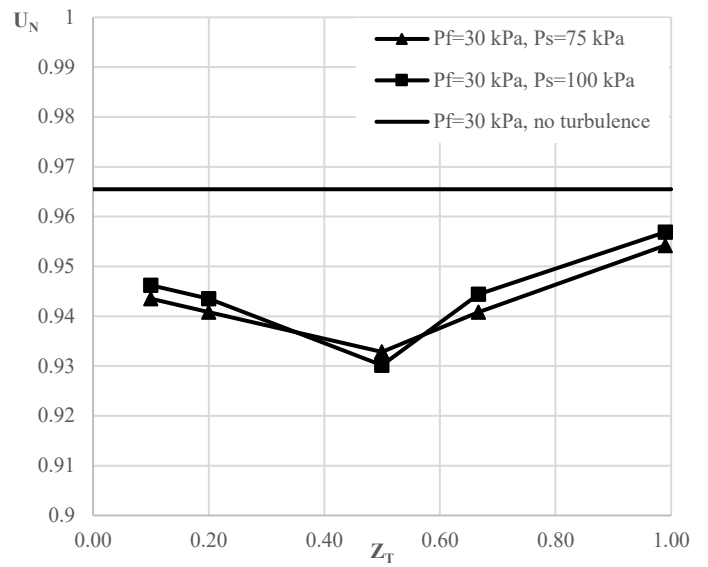


(c) Inlet 3

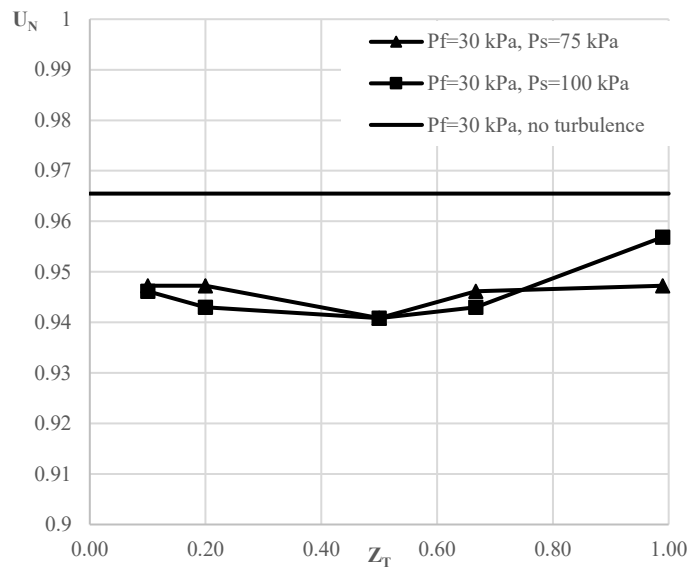
Figure 37: Normalized velocity U_N versus Z_T for $P_f=20$ kPa



(a) Inlet 1



(b) Inlet 2



(c) Inlet 3

Figure 38: Normalized velocity U_N versus Z_T for $P_f = 30$ kPa

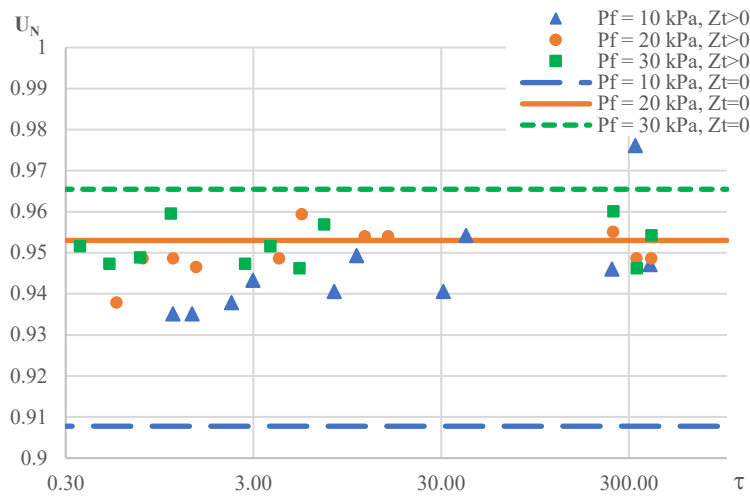
At 10 kPa fill pressure (figure 36), injecting through inlet 1 results in steady increases in speed with injection time for 75 kPa and 100 kPa supply pressures. The velocity increase is more pronounced for 100 kPa supply pressure. The presence of turbulence increases the wave speed by more than 60-154 m/s above U_P for all injection times. When injecting through inlet 2, wave speeds increase by up to 93 m/s above U_P for higher values of Z_T , with the smallest injection times give a speed very near U_P , for both supply pressures. When injecting through inlet 3, a deviation from U_P is only seen at values of Z_T 0.8 and above, as the speed increases by 80-90 m/s. The steady velocity increase with increased injection time for inlet 1 (figure 36a), shows that increased local turbulence levels result in a higher velocity. For inlets 2 (figure 36b) and 3 (figure 36c), the sharp transition is due to the edge of the turbulent region passing over the viewing section.

At 20 kPa (figure 37), there is no clear change in the wave speed as it hovers around U_P with no noticeable trend with change in injection time, for both supply pressures, when injecting through inlet 1. When injecting through inlet 2, the wave speed is near U_P for lower values and higher values of Z_T but drops well below for $Z_T=0.5$ and 0.8 , for a deficit of up to 110 m/s. When injecting through inlet 3, the wave speed behaves similarly to inlet 2 but with a smaller deficit (54 m/s) below U_P .

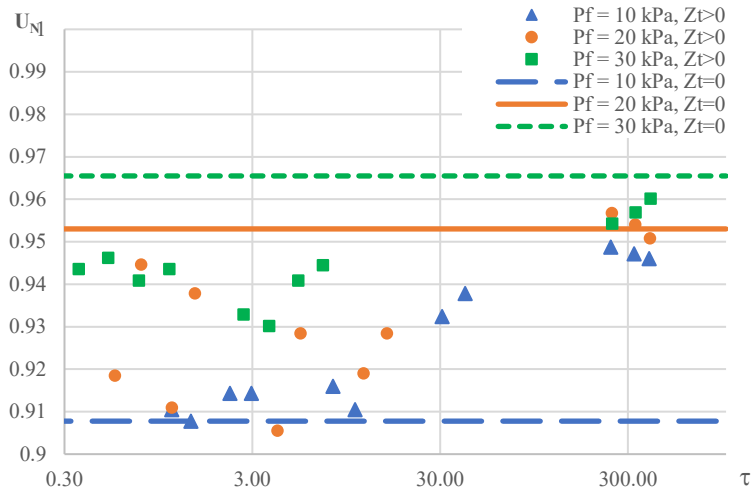
At 30 kPa, (figure 38), the speed drops up to 106 m/s below U_P , with no noticeable trend with change in injection time for injection through inlet 1. When injecting through inlet 2, the wave speed deficit is up to 143 m/s and approaches U_P at higher values of Z_T . A similar effect is observed for inlet 3.

At 10 kPa, a clear trend is seen for all 3 inlets where an increase in injection time sees an increase in wave speed of up to 154 m/s above U_P , with this increase more prominent for inlet 1, less for inlet 2, and least for inlet 3. However, for 20 kPa and 30 kPa, the effect of increased injection time on the wave speed is less, though clearly detrimental for all levels of turbulence, and more detrimental when injecting through inlets 2 and 3 than through inlet 1.

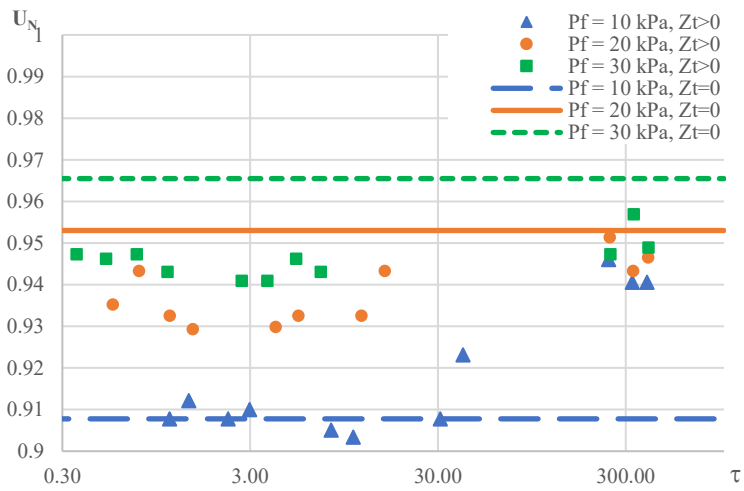
Figure 35 plots U_N versus τ for each inlet and is meant to provide a bigger picture of the impact of turbulence on the wave speed by examining velocity variations for all fill and supply pressures against a single metric.



(a) Inlet 1



(b) Inlet 2



(c) Inlet 3

Figure 39: Normalized velocity U_N versus τ

When injecting through inlet 1 (figure 39a), at 10 kPa, the wave speed is increased in the presence of turbulence and increases with increasing τ . At 20 kPa, little change is observed as the data points hover around U_P . At 30 kPa, a slight deficit is observed but remains near U_P .

When injecting through inlet 2 (figure 39b), at 10 kPa, the wave speed increases with increasing τ , but travels at approximately U_P for lower values of τ . At 20 kPa, no observable trend is seen with an increasing τ , but a large deficit is noted, and the wave travels at U_P for higher values of τ . At 30 kPa, a significant drop in wave speed below U_P is observed for an increasing τ and then an increase back to U_P for higher values of τ .

When injecting through inlet 3 (figure 39c), at 10 kPa, the wave speed increases above U_P only for higher values of τ . For 20 kPa and 30 kPa, a drop in speed is observed for all levels of turbulence except for the higher ones where the wave speed approaches U_P again.

Once again we see the positive impact turbulence has on lower pressure (10 kPa) detonations, and its detrimental impact on higher pressure (20 kPa and 30 kPa) detonations.

Physical Effect of Turbulence on Detonation Front:

Most of the detonations seem physically unaffected after interacting with turbulence. Only 16 experiments out of 99 exhibited some form of change either in orientation or shape of the front. One frame from each of the 16 experiments are shown in figure 36. Each image is described by the inlet through which turbulence was injected and the row number in brackets, referring to table 9.

The following observations were made:

- Four out of the 16 shots were from detonations that have interacted with turbulence from inlet 2, and 12 shots with turbulence from inlet 3. Injecting through inlet 1 does not seem to have an impact on the front. This implies that turbulence will affect the orientation or shape of the front if given sufficient time to interact with it.
- Experiment 7 (inlet 2) and 2, 16, 17, 31 (inlet 3) have exhibited a very slight tilt but more prominently a curved front. In the remaining 11 experiments, the waves were only tilted forward, some more substantially than others.
- Four out of the 16 experiments that have shown some changes are at 10 kPa fill pressure, 6 are at 20 kPa, and 6 at 30 kPa.
- All 4 experiments at 10 kPa have shown a curved front.
- The experiments that exhibited the most tilt are of 20 kPa and 30 kPa. This was observed in the detonation experiments with argon as well.

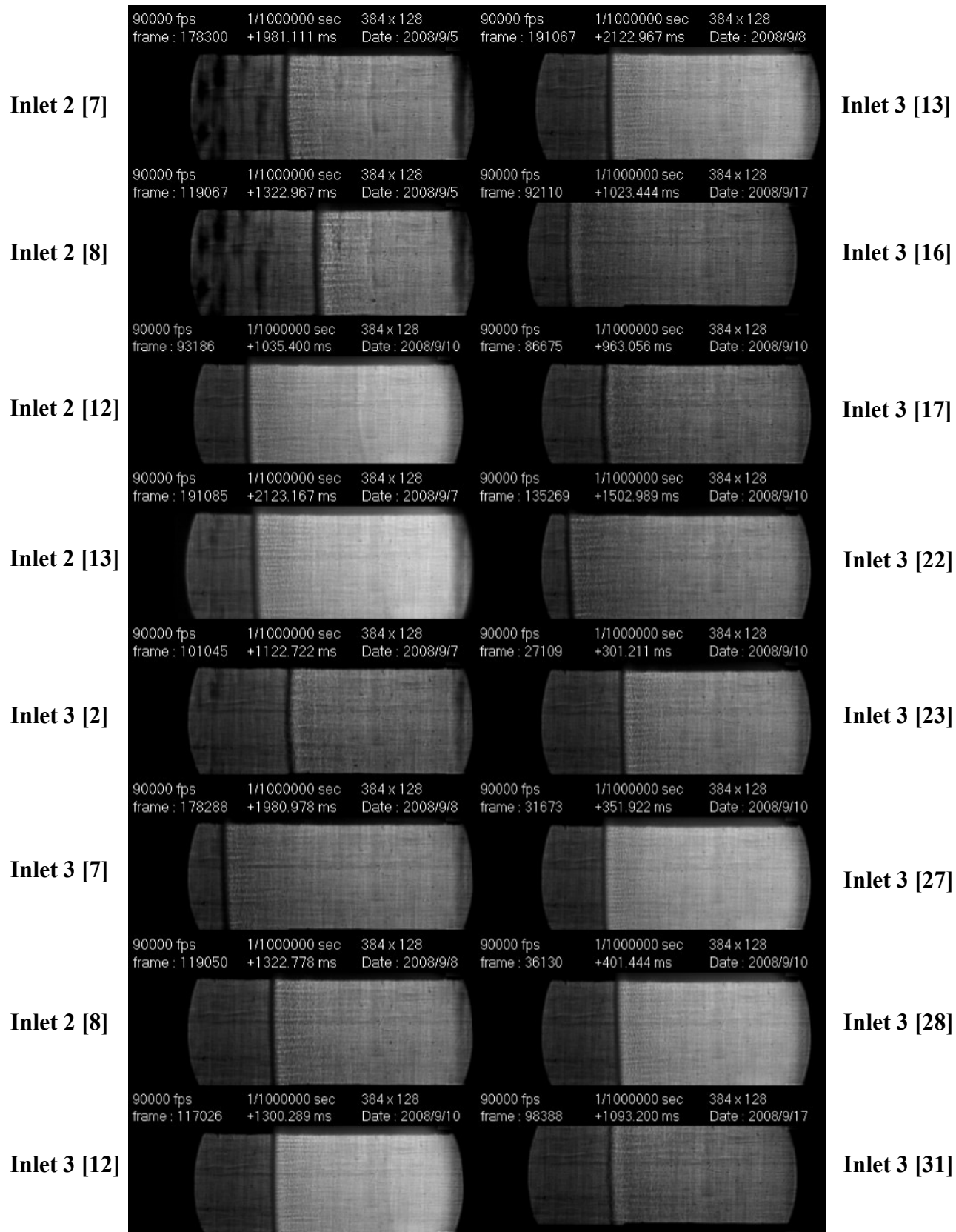


Figure 40: One frame from each of the 16 detonations that have exhibited change in shape or orientation upon interaction with turbulence

5.3 Errors and Uncertainties

The errors and uncertainties associated with the detonation experiments conducted in this study are summarized as follows:

- 1- As mentioned earlier in this chapter, measuring the velocity of the detonation front using the on-screen pixel ruler incorporates an error of 2 pixels per time frame (0.044/0.056 s) which corresponds to ± 9.9 -12.4 m/s. All considered variations were greater than at least one error bar.
- 2- During the firing of detonation waves with turbulence, the final pressures were reached using pre-determined injection times, and not using the 15 psi pressure sensor, which had to be removed because the detonation bypassed a closed S1 and damaged the sensor on more than one occasion. Completely evacuating the region that the sensor occupies induces a delay of more than 1 second after turbulence is injected – which may give the turbulence enough time to decay. Therefore, there was a need to fire “blindly”. Consequently, the actual pressures at which detonations were fired were $P_f \pm 1$ kPa, as tested with some dry runs.
- 3- The accuracy of the 15 psi sensor is $\pm 0.25\%$, which amounts to ± 0.26 kPa on all pressure readings. The accuracy of the 5 psi sensor amounts to ± 0.086 kPa, making it ideal for reading initial pressures in the tube.
- 4- Errors were incurred in setting the supply pressure of the injection line during detonations with argon turbulence as the pressure was set using a pressure gauge on the regulator. This led to slight inconsistencies between experiments in the set supply pressure. The supply pressure during detonations with ethylene-oxygen turbulence was set using the 50 psi sensor connected to Panel 2, as cylinder C2 is not regulated. The accuracy of this sensor is $\pm 0.25\%$ which amounts to ± 0.86 kPa.
- 5- The leak rate in the system ranged between 0.1-0.2 kPa/minute at a pressure of 0.5 kPa. The maximum duration of all the experiments did not exceed 3 minutes. In addition to the average pressure value of 0.2 kPa in the system before filling begins, the partial pressure of air/products does not exceed 0.8 kPa at all times.
- 6- As mentioned earlier in this section, the fact that the manifold had to be evacuated to a pressure of 5.5 kPa induced a delay of 200-400 ms. Although this delay is small, the turbulence would have decayed to a certain degree by the time the detonation interacts with the flow-field. Injecting turbulence at a higher supply pressure increases this delay further.

Chapter 6

Conclusion

A macroscopic analysis of the impact of turbulence on shock and detonation dynamics was conducted in this study. The understanding of how detonation waves interact with turbulence is vital for the development of RDEs. Turbulence was generated by injecting jets of gas through three different inlets located at the top of the shock tube while varying the supply pressure and injection time to control the degree of turbulence. Shock wave speeds increased upon interaction with turbulence and the most prominent effects were seen when injecting through inlet 3. Detonation wave speeds increased at fill pressures of 10 kPa with the most prominent effects seen close to the injection port. Wave speeds decreased at fill pressures of 20 kPa and 30 kPa with the most prominent effects seen further away from the injection port. This means two things: first, turbulence helps recover lost energy for larger cell size detonations as wave speeds approach U_{CJ} more, and leads to more energy loss for smaller cell size detonations as a significant drop in wave speeds below U_{CJ} is observed; second, smaller cell size detonations need more interaction time with turbulence to exhibit changes in wave speed as opposed to larger cell size detonations which exhibit changes in speed with minimum interaction time. This implies that there is a boundary between 10 kPa and 20 kPa at which a switch in behavior occurs.

6.1 Future Works

Setup improvement:

The setup used in this study serves as a basis for future experiments that involve detonation-turbulence interactions. The first issue to be addressed is the inability to fire with the pressure sensor installed. The sensor is to be electrically and mechanically protected in order to use it during ignition and enhance the accuracy of the pressures at which detonations are being fired. The second issue is to find a way to minimize the delay between turbulence injection and ignition in order to maximize the effect of the turbulent flow-field on the propagating wave. This will allow one to inject at higher supply pressures without worrying about any delays before ignition. However, even with the incurred delays of 200-400 milliseconds in this study, significant changes in wave speed have been observed.

Further exploring the effect of turbulence:

Analysis based on changes in detonation speeds gives an understanding of energy conservation and dissipation, but does not reveal clear information about the detonation structure. Future work includes measuring the cell size for detonations propagating in a quiescent medium and for

detonations interacting with turbulence for different fill pressures. The cell size can be measured by inserting a soot foil inside the shock tube and physically measuring the cells imprinted on the foil. Another set of experiments are to be done at fill pressures between 10 kPa and 20 kPa in order to find the boundary pressure/cell size at which the switch in behavior occurs. The minimum cell size found, call it λ_{min} , would be a characteristic of the reactive mixture used. To further expand on this, different reactive mixtures can be used and compared.

Previous work on RDE design provides us with a minimum number of cells (hence maximum cell size, λ_{max}) for a given annular height, h , required for a detonation to maintain propagation in an annular chamber [35]. Further expanding on the experiments in this study provides us with a range of cell sizes bounded by λ_{min} and λ_{max} .

Numerical analysis:

A CFD analysis on the varied levels of turbulence should be done to attribute the turbulence intensities to the cell sizes that have seen an increase or decrease in wave speed. This is important in order to compare the impact of turbulence on detonations in different reactive mixtures and also the intensities seen in this study to those encountered in the injector orifices of an RDE. The turbulence intensity could also be measured using PIV techniques.

Bibliography

1. Lu, F.K., Braun, E.M.: Rotating Detonation Wave Propulsion: Experimental Challenges, Modeling, and Engine Concepts. *J. Propuls. Power.* 30, 1125–1142 (2014). <https://doi.org/10.2514/1.B34802>
2. Wolański, P.: Detonative propulsion. *Proc. Combust. Inst.* 34, 125–158 (2013). <https://doi.org/10.1016/j.proci.2012.10.005>
3. Maxwell, B.McN., Bhattacharjee, R.R., Lau-Chapdelaine, S.S.M., Falle, S.A.E.G., Sharpe, G.J., Radulescu, M.I.: Influence of turbulent fluctuations on detonation propagation. *J. Fluid Mech.* 818, 646–696 (2017). <https://doi.org/10.1017/jfm.2017.145>
4. Jackson, T.L., Kapila, A.K., Hussaini, M.Y.: Convection of a pattern of vorticity through a reacting shock wave. *Phys. Fluids Fluid Dyn.* 2, 1260–1268 (1990). <https://doi.org/10.1063/1.857626>
5. Lasseigne, D.G., Jackson, T.L., Hussaini, M.Y.: Nonlinear interaction of a detonation/vorticity wave. *Phys. Fluids Fluid Dyn.* 3, 1972–1979 (1991). <https://doi.org/10.1063/1.857928>
6. Jackson, T.L., Hussaini, M.Y., Ribner, H.S.: Interaction of turbulence with a detonation wave. *Phys. Fluids Fluid Dyn.* 5, 745–749 (1993). <https://doi.org/10.1063/1.858657>
7. Massa, L., Chauhan, M., Lu, F.: Numerical Study of Detonation-Turbulence Interaction. In: 49th AIAA Aerospace Sciences Meeting including the New Horizons Forum and Aerospace Exposition. American Institute of Aeronautics and Astronautics, Orlando, Florida (2011)
8. Massa, L., Lu, F.K.: The role of the induction zone on the detonation–turbulence linear interaction. *Combust. Theory Model.* 15, 347–371 (2011). <https://doi.org/10.1080/13647830.2010.540353>
9. Massa, L., Chauhan, M., Lu, F.K.: Detonation–turbulence interaction. *Combust. Flame.* 158, 1788–1806 (2011). <https://doi.org/10.1016/j.combustflame.2011.01.014>
10. Lu, F.K., Chauhan, M., Massa, L.: Evolution of Autocorrelation in Detonation Interaction with Homogeneous, Isotropic Turbulence. In: Kontis, K. (ed.) 28th International Symposium on Shock Waves. pp. 349–354. Springer Berlin Heidelberg, Berlin, Heidelberg (2012)
11. Massa, L., Chauhan, M., Lu, F.K.: Effects of Vortical and Entropic Forcing on Detonation Dynamics. In: Kontis, K. (ed.) 28th International Symposium on Shock Waves. pp. 281–286. Springer Berlin Heidelberg, Berlin, Heidelberg (2012)
12. Jin, T., Luo, K., Dai, Q., Fan, J.: Simulations of Cellular Detonation Interaction with Turbulent Flows. *AIAA J.* 54, 419–433 (2016). <https://doi.org/10.2514/1.J054538>
13. Huete, C., Sánchez, A.L., Williams, F.A.: Theory of interactions of thin strong detonations with turbulent gases. *Phys. Fluids.* 25, 076105 (2013). <https://doi.org/10.1063/1.4816353>
14. Huete, C., Sánchez, A.L., Williams, F.A.: Linear theory for the interaction of small-scale turbulence with overdriven detonations. *Phys. Fluids.* 26, 116101 (2014). <https://doi.org/10.1063/1.4901190>
15. Hussein, S.M., Blaiszik, E.M., Baydar, E., Lu, F.K.: Velocity Fluctuations in the Interaction of Homogeneous, Isotropic Turbulence and a Detonation Wave. In: Bonazza, R. and Ranjan, D. (eds.) 29th International Symposium on Shock Waves 1. pp. 289–294. Springer International Publishing, Cham (2015)
16. Huete, C., Jin, T., Martínez-Ruiz, D., Luo, K.: Interaction of a planar reacting shock wave with an isotropic turbulent vorticity field. *Phys. Rev. E.* 96, 053104 (2017). <https://doi.org/10.1103/PhysRevE.96.053104>

17. Andreopoulos, Y., Agui, J.H., Briassulis, G.: Shock-wave turbulence interactions. (2000)
18. Zhang, F. ed: Shock Waves Science and Technology Library, Vol. 6. Springer Berlin Heidelberg, Berlin, Heidelberg (2012)
19. Chapman, D.L.: VI. On the rate of explosion in gases. Lond. Edinb. Dublin Philos. Mag. J. Sci. 47, 90–104 (1899)
20. Jouguet, M.: Sur la propagation des réactions chimiques dans les gaz. J. Mathématiques Pures Appliquées I. 347–425 (1905)
21. Fickett, W., Davis, W.C.: Detonation: theory and experiment. Dover Publications, Mineola, N.Y (1979)
22. Dove, J.E., Wagner, H.G.: A photographic investigation of the mechanism of spinning detonation. In: Symposium (International) on Combustion. pp. 589–600. Elsevier (1961)
23. Schott, G.L.: Observations of the Structure of Spinning Detonation. Phys. Fluids. 8, 850 (1965). <https://doi.org/10.1063/1.1761328>
24. White, D.R.: Turbulent Structure of Gaseous Detonation. Phys. Fluids. 4, 465 (1961). <https://doi.org/10.1063/1.1706350>
25. Bastea, S., Fried, L.E.: Chemical Equilibrium Detonation. In: Zhang, F. (ed.) Shock Waves Science and Technology Library, Vol. 6. Springer Berlin Heidelberg, Berlin, Heidelberg (2012)
26. Higgins, A.: Steady One-Dimensional Detonations. In: Zhang, F. (ed.) Shock Waves Science and Technology Library, Vol. 6. pp. 33–105. Springer Berlin Heidelberg, Berlin, Heidelberg (2012)
27. Vasilev, A.A.: Detonation Dynamic Parameters. In: Zhang, F. (ed.) Shock Waves Science and Technology Library, Vol. 6. Springer Berlin Heidelberg, Berlin, Heidelberg (2012)
28. Mazaheri, K., Mahmoudi, Y., Sabzpooshani, M., Radulescu, M.I.: Experimental and numerical investigation of propagation mechanism of gaseous detonations in channels with porous walls. Combust. Flame. 162, 2638–2659 (2015). <https://doi.org/10.1016/j.combustflame.2015.03.015>
29. Pintgen, F., Shepherd, J.E.: Detonation diffraction in gases. Combust. Flame. 156, 665–677 (2009). <https://doi.org/10.1016/j.combustflame.2008.09.008>
30. Chao, J., Otsuka, T., Lee, J.H.S.: An experimental investigation of the onset of detonation. Proc. Combust. Inst. 30, 1889–1897 (2005). <https://doi.org/10.1016/j.proci.2004.08.193>
31. Chao, J., Lee, J.H.S.: The propagation mechanism of high speed turbulent deflagrations. Shock Waves. 12, 277–289 (2003). <https://doi.org/10.1007/s00193-002-0161-2>
32. Hlouschko, S., Ciccarelli, G.: Interaction of a high-speed combustion front with a closely packed bed of spheres. Shock Waves. 18, 317–327 (2008). <https://doi.org/10.1007/s00193-008-0132-3>
33. Lee, J.H.W., Chu, V.H.: Turbulent Jets. In: Turbulent Jets and Plumes - A Lagrangian Approach. Springer (2003)
34. California Institute of Technology: Detonation Database, http://shepherd.caltech.edu/detn_db/html/db.html
35. Bykovskii, F.A., Zhdan, S.A., Vedernikov, E.F.: Continuous Spin Detonations. J. Propuls. Power. 22, 1204–1216 (2006). <https://doi.org/10.2514/1.17656>
36. Settles, G.S.: Schlieren and Shadowgraph Techniques. Springer Berlin Heidelberg, Berlin, Heidelberg (2001)

Appendix

A1 List of Components

Below is the list of mechanical and electrical components used in the shock tube setup:

No.	Description	Manufacturer	Part/Model Number	Quantity
1	Solenoid Valve (3/8")	ASCO	8210G093	5
2	Ball Valve (1/2")	Swagelok	SS-45S8	3
3	Ball Valve (1/4")	Parker	4A-MB4LPFA-SSP	5
4	Needle Valve (1/2")	Swagelok	SS-1VS8	1
5	Needle Valve (1/4")	Swagelok	SS-1RS4	2
6	Check Valve (1/4")	HAM-LET	H400SSL1/41/3PSI	3
7	Pressure Regulator	Festo	LFR-D-MIDI	1
8	Pressure Regulator	The Harris Products Group	425-200	1
9	2-Stage Rotary Vane Vacuum Pump	EDWARDS	RV-5	1
10	Absolute Pressure Transducer (15 psi)	Honeywell	PX2EN1XX015PAAAX	1
11	Absolute Pressure Transducer (30 psi)	Honeywell	PX2AN1XX030PAAAX	1
12	Absolute Pressure Transducer (50 psi)	Honeywell	PX2AN1XX050PAAAX	1
13	Absolute Pressure Transducer (5 psi)	OMEGA	PX309-005AI	1
14	Arduino Mega2560	Arduino	-	1
15	5V DC 4-Channel Relay Module	Songle	JQQ-3FF-S-Z	1
16	5V DC 1-Channel Relay Module	Songle	SRD-05VDC-SL-C	1
17	5V DC 1-Channel Relay Module	OMRON	G3MB-202P	1
18	High Voltage 30 kV Trigger Module	EG&G	TM-11	1
19	Capacitor	The Condenser Products Corporation	EC104-30M	4
20	Variable Transformer	Superior Electric	Type 10C	1
21	High Voltage Power Supply	-	-	1

Table 12: List of components used in the experiments

A2 Schlieren Setup Procedure

- 1) Mount the two first surface mirrors at 45 degree angles with the structure of the shock tube, bending inwards towards the tube.
- 2) Place the first concave mirror at an arbitrary distance from one of the square mirrors facing it, keeping the central axes joining them parallel to the structure. Do the same with the remaining two mirrors. Ensure that the concave mirrors are at the exact same level using the laser, and that their positions are symmetrical about the center of the structure.
- 3) Identify the locus of points that are at a distance of a focal length (48") away from each concave mirror. This set of points is the possible locations of the slit and of the knife edge required to form the Z-shape. Calculate the minimum acceptable angle (to avoid blockages in the light path) between the axis joining the two mirrors, and the angle of reflection of a light source if it were placed along this axis.

$$2\theta_{min} = \sin^{-1} \frac{d}{2f} = 3.6^\circ$$

In our setup, the angle was set at 10.4°.

- 4) Place the slit at a distance of one focal length away from the first mirror to produce a collimated beam, and similarly for the knife edge at the other mirror. Using the laser, ensure that the slit-light source arrangement is correctly oriented at the angle chosen in step 3.
- 5) The next step is to ensure that the slit is also at the focal length of the converging lens placed in the light source housing. It is recommended that the condenser f-number is 1.5 to 2 times smaller than that of the field mirror [36]. The light source housing contains a 1" condenser followed by a focusing lens of f-number $f/5$ making the lens-slit cone angle larger than the mirror-slit cone angle, which in turn causes some light spillage out of the first field mirror.
- 6) Check the beam diameter at various distances along the light path between the mirrors and ensure it is constant and exactly fills both spherical mirrors.
- 7) Adjust the percentage of knife-edge cutoff to obtain the desired sensitivity. Slide the knife edge in to cut off part of the image. If the spot darkens non-uniformly, note the side. If it is the same side as the knife edge, increase the axial distance between the knife edge and the second mirror. If it is the opposite, decrease the axial distance. Once the image darkens uniformly, you know the knife edge is in the correct position.

A3 Shock Test Procedure

A3.1 Shocks with no Turbulence

Referring to figure 14 from Chapter 3:

- 1) The injection line is disconnected and the inlet is plugged. Connect the regulated shop air line to B5. Replace the 15 psi sensor with the 30 psi sensor.
- 2) Evacuate the shock tube
 - a. Turn on the evac motor and the vacuum pump, and connect its outlet to the evac hose.
 - b. Plug the Arduino into the power supply, this opens S1 and keeps S2 closed.
 - c. Open B1, B2, B3, and B4 in order to evacuate the entire system including the shock tube and the panels until the pressure reaches 0.2 kPa.
- 3) Fill tube with air
 - a. Slowly open B5 until pressure in tube reaches the desired value (P_f)
 - b. Close B5 and B1.
- 4) Prepare for ignition
 - a. Turn on trigger module then power supply
 - b. Remove the safety shaft from the capacitors
 - c. Turn up the power supply potentiometer to the desired voltage of 16.5 kV. Monitor the capacitor charge with the high voltage probe.
 - d. When the desired voltage is reached, turn off the power supply.
 - e. Press the red button – S1 is closed to protect the sensor → trigger the camera → ignition
 - f. Lower the safety shaft

A3.2 Shocks with Turbulence

Referring to figure 14 from Chapter 3:

- 1) Disconnect B6 from cylinder C2 and connect it to the regulated shop air line.
- 2) Evacuate the shock tube
 - a. Turn on the evac motor and the vacuum pump, and connect its outlet to the evac hose.
 - b. Plug the Arduino into the power supply, this will open S1 and close S3. S2 & S4 remain closed at all times and S5 & B6 remain open at all times.
 - c. Open B1, B2, B3, and B4 in order to evacuate the entire system including the shock tube and the panels until the pressure reaches 0.2 kPa. Close B4.
- 3) Fill tube with air
 - a. Slowly open the side of B5 that is open to the atmosphere until pressure in tube reaches the desired value (P_i)
 - b. Close B5
- 4) Prepare for ignition
 - a. Turn on trigger module then power supply
 - b. Remove the safety shaft from the capacitors
 - c. Turn up the power supply potentiometer to the desired voltage of 16.5 kV. Monitor the capacitor charge with the high voltage probe.
 - d. When the desired voltage is reached, turn off the power supply.
 - e. Press the red button to:
 - i. Open S3 for t_{inj} seconds until P_f is reached.
 - ii. Close S1 to protect the sensor
 - iii. Trigger the camera → ignition
 - iv. Lower the safety shaft.

A4 Detonation Test Procedure

A4.1 Detonations with no Turbulence

Referring to figure 14 from Chapter 3:

- 1) The fill and injection lines are disconnected and the inlets are plugged. Keep B1 connected to B2 and Panel 1.
- 2) Evacuate the shock tube
 - a. Turn on the evac motor and the vacuum pump, and connect its outlet to the evac hose.
 - b. Plug the Arduino into the power supply.
 - c. Open B1, B2, B3, and B4 in order to evacuate the entire system including the shock tube and the panels until the pressure reaches 0.2 kPa. Keep N1 and N2 closed.
 - d. For the first test of the day only, open N2 while keeping N1 closed to evacuate the hose that connects C1 to Panel 1.
- 3) Prepare to fill tube with reactive mixture
 - a. Close B3 and B4 to isolate the tube's vacuum line and Panel 2 from Panel 1 and the fuel injection line.
 - b. Open N1 to fill the hose connecting C1 to Panel 1.
- 4) Fill tube with reactive mixture
 - a. Slowly open N2 until pressure in tube reaches the desired value (P_f)
 - b. Close N2 and B1.
- 5) Evacuate Panel 1
 - a. Open B3 and B4 until Panel 1 and the fill line are fully evacuated. Close B3 and B4.
 - b. Close B5 to protect the 5 psi sensor.
- 6) Prepare for ignition
 - a. Turn on trigger module then power supply
 - b. Remove the safety shaft from the capacitors
 - c. Turn up the power supply potentiometer to the desired voltage of 16.5 kV. Monitor the capacitor charge with the high voltage probe
 - d. When the desired voltage is reached, turn off the power supply
 - e. Press the red button to trigger the camera and ignition
 - f. Lower the safety shaft
- 7) Evacuate the shock tube and panels
 - a. Open B1-B5 to evacuate the shock tube

A4.2 Detonations with Turbulence

- 1) Evacuate the shock tube
 - a. Turn on the evac motor and the vacuum pump, and connect its outlet to the evac hose.
 - b. Plug the Arduino into the power supply, this will open S1, S2, S3, and S4 to prepare for evacuation.
 - c. Open B2, B3, B4, and B5 in order to evacuate the entire system including the shock tube and the panels until the pressure reaches 0.2 kPa. Keep N1, N2, and B1 closed.
 - d. For the first test of the day only, open N2 while keeping N1 closed to evacuate the hose that connects C1 to Panel 1, and open S5 to evacuate the injection line as well.
- 2) Prepare to fill tube with reactive mixture
 - a. Close B3 and B4 to isolate the tube's vacuum line and Panel 2 from Panel 1 and the fuel injection line.
 - b. Open N1 to fill the hose connecting C1 to Panel 1.
 - c. Press the green button to close S3 and S4, and open S5. This will fill the T-branch on the injection line and prepare the tube for filling.
 - d. Set the supply pressure on cylinder C2 (argon or ethylene-oxygen) to prepare for jet injection.
 - i. If the experiment is with argon turbulence then set the supply pressure using the regulator while reading off the pressure gauge.
 - ii. If the experiment is with ethylene-oxygen turbulence then first close B2 to isolate the tube from the panels, then open B8, B3, B5, N3, and N2 to fill the cylinder to the required supply pressure while reading off the 50 psi sensor. Close N3, B5, and N2. Open B4 to evacuate Panels 1 and 2 then close B3 and B4 to re-isolate the panels from each other. Open B2 again.
- 3) Fill tube with reactive mixture
 - a. Slowly open N2 until pressure in tube reaches the desired value (P_i)
 - b. Close N2
- 4) Evacuate Panel 1 and manifold
 - a. Press the green button to close S2 and isolate the shock tube from the panels
 - b. Open B3 and B4 until Panel 1 and the branches are fully evacuated
 - c. Close B5 and B8 to protect the 5 psi and 50 psi sensors.
- 5) Prepare for ignition
 - a. Turn on trigger module then power supply
 - b. Remove the safety shaft from the capacitors
 - c. Turn up the power supply potentiometer to the desired voltage of 16.5 kV. Monitor the capacitor charge with the high voltage probe.
 - d. When the desired voltage is reached, turn off the power supply.
 - e. Press the red button to:
 - i. Open S3 for t_{inj} seconds
 - ii. Close S1 and open S2 and S4 for t_{delay} seconds to evacuate the manifold
 - iii. Close S2 and S4
 - iv. Trigger the camera and ignition.
 - f. Lower the safety shaft
- 6) Evacuate the shock tube and panels
 - a. Open B1-B5 to evacuate the shock tube. Close B1.
 - b. Press the green button to open S1, S2, S3, S4 and evacuate the entire system.

A5 Arduino Scripts

This section contains the code used for the Arduino during the detonation experiments with and without turbulence.

A5.1 Detonations with no Turbulence

```
int ledPin = 4;
int redbuttonPin = 13;
int redbuttonState = 0;
int triggerPin = 8;
int bncPin = 39;
int ignitionToCameraDelay = 1;
int triggerdelay = 350;
int cameraPulseWidth = 250;

void setup() {

    //initialize ignition parameters
    pinMode(ledPin, OUTPUT);
    pinMode(redbuttonPin, INPUT);
    pinMode(bncPin, OUTPUT);
    pinMode(triggerPin, OUTPUT);
    digitalWrite(ledPin, LOW);
    digitalWrite(bncPin, LOW);
    digitalWrite(triggerPin, HIGH);

}

void loop() {

    redbuttonState = digitalRead(redbuttonPin);
    if (redbuttonState==HIGH) {

        digitalWrite(triggerPin, LOW);
        Serial.println("IGNITION!");
        delay(ignitionToCameraDelay);
        digitalWrite(bncPin, HIGH);
        delay(cameraPulseWidth);
        digitalWrite(triggerPin, HIGH);
        digitalWrite(bncPin, LOW);

    }

}
```

```

void readpressure15{
const int abspressureinput15 = A1;
const float pressurezerol5 = 102.3; //analog reading at 0 kPa
const float pressuremax15 = 920.7; //analog reading at 103.42 kPa
const float pressuremaxkPa15 = 103.42; //maximum pressure reading of
//pressure transducer in kPa

float readpressure15()
{
pressurevalue15 = analogRead(abspressureinput15);
pressurevalue15 = (pressurevalue15-
pressurezerol5)*(pressuremaxkPa15)/(pressuremax15-pressurezerol5);
return pressurevalue15;
}

}

```

A5.2 Detonations with Turbulence

```

int ledPin = 4;
int redbuttonPin = 13;
int redbuttonState = 0;
int triggerPin = 11;
int bncPin = 39;
int ignitionToCameraDelay = 1;
int cameraPulseWidth = 250;

float pressurevalue15 = 0;
int I1Pin = 2;
int I2Pin = 6;
int I3Pin = 11;
int R1Pin = 3;
int R2Pin = 5;
int greenbuttonPin = 9;
int greenbuttonState = 0;
int Pf = 10;
float t1;
float t2;
float tinj;
float tdelay;

void setup() {
Serial.begin(9600);
//initialize valve pins
pinMode(I1Pin, OUTPUT);
pinMode(I2Pin, OUTPUT);
pinMode(I3Pin, OUTPUT);
pinMode(R1Pin, OUTPUT);
pinMode(R2Pin, OUTPUT);
digitalWrite(I1Pin, LOW);
digitalWrite(I2Pin, LOW);

```

```

digitalWrite(I3Pin, HIGH);
digitalWrite(R1Pin, LOW);
digitalWrite(R2Pin, LOW);

//initialize ignition parameters
pinMode(ledPin, OUTPUT);
pinMode(redbuttonPin, INPUT);
pinMode(greenbuttonPin, INPUT);
pinMode(bncPin, OUTPUT);
pinMode(triggerPin, OUTPUT);
digitalWrite(ledPin, LOW);
digitalWrite(bncPin, LOW);
digitalWrite(triggerPin, HIGH);

readpressure15();
Serial.println("Tube pressure is:\n");
Serial.println(pressurevalue15, 4);
while (greenbuttonState==LOW) {
    greenbuttonState = digitalRead(greenbuttonPin);
    Serial.println("Evacuating System");
    readpressure15();
    Serial.println(pressurevalue15, 4);
    delay(1000);
}
digitalWrite(I1Pin, HIGH);
digitalWrite(I2Pin, HIGH);
delay(200);
digitalWrite(I3Pin, LOW);
Serial.println("Ready to fill");
greenbuttonState = LOW;
while (greenbuttonState==LOW) {
    greenbuttonState = digitalRead(greenbuttonPin);
    Serial.println("Filling shock tube");
    readpressure15();
    Serial.println(pressurevalue15, 4);
    delay(1000);
}
digitalWrite(R2Pin, HIGH);
greenbuttonState = LOW;
}

void loop() {

    redbuttonState = digitalRead(redbuttonPin);
    if (redbuttonState==HIGH) {
        digitalWrite(ledPin, HIGH);
        t1=millis();
        digitalWrite(I1Pin, LOW);
        do{
            readpressure15();
            Serial.println(pressurevalue15, 4);
            readpressure15();

```

```

    } while (pressurevalue15 < Pf);

t2=millis();
digitalWrite(I1Pin, HIGH);
tinj=t2-t1;
Serial.println("Injection time is: ");
Serial.println(tinj, 4);
readpressure15();
Serial.println("Tube pressure before ignition is: ");
Serial.println(pressurevalue15, 4);
t1=millis();
digitalWrite(R1Pin, HIGH);
digitalWrite(I3Pin, HIGH);
digitalWrite(R2Pin, LOW);
digitalWrite(I2Pin, LOW);

do{
readpressure15();
Serial.println(pressurevalue15, 4);
readpressure15();
} while (pressurevalue15 > 5);

digitalWrite(I2Pin, HIGH);
digitalWrite(R2Pin, HIGH);
t2=millis();
tdelay = t2-t1;
digitalWrite(triggerPin, LOW);
Serial.println("IGNITION!");
delay(ignitionToCameraDelay);
digitalWrite(bncPin, HIGH);
delay(cameraPulseWidth);
digitalWrite(triggerPin, HIGH);
digitalWrite(bncPin, LOW);

Serial.println("Delay after injection is: ");
Serial.println(tdelay, 4);
readpressure15();
Serial.println("Tube pressure is:\n");
Serial.println(pressurevalue15, 4);
delay(500);

while (greenbuttonState==LOW) {
    greenbuttonState = digitalRead(greenbuttonPin);
    digitalWrite(ledPin, LOW);
    delay(250);
    digitalWrite(ledPin, HIGH);
    delay(250);
}
digitalWrite(R1Pin, LOW);
digitalWrite(R2Pin, LOW);
digitalWrite(I1Pin, LOW);
digitalWrite(I2Pin, LOW);

```

```

        digitalWrite(ledPin, LOW);
        greenbuttonState = LOW;
    }
    else {
        readpressure15();
        Serial.println("Tube pressure is now:\n");
        Serial.println(pressurevalue15, 4);
        delay(500);
    }
}

void readpressure15{
const int abspressureinput15 = A1;
const float pressurezero15 = 102.3; //analog reading at 0 kPa
const float pressuremax15 = 920.7; //analog reading at 103.42 kPa
const float pressuremaxkPa15 = 103.42; //maximum pressure reading of
//pressure transducer in kPa

float readpressure15() {

    pressurevalue15 = analogRead(abspressureinput15);
    pressurevalue15 = (pressurevalue15-
    pressurezero15)*(pressuremaxkPa15)/(pressuremax15pressurezero15);
    return pressurevalue15;
}

}

```

A6 Schlieren Images of Detonations with Turbulence

Eighteen images of detonations with ethylene-oxygen turbulence are shown below. For each inlet and fill pressure, images for a supply pressure of 100 kPa and two modes of turbulence are shown: $Z_T = 0.99$ and $Z_T = 0.2$. The number next to each row of images represents the experiment number that the row corresponds to referring to table 9.

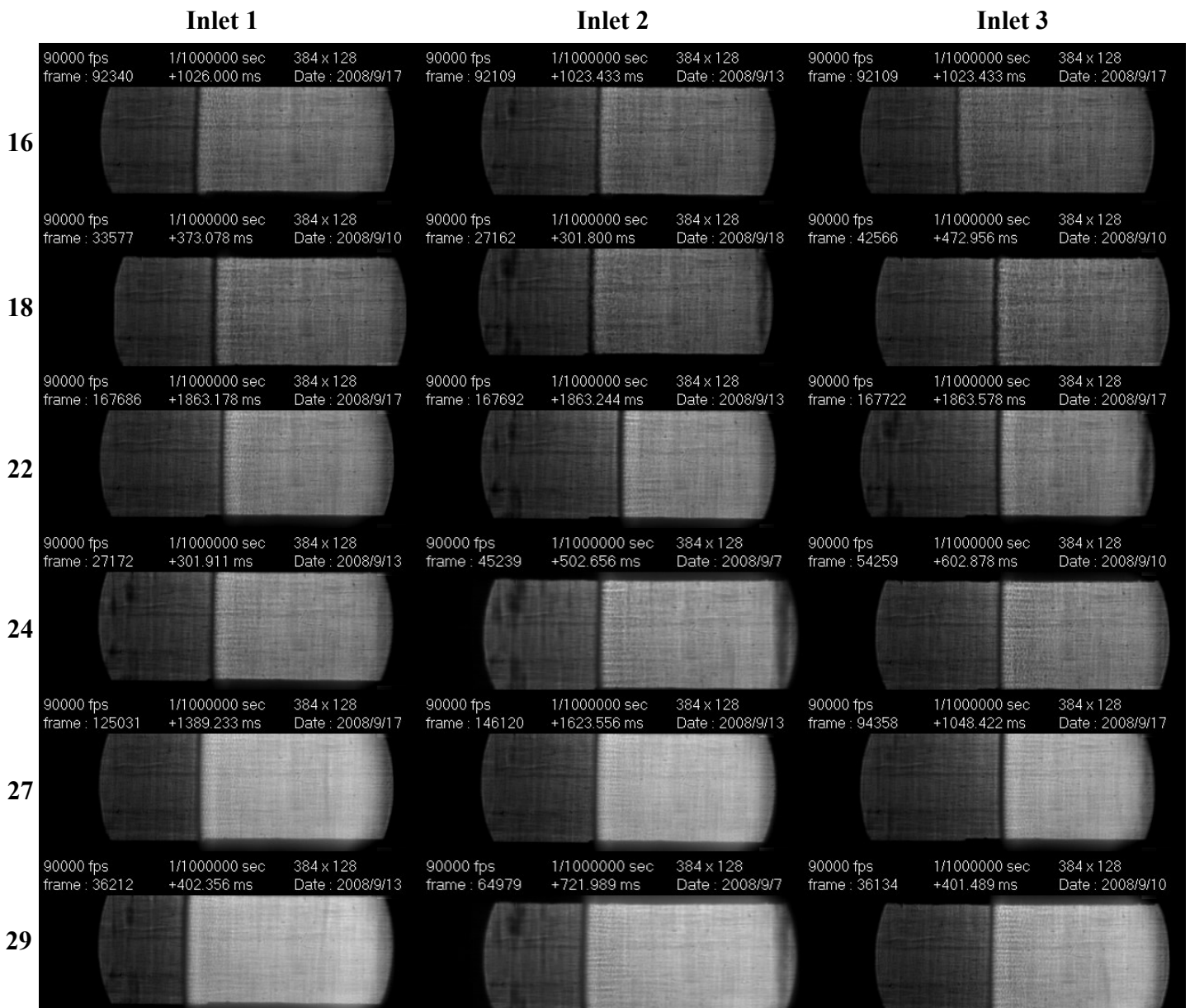


Figure 41: Schlieren images of detonations with ethylene-oxygen turbulence at $P_s=100$ kPa and $Z_T=0.99$ & $Z_T=0.2$.